# Robotically Assisted Active Vibration Control in Milling

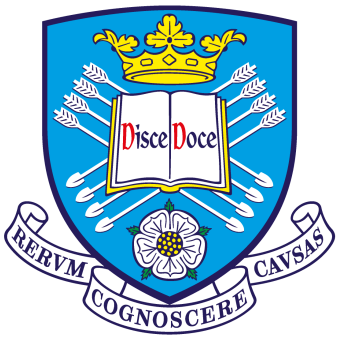


**Muhammet Ozsoy**

Supervisors: Prof. Neil D. Sims

Dr. Erdem Ozturk

Department of Mechanical Engineering

University of Sheffield

This dissertation is submitted for the degree of

*Doctor of Philosophy*

September 2022

# Acknowledgements

I express my sincere gratitude to my supervisors Prof. Neil Sims and Dr. Erdem Ozturk, for their continuous support, encouragement, guidance and patience from the beginning to the end of my PhD. They always supported me and my research by sharing their profound knowledge and experiences with me. Furthermore, their ideas and advice in our weekly meetings were inspirational for me accomplishing my PhD studies and developing my research and engineering skills. It was a privilege to have two supervisors like them, who have high standards in research and supervision.

I would like to thank Dr. Huseyin Celikag and Dr. Hakan Dogan for fruitful discussions and help in machining tests. I thank Jamie Booth and Mathew Hall for their help and technical support in the experiments. I wish to extend a special thanks to my friends who made my years at the University of Sheffield memorable. I would like to acknowledge the financial support of the Turkish Ministry of National Education for this research.

Finally, I am most thankful to my beloved family, specifically my parents, brother, and his family for their love, support and encouragement throughout the years. This accomplishment would not be possible without them. Also, I would like to thank Semra Ismailova Saidova for her love and invaluable support from London and then Sheffield. There is no greater support and encouragement besides you.

# Abstract

The role of robots has been increasing in machining applications, with new concepts such as robotic-assisted machining where a robot supports the workpiece while it is machined by a machine tool. This method improves chatter stability to a certain extent. However, forced vibrations or unstable vibrations such as chatter can still be a limiting factor for the productivity and quality of the machining process. In this thesis, the robotic-assisted milling approach is extended to consider an actively controlled robot arm, to suppress the chatter vibrations for milling operation. To assess the feasibility of the method, a proof-mass actuator is assembled on a beam structure that is representative of the robot system. The beam structure is designed to exhibit two degrees of freedom in its structural dynamics, thereby emulating the robots' dynamic response. Many standard active control methods are evaluated, namely direct velocity feedback (DVF), virtual passive absorber (VPA), proportional integrated derivative (PID), linear quadratic regulator (LQR), H infinity ($H_\infty$) and $\mu$ synthesis control. To optimise the controller parameters, a self adaptive differential (SADE) algorithm is used. To validate the simulated frequency response function (FRF) results, several experimental tests are carried out for each control method. It is shown that the critical limiting depth of cut can be significantly increased, compared to the scenario where the robot has no active control applied. Then, the concept was examined under the real milling conditions. The experimental results showed that the chatter stability and the critical limiting depth of cut ($b_{min}$) were considerably improved. An actuator saturation model is proposed and the predicted results are considerably matched with the experimental results.

# Table of contents

# List of figures

# List of tables

# Chapter 1

# Introduction

## 1.1 Background

Cutting operations are used to remove the material from parts. The most common operations are turning, milling, drilling and grinding. Milling where a rotating tool is used to remove the material from a workpiece, is one of the most used manufacturing techniques in industry. The productivity, surface roughness and quality of parts are influenced by milling process parameters. The wrong selection of these milling parameters, such as spindle speed or depth of cut, can result in varying cutting force and chatter vibration which is a self-excited vibration. Chatter may result in low surface quality, unacceptable tolerance, machine tool damage or even breakage.

The chatter is classified as primary and secondary chatter. Since the secondary chatter mechanism, also known as regenerative chatter is mostly seen in machining operations and more detrimental, the focus of this thesis is on regenerative chatter. The basic regenerative chatter mechanism was first explained by Tobias and Fishwick [4–6], and Tlusty and Polacek [7–10]. It is induced by regeneration of waviness on the surface of the workpiece to be machined. Tobias and Fishwick [4] presented the relation between the critical limiting depth of cut and the time delay of the machining process. They described the stability pockets, the

so-called stability lobe diagram (SLD), as illustrated in Figure 1.1. The diagram shows the stability boundary as a function of spindle speed and the axial depth of cut. The productivity of a machining is proportional to the material removal rate, which is the amount of the material removed from the workpiece per second. It can be improved by selecting the cutting parameters from a stable region with a larger depth of cut at higher spindle speed in the SLD. Thus, the SLD has a critical importance to improve the productivity of a machining operation.

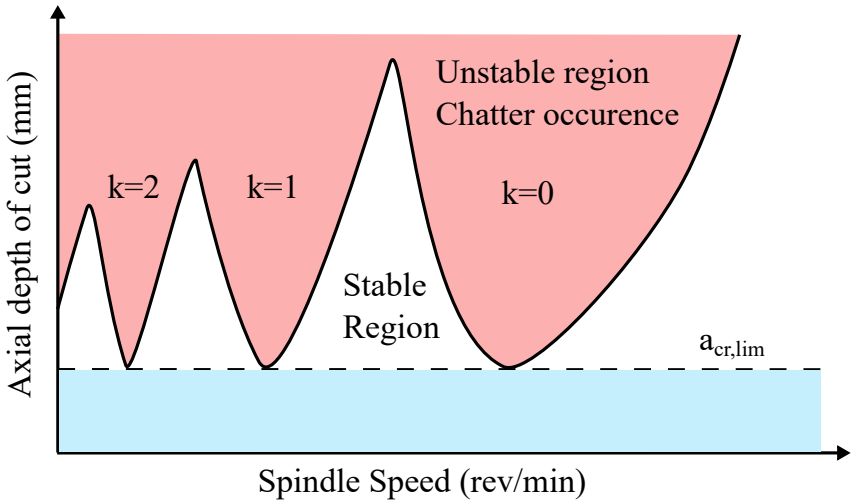


Fig. 1.1 Stability lobe diagram with red region shows the unstable/chatter region, while the blue region shows the absolute critical limiting depth of cut border for any spindle speed.

Although the method improves the productivity of the milling operation, it does not improve the stability limit. One way that this can be improved and manipulated is by changing the dynamics of the milling system through a novel method called robotic-assisted milling [11] where a robot supports the structure while it is machined by a machine tool. The concept provides a promising effect on the productivity since it increases the stiffness and damping ratio of the structure by supporting it during machining. However, the forced and chatter vibrations can still be a limiting factor for the productivity of the robotic-assisted milling. To deal with this potential problem, an active control method could be one solution. Hence, the robotic-assisted milling is extended to consider an actively controlled robot arm

to improve the chatter stability in this thesis. To the author's knowledge, the only study related to application of the active control method in robotic assisted machining is the work of Esfandi and Tsao [12]. They suggested using an industrial robotic manipulator to avoid machining vibrations for turning process of the thin walled cylindrical workpieces. However, the concept is considered for the turning operation. Hence, the investigation of the benefits of the active control method in robotic assisted milling has remained a research gap in the literature.

This thesis therefore investigates the benefits of the employing of active control methods in improving the chatter stability and critical limiting depth of cut in robotic assisted milling.

## 1.2 Motivation and objectives

The aim of the research is to explore how active vibration control can be deployed on a robot arm to support a workpiece during milling operation, to improve chatter stability. This would provide a novel and useful contribution to knowledge compared to the existing machining literature. To achieve this aim, the following objectives are defined:

1. Numerically evaluate the performance of device performance using well-established active control methods.

2. Use outcomes from (1) to specify plausible actuators and configure an experimental system.

3. Design a test system to explore the dynamic performance of the chosen actuator.

4. Elucidate challenges with the proposed configuration, such as end-effector loss-of-contact, end-effector stiffness/damping, and robot dynamic nonlinearity.

5. Validate the control performances on the chatter stability improvement and critical limiting depth of cut under real milling experiments.

6. Benchmark the performance of different control algorithms to demonstrate the practical utility of the method.

7. Validate the actuator saturation points predicted by the proposed actuator saturation model.

## 1.3 Thesis outline

The rest of the thesis is organised as follows:

Chapter 2 introduces the literature review of machining and robotic-assisted milling applications. The machining stability prediction methods are reviewed in the part of machining literature. Then, the chatter mitigation and suppression methods are presented including the passive and active control methods. In the robotic-assisted milling literature, the concept and additional support system are presented. Its applications and details are introduced including the support force and contact type.

Chapter 3 presents the theoretical background of the milling stability analysis. A basic chatter mechanism considering a single-point cutting operation is given. Then, the stability lobe diagram (SLD) is presented. Afterwards, the chatter stability analysis is extended for the milling which is an intermittent cutting operation due to a rotating cutting tool. The method is based on expanding the time-varying dynamic cutting coefficients into Fourier series to obtain averaged constant term (zeroth order) of the series. The critical limiting depth of cut $a_{cr}$ is derived for a general two-dof milling operation. Finally, the method accuracy is discussed in terms of low radial immersion and cutting force harmonics due to the cutting parameters.

Chapter 4 introduces the analysis of the concept of the robotic-assisted milling where a robot supports a flexible structure while it is machined by a machine tool to suppress and improve the regenerative chatter. Six different control methods are investigated. In order to evaluate the feasibility of the method, a proof-mass (inertial) actuator is assembled to a beam which emulates the dynamic behaviour of the robotic arm to improve the dynamic response of a flexible structure. A numerical optimisation method is used to optimise the controller gains to obtain the best performance in terms of chatter suppression. Finally, the performance of each controller is evaluated with the experimental frequency response functions (FRFs) and predicted stability lobe diagrams (SLDs) considering a milling scenario. It is shown that the concept can improve the chatter stability and also can increase the criticial limiting depth of cut significantly, comparing to the scenario where the robot has no active control applied.

In Chapter 5, an actuator saturation model is proposed. The regeneration effect is neglected in the model; only forced vibrations are taken into account. Fourier force model is utilised to predict the actuator saturation considering the type of the milling. The saturation points are determined up to the stability boundary for each control method. It is seen that the saturation predictions in frequency-domain (proposed method) match with the time-domain results. Besides, the effect of the helix angle on the saturation is presented. It is shown that the higher number of helix angle can affect the location of the saturation points and actuator force now that the forced vibrations are reduced in the controlled direction and the delay of the process is affected due to the helix angle of the cutting tool.

Chapter 6 evaluates the predicted SLDs of the robotic-assisted milling concept. The concept is first tested considering the FRF results for each control method. It is shown that the concept can effectively improve the dynamic response of the flexible structure. Close responses are obtained from the experimental FRF tests by a hammer in the machine tool. Then,

the concept is examined under the real milling conditions. The experimental results shows that the chatter stability and the critical limiting depth of cut ($b_{min}$) are considerably improved.

Chapter 7 draws conclusions and discusses the limitations and future works.

The research outcomes have been published as journal and conference papers. The active chatter control in robotic-assisted milling has been presented by Ozsoy et al. [13, 14] as a first attempt to improve stability of the robotic-assisted milling.

# Chapter 2

# Literature Review

## 2.1 Introduction

This chapter presents a literature review of machining and robotic assisted milling. In the first section of this chapter, the machining literature including the chatter, stability prediction methods, chatter avoidance and mitigation methods, is presented. In the second section, the robotic assisted milling applications and its performance are discussed.

## 2.2 Machining

### 2.2.1 Introduction

Cutting operations are used to remove the material from parts. The most common operations are turning, milling, drilling and grinding. The research studies of machining operations started in the early 19th century [15]. The early studies are to used to optimise the production by selecting the spindle speed and axial depth of cut without causing the chatter. One of the most famous research programme about machining was F. W. Taylor's research which was practical research. It was published in 1906, entitled "On the art of cutting metals"

[16]. F. W. Taylor stated that "chatter is the most obscure and delicate of all problems facing the machinist, and in the case of casting and forgings of miscellaneous shapes probably no rules and formulae can be devised which will accurately guide the machinist in taking the maximum cuts and speeds possible without producing chatter". The early studies were limited only to general explanations of the chatter, and no mathematical model or formula was expressed for the chatter occurence.

The research in the field of machining has shown rapid development in the middle of the 1940s. The chatter mechanism, which accelerated the development of the field, was expressed by Merchant [17–19]. Merchant developed the orthogonal cutting force model assuming continuous chip of Ernst [20]. Then, the tool vibration of steel cutting was investigated by Arnold [21, 22]. The research led to study on regenerative chatter mechanism by Tobias and Fishwick [4, 5, 7], and by Tlusty and Polacek [6, 8–10]. Furthermore, many researchers studied the chatter mechanism to establish accurate mathematical models. For instance, Altintas and Budak [23–26] extended the theory of regenerative chatter mechanism modelling the tool and workpiece as multi-degree-of-freedom structures. The stability model was developed expanding the periodic matrix into Fourier series. The chatter limits can be predicted accurately using the analytical model. Insperger and Stepan [27–29] developed the analytical chatter model introducing the semi-discretisation method for delayed systems. Then, Ding [30] proposed a full-discretisation algorithm for milling operation, reducing the computational time compared with the semi-discretisation method for the same discretisation step size.

Several suppression methods have been studied by researchers. They can be divided into two main groups: using the stability lobe effect and changing the system behaviour, as seen in Figure 2.1. The first group is about selecting optimum cutting parameters such as spindle speed and critical limiting depth of cut. The second one is about changing the stiffness and/or

the damping ratio of the system [31].

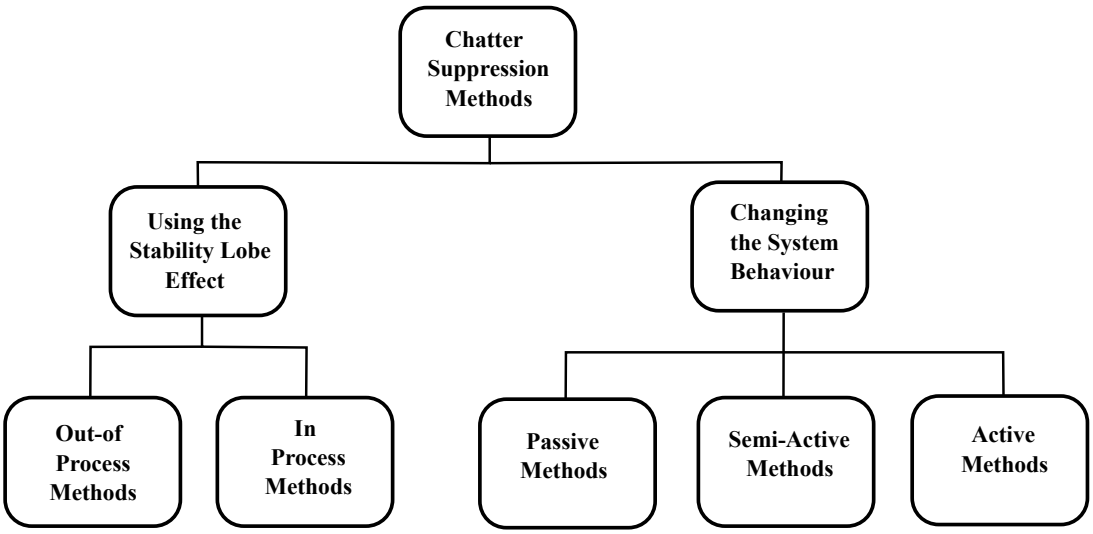


Fig. 2.1 Chatter Suppression Methods

The out-of process subcategory is related to the cutting parameters. To identify the stability lobes, the process aims to select proper cutting parameter combinations. To develop the stability lobe diagram, there are different models such as zero order approach, semi-discretisation and full-discretisation described in the literature [4, 9, 27, 29, 30, 32–37]. The dynamic properties of the system are measured by impact hammer test [38]. The out-of process method must be applied before the machining operation. The other method is to aim to avoid chatter while the machining operation is proceeding. It is called in-process chatter avoidance method. It is applied by modifying the cutting parameters as soon as chatter occurs thanks to the sensors, accelerometers and the microphone[39–54].

The second group is changing the system behaviour. The first subcategory, passive strategy, includes changing the machine tool assemblies. In order to suppress the chatter using passive strategy, the cutting tool and the tool holder can be modified or a damper can be added [55–62]. The second subcategory, semi-active strategy, acts like a passive strategy method, and can change the passive properties with an energy input. The difference between passive and semi-active method is that the passive strategy can only be applied once

to change the system behaviour, whereas the semi-active strategy's properties can be changed many times [63–67]. If the system behaviour is changed with an energy input to generate force, it is called active chatter suppression method. It supplies or absorbs the energy from the system.

In the first group, the chatter suppression methods depend on the regenerative chatter mechanism while the second group depends on structural dynamics. Thus, the chatter mechanism will be presented first. Then, the chatter suppression methods will be given.

### 2.2.2 Chatter prediction

After twenty-six years of Taylor's initial factory-based investigation on chatter, Merchant [17–19] developed the orthogonal force model considering continuous chip by Ernst [20]. Indeed, Arnold's research [21, 22] was the initial effort for the investigation of the tool vibration while cutting steel. Afterwards, Tobias and Fishwick [4], Tlusty and Polacek [6, 9, 10] studied the fundamental chatter mechanism that was the way we understand how to predict and mitigate unwanted vibrations. Tlusty and Polacek [9] showed a relation between the dynamic stiffness of the machine tool and the critical limiting depth of cut, also the relation between the force and chip thickness. Tobias and Fishwick [4] presented the relation between the critical limiting depth of cut and the time delay of the machining process. This relation brought the stability pockets, the so-called stability lobe diagram (SLD). The diagram shows the stability boundary as a function of spindle speed and the axial depth of cut. Furthermore, Merritt [68] represented the chatter theory as a feedback loop system neglecting the behaviour presented by Tobias at the lower spindle speeds, and accomplished the stability by using the Nyquist stability criterion. The behaviour at the lower spindle speeds was explained in more detail by Kegg [69]. Kegg explained the rubbing effect between the wavy surface of the workpiece and cutting tool at lower spindle speeds, known as process damping. According to Merritt's model, a milling model was formulated with two degrees of freedom by Sridhar

et. al. [70, 71]. The force coefficients were time-periodic due to the cutting tool rotation in milling. A stability algorithm that allowed a more realistic model, was applied to a milling process using a digital computer. Some researchers utilised an average directional cutting coefficient value [72] and time-averaged directional force coefficient values [73, 74] in order to obtain fast stability analysis. Yet, the stability diagrams showed that the accuracy of the stability analysis was inaccurate in milling operations [75].

Time domain models can analyse the nonlinearities such as loss of contact between the tool and workpiece, and the process damping in machining process [76–80]. However, they require simulation that can be computationally intensive and time consuming. An analytical solution had been studied by Minis and Yanushevsky [81]. They applied Floquet's theorem to Sridhar's model [70] for the stability analysis of the two degree of freedom milling model. Nevertheless, they used the numerical evaluation for the characteristic equation. Then, Budak and Altintas [23–26] developed an analytical model called the zero order approximation (ZOA) by expanding the periodic matrix into Fourier series. The model was updated by Altintas [25] for the three dimensional milling operations. The model offered an accurate and fast solution for the cutting with high immersion. At high speeds with low immersion, additional lobes due to the period doubling bifurcations were explored by some researchers [82–85]. The ZOA model could not predict these additional lobes since the model only considered the constant term of the Fourier expansion. Many Fourier terms were needed to analyse the stability lobes accurately as the several harmonics occurs at high intermittent cutting operations. Insperger and Stepan [27–29] developed the semi-discretization method (SDM) to predict the additional lobes which occur at high speeds with a very low radial immersion. They updated the method [86] to investigate different orders of the semi-discretization method. It was shown that the first order term provided better convergence than the second and higher order approximations. Also, the effectiveness of the SDM has been proved for the unstable islands

[60], as well as variable helix and pitch milling tools [62, 87]. Yet, the method requires more computational effort. The stability analysis in frequency domain was established by Merdol and Altintas [88]. They extended the ZOA to the multi-frequency approach (MFA) to predict the additional lobes at high speed cutting with a small radial depth of cut. Bachrathy and Stepan [89] extended the MFA model considering the general tool geometries. Moreover, a full-discretization method (FDM) was proposed by Ding [30] to reduce the consumed time for the SDM without any loss of numerical precision.

There have been efforts to find an accurate model to predict the stability of machining process. An accurate mode can provide the chatter mitigation. It can be simply done selecting the spindle speed and depth of cut from the predicted SLD. All the mentioned chatter prediction models can be evaluated as out-of process method. Alternatively, the chatter can be avoided by changing the spindle speed and depth of cut during the machining operation. It is called as in-process method, these parameters can be set in the moment chatter occurs. The details of the method are explained in the next subsection.

### 2.2.3 In-process methods

The chatter can be detected thanks to the sensors, accelerometers and microphones [40–54]. Yet, the method may result in detrimental effects such as tool breakage and surface roughness as the parameters are set just after the chatter occurence. For instance, Smith and Tlusty [90] presented the changing spindle speed effect on stability in high-speed milling. The chatter was detected using Fast Fourier Transform (FFT) of the sound pressure during the operation. Then, the operation was stopped and the spindle speed was adjusted according to the chatter frequency [91, 92]. This method provided the spindle speed setting without knowledge of dominant natural frequency in the industry. The model also extended to a wide tange of spindle speed selection [93, 94]. Some researchers proposed the variable spindle speed by

disturbing the chatter mechanism. Sexton and Stone [95] presented the variable spindle speed effect in turning. However, changing the spindle speed continuously caused poor surface finish. Sastry et al. [44] extended the model to milling operation using time-varying cutting force coefficients.

The variable spindle speed effect was also investigated by using the semi-discretisation method (SDM) [41, 45, 96, 97]. SDM [27] was proven for the constant spindle speed to obtain the additional lobes due to the bifurcations. It was shown that the utilising continuous spindle speed variable was successfully verified by experiments. Furthermore, different form of spindle speed variations such as sinusoidal [96, 98–100], rectangular [95], triangular [45, 96, 101], and random [46] were tested. The sinusoidal variation was the most successful one to suppress the chatter vibrations. Moreover, Al-Regib et al. [43] proposed an automatic spindle speed variation based on for minimum energy input. Nonetheless, the model did not take into account the machine limitations. The optimum criteria of the model was very high and beyond the allowable range for the current spindle-drive systems at high spindle speeds. In the allowable range, the effectiveness of the method was experimentally verified.

With reference to Figure 2.1, the second chatter suppression group is changing the system behaviour. The details of the group are explained in the following sections.

### 2.2.4 Passive methods

The first subcategory, passive strategy, includes changing the machine tool assemblies. In order to suppress the chatter using passive strategy, the cutting tool and the tool holder can be modified or a damper can be added. One of the most used passive devices is the tuned mass damper (TMD). For instance, Kato et al. [102] applied the TMD using Lanchester damper for the boring operation. The chatter improvement was verified by experiments. The impact and friction dampers were also investigated by some researchers [103–107]. The damping

of the machining system was increased using the impact and friction dampers. Seto and Tominari [108] utilised the variable stiffness for the TMD method. The experiments showed that the critical limiting depth of cut was increased considerably. The TMD was investigated in milling by Liu and Rouch [109]. The optimal parameters were found numerically. To obtain the best performance from the TMD, tuning the parameters is important. Den Hartog's method [55] was firstly used tuning method in machining. However, the critical limiting depth of cut is inversely proportional to the negative real part of the FRF [4, 9]. Using this knowledge, Sims [62] proposed an analytical tuning method based on equal real part peaks. It was shown that the Sims tuning method improved the stability performance by 40-50% compared to Den Hartog's method. TMD method was also investigated for the multiple and nonlinear TMDs. Yang et al. [110] used multiple TMDs for the turning operation. The performance of the using multiple TMDs was more compared to the single TMD usage. Nakano et al. [111] applied the multiple TMDs to the milling operation. Using multiple TMDs in milling was verified successfully. In addition, the nonlinear TMDs [112–114] were also employed in machining.

Instead of using TMD, the other damping element, viscoelastic dampers have also been studied. Kim and Ha [115] presented a viscoelastic damper tuned by Den Hartog's method. The damper was assembled to the tool holder and obtained successful results in turning. Rashid and Nicolescu [116] applied the viscoelastic damper to reduce the vibrations in milling. Saffury and Altus [117] investigated the tuning of the viscoelastic cantilever beam parameters regards to the real part of the FRF. They concluded that the viscoelastic damper had some advantages comparing to TMD. As an alternative passive control device, eddy current dampers [118–120], were investigated for thin-walled structure machining. It was reported that the damper was effective for the dynamic properties change due to the material removal, unlike TMD. One of the other methods is increasing the damping of the machining

system using a viscous fluid [121, 122]. The machining system was submerged into a tank filled with a viscous fluid. It was shown that the cutting force coefficients was significantly decreased owing to the lubrication effect of the viscous fluid. Also, the noise of the milling operation was reduced thanks to the isolated environment.

Supporting flexible structures can increase their chatter stability. Fei et al. [123] proposed a moving damper to increase the chatter stability. The damper moves along with the milling tool to support the flexible structure. However, as the moving damper is fixed to the machine itself, it can be used only for a particular workpiece. The authors also investigated the deformation model for the moving fixture [124]. The results showed that it improved surface quality and decreased machining errors due to vibrations. The passive control devices can also be used to support the fixtures. Munoa et al. [125] presented a tuneable clamping table with adjustable stiffness for milling operations. It was shown that the stability was increased by using the clamping table. Wan et al. [126] applied tensile prestress to the structure to improve the chatter stability. The stress was utilised according to the finite element simulations to indicate the stress level. The method was experimentally verified by comparing without prestress results in milling operation.

The special tool geometries can also be used to improve the chatter stability. Variable helix and variable pitch tools are employed to suppress the regenerative mechanism by disturbing the delay between consecutive cuts. Variable pitch angle was presented by Hanh [127] to suppress the chatter vibrations. It was reported that selecting random pitch angles does not guarantee the stability improvement. Hence, the tool geometry optimisation is required to obtain the best performance from the irregular tools [128, 129]. For example, Altintas et al. [130] adopted ZOA taking into account the tools with variable pitch angles. Budak [131, 132] developed an analytical method to optimise the pitch angles considering

the chatter frequency. Sims et al. [62] presented semi-analytical stability prediction for irregular tools.

The variable helix tools have been researched to improve the chatter stability. Turner et al. [133] introduced an analytical prediction for helix angle variation. The tools have variable pitch angles were compared with the tools have variable helix angles experimentally. A better performance was achieved with variable helix tools in experiments. Sims [134] proposed alternative MFA using harmonic transfer function approach. Also, Yusoff and Sims [135] optimised the variable helix angles utilising differential evolution algorithm to the SDM. The special tools are one of the cost-effective ways implemented in the industry. For both special tools, an optimisation is required to achieve the optimum pitch and/or helix angles to improve the chatter stability considerably.

### 2.2.5 Semi-active methods

The second subcategory, semi-active strategy acts like a passive strategy method, and can change the passive properties with an energy input. The difference between passive and semi-active methods is that for the passive strategy can be applied only once to change the system behaviour, but for semi-active strategy the passive properties can be changed many times [63–67]. If the system behaviour is changed with an energy input to generate force, it is called active chatter suppression method. It supplies or absorbs the energy from the system. As an example of semi-active control method, Munoa et al. [64, 125] proposed a clamping table with rotary spring to change the natural frequency of the system. The experiments were carried out to verify the clamping mechanism in heavy-duty milling operations. It was shown that the clamping mechanism increased the performance of the stability. Besides, smart fluids such as Magnetorheological (MR) and Electrorheological (ER) fluids are also studied for the machining stability. Applying an electric or magnetic field improves the dynamic properties of the machining system. For instance, Lei [136] , and Aoyama and Inasaki [137]

used ER damper to increase the chatter stability in milling. Wang and Fei [138] also utilised the ER fluid in turning operation. Although ER and MR fluids have similar viscosity while non-active state, MR fluids have higher yield strength than ER fluids. Also, MR fluids require low voltage and high current power. Hence, MR fluids were applied by some researchers [139–142]. Batterbee and Sims [143] investigated the performance of MR dampers considering the temperature variation. Their model was validated by experimental data according to the temperature variation. The smart fluids were also studied using a varying magnetic or electric field. The performance of sinusoidal waves for the ER fluid research was the better as reported by Segalman [144]. Mei et al. [145, 146] conducted a comparison research in terms of waveforms using MR fluids for a boring operation. Their conclusion was the square waveform had a better performance than the sinusoidal and triangular waveforms.

In the following section, active chatter strategies will be explained in more detail.

### 2.2.6 Active control methods

An active strategy is based on supplying or absorbing energy from the system to suppress the chatter by measurement of system vibration value by means of sensors. Actuators can be used to change the system's natural frequency and damping ratio.

Earlier active chatter control researches were applied for boring operations. Klein and Nachtigal [147, 148] presented an active control scheme to improve the boring bar performance. The boring bar was controlled by an electrohydraulic servo system. The experimental results showed that the critical limiting depth of cut was significantly improved. Yet, they concluded that the performance of the active vibration control was dependant on the knowledge of the principal modes and cutting force angle. Glaser and Nachtigal [149] conducted a research using a special boring bar with two hydraulic chambers for the actuation system.

A pressure difference between two hyraulic chambers was used to control the tool tip motion. Nevertheless, the chatter control performance was not improved as modelled since the controller and measurement system were not properly selected. Furthermore, Tewani et al. [150] utilised active chatter control by using piezoelectric actuator in boring operation. Comparison experiments were carried out to obtain the performance differences between the active and passive absorber. The results showed that using active dynamic absorbers provided considerably improvements in boring operation. Similarly, Tanaka et al. [151] proposed an active damping system for slender boring bar using a piezoelectric actuator. The direct velocity feedback (DVF) control strategy was implemented for chatter suppression. Besides, actuator locations for chatter suppression were investigated. Pratt and Nayfeh [152] developed a nonlinear model for slender boring bars using a biaxial magnetostrictive actuator.

Fallah and Imani [153] proposed a new adaptive chatter control system in boring operation. A shaker was utilised as the actuation system to control the vibration of a boring bar. Proportional integral derivative (PID) and direct velocity feedback (DVF) control methods were compared in terms of frequency response function (FRF) improvement. Since DVF control presented a better performance in terms of improving the dynamic stiffness of the boring bar by a factor of 20, the adaptive control algorithm was proposed using DVF control considering the actuation cost of the control system and intensity of vibrations. To stabilize the unwanted signals, a low-pass filter was applied to the integrated signal. Once the minimum and maximum control gains were indicated by the proposed adaptive control algorithm, several experimental tests were conducted for an aluminium alloy (6063-T6) for the verification. The chatter vibrations were significantly reduced by the proposed control system providing significant improvement of the critical limiting depth of cut by a factor of 10. Indeed, the surface roughness of the machined part was also reduced by a factor of 7 for

the industrial application.

Although piezoelectric and electromagnetic actuators have a good performance on chatter stability improvement in turning/boring, a new type of actuators are also investigated in boring operation [154]. For instance, Chen et al. [155, 156] presented a novel magnetic actuator design which can reduce the vibration in two radial and torsional directions for a boring operation. The design consists of four magnetic units with a permanent magnet, two excitation coils, stators, and an armature core. Fiber optic sensors were used to measure the chatter vibrations. To reduce the heat generation and eliminate the eddy current in the actuator, a soft magnetic material, Samoloy 500 was selected. Finite element method (FEM) was performed in order to detect the nonlinearities such as magnetic saturation and flux leakage. The cutting test results showed that the proposed magnetic actuator considerably reduced the chatter vibrations.

The active regenerative chatter control was also applied in milling operations. For instance, Chung et al. [157] presented an active damper design for a spindle unit in milling. The damping system used an electromagnetic actuator. Authors targeted some structural modes to damp, as the tool modes could not be damped due to the lack of the access to location. Predicted and measured stability limits were found to disagree slightly due to the nonlinearity of the actuator when implemented near the limits of its bandwidth. Also, Munoa et al. [158] developed a biaxial active actuator. In experiments, one and two axis actuators were compared, and two axis actuators provided more accurate machining by improving the stability of the system. In spite of this, since the biaxial actuator was controlled in two orthogonal directions, more space was needed to provide required high actuation forces. Different control laws which were direct acceleration feedback control, direct velocity feedback control, direct position feedback control, and delayed position feedback control, were

compared for active chatter vibration control. However, in order to compare the control laws, an actuation force limit was introduced. Optimal gain was applied for each control system, and the direct velocity feedback control was the most effective control strategy for chatter suppression. Yet, as the spindle speed increased, the DVF control system outcome reduced. Monnin et al. [159, 160] presented an active control system integrated into a spindle unit to suppress the chatter vibrations in milling. Two optimal control designs, which were considering only the structure modes of the machine and overall close-loop system for the machining system, were compared. Four piezoelectric stack actuators were mounted to the spindle unit with equal spacing. They reported that the active control system provided more than 50% improvement for the critical limiting depth of cut using disturbance rejection. The piezoelectric stack actuators integrated to a spindle unit were also investigated utilising different control methods, adaptive control [161, 162], model-predictive control [163], $H_\infty$ [164, 165], and a robust control [166, 167].

Zhang and Sims [168] investigated a piezoelectric patch actuator for active damping strategy in milling. A series of experiments was performed and the results showed that the critical depth of cut was increased by using a piezoelectric actuator with a positive position feedback control strategy. Despite this, for a specific region of the stability lobe diagram, bonding of the actuator (with glue) was degraded. This resulted in less performance of the actuator and the stability limit was decreased. Using the piezoelectric patch actuator can be a problem in terms of mounting issues. They reported that one of the problems was that the actuator must be sealed to protect it from coolant. Also, the controller performance was corrupted due to the actuator saturation in many tests.

Active magnetic bearing (AMB) systems [162, 169–173] are also applied for the chatter stability improvement. For instance, Knospe [174] designed an active magnetic bearing

system for the spindle. In experiments, it was seen that the stiffness of the system had been increased significantly. Multivariable controllers were developed utilising $\mu$-synthesis. In experiments, a 40% reduction in compliance was obtained. As control strategies, PID and $\mu$-synthesis were applied and $\mu$-synthesis had better performance than the PID control system for active magnetic bearing. Even though active magnetic bearings are a promising technology, there are some technical problems such as low specific load, low bandwidth and complexity of the spindle dynamics which should be overcome for future applications.

There are also another control methods presented to improve the chatter stability. Huyanan and Sims [175] presented three control methods, the skyhook controller (DVF), the virtual passive absorber (VPA), and the virtual active tuned mass damper (VATMD). A proof-mass actuator was attached to the workpiece to reduce the vibrations. The FRF results showed that the virtual passive absorber had better performance since it was not affected by the measurement noise. The cutting tests were presented using the virtual passive absorber method tuned by Sims method [176]. Due to the material removal effect, the dynamic properties of the structure were changed, which caused stability degradation. To overcome this problem, automatically tuned actuators were examined. Beudaert et al. [177] developed a portable inertial actuator which can tune the controller parameters automatically for specifically flexible structures. Frequency domain was employed for the auto-tuning algorithm. Experimental and industry tests showed that the portable active damping device improved the dynamic properties of the flexible structure. They concluded that the portable damper can be successfully attached to different flexible structures instead of designing new fixtures or complex supporting units. Also, Zaeh et al. [178] presented an automatically tuned inertial actuator to suppress the machining vibration. In order to improve the stability, direct velocity feedback (DVF) and $H_\infty$ control methods were applied. An automatic tuning methodology was presented considering the actuator saturation. They reported that the critical limiting

depth of cut was increased around 50-60% experimentally. Moreover, Kleinwort et al. [179] proposed a new automatic tuning method for the active vibration control. The method uses particle swarm optimisation to obtain a robust controller. The comparison cutting tests were carried out for DVF, $H_\infty$ and a novel adaptive FxLMS control presented earlier in [180]. All control methods considerably improved the chatter stability according to the experimental results. The best performance was achieved by $H_\infty$ control method in terms of the critical limiting depth of cut by the factor of 2.3.

The new machine tool feed drive system is also presented as an alternative active control solution to mitigate the chatter [181–185]. Alter and Tsao [186, 187] presented improvement of stability using an actively controlled linear motor feed drive for turning processes. They implemented a proportional-derivative (PD) and $H_\infty$ controllers. It was shown that $H_\infty$ controller had a promising performance on the chatter stability in turning. Munoa et al. [188] developed stability limits using the rack and pinion drive system, and external accelerometers that were located at ram, for heavy duty milling operation. Not only the targeted modes but also the other modes were suppressed with the actuator. It was reported that the proposed chatter control system improved the stability significantly.

Researchers [189–194] have investigated the suppression methods of chatter vibrations by designing an active workpiece holder. For example, Mohring et al. [195] designed two different designs as clamping setups and intelligent fixtures. In experiments, different intelligent fixtures are used for thin walled structures and large thin walled structures. Thanks to sensors and actuators, deformations and the critical positioning problems have radically been overcome. Also, finite element analysis is employed for the improvement of active fixtures. The results showed that clamping issue and intelligent fixtures have significantly contributed to reduce machining operation vibrations. Brecher and Schulz [196] presented an active

system based on electrohydraulic actuator that can generate higher forces. The vibration measurement was provided by an accelerometer which was based on velocity feedback control. The authors used the electrohydraulic actuator to improve the dynamic flexibility of the machine table since larger damper masses are needed for the desired improvement. They concluded that dynamic flexibility was considerably improved experimentally.

Dynamic properties of the machining system change due to the material removal during the machining. Also, the control systems may degrade or provide less performance due to the uncertainties such as actuator saturation, limiting bandwidth, cutting parameters, and machine tool itself. Therefore, more robust control systems are required for the machining operations. Several researches have been conducted recently [159, 160, 166, 170, 171, 197]. For instance, Van Dijk et al. [198, 199] presented a robust active control system considering the uncertainties such as spindle speed, and depth of cut in high-speed milling operations.

Robots have been used in many machining applications such as drilling, trimming, deburring, and milling recently [200]. However, they tend to vibrate more than CNC machine tools during machining. There have been researches to improve the chatter stability during robotic milling. For instance, Nguyen et al. [201] presented an active vibration suppression in robotic milling using optimal control. They analysed the dynamic properties of the robot according to the robot's pose by Gaussian Process Regression (GPR), and proposed linear quadratic regulator (LQR) control method considering the robot's position. The controller provided 50% vibration suppression of milling vibration amplitudes. Wang et al. [202] proposed a force control-based vibration suppression in robotic grinding of large thin-wal shells. The vibration suppression mechanism was validated by hammer tests and finite element method (FEM) simulations. Experimental results showed that the vibration was suppressed by around 75% in stable grinding. Morever, the surface roughness was also decreased by a factor of

3.2. The industrial robots have also been used for high speed machining operations. Sornmo et al. [203] used an industrial robot to suppress the vibrations during high speed milling using a piezo-actuated compensation mechanism. The actuator position was controlled by PID controller while the micro manipulator position was controlled by linear quadratic gaussian (LQG) controller. It was shown that the workpiece surface roughness was improved significantly. Wang et al. [204] proposed an active vibration control using a voice coil for robotic machining. Once the eccentric mass experiments were conducted successfully, they showed the vibration suppression improvement by 25% during milling.

Robots have also been utilised for the thin-walled structure milling [205–207]. Zhu et al. [208] proposed an intelligent machining system in robotic grinding of complex components such as aviation parts. They concentrated on geometrical accuracy, high precision online measurement, and constant contact force control. The applications of robotic grinding of turbine blades and large-scale complex structures are discussed. They suggested more intelligent and efficient solutions for robotic grinding operation. The path planning is also considered by researchers. Zhou et al. [209] used a robot for grinding of large flexible workpiece taking into account the tool path planning. In order to avoid the fluctuation of the cutting force, a time-varying isobaric surface (TVIS) was defined. An automatic method was proposed to calculate the TVIS considering the contact trials. The proposed method was verified experimentally. It was shown that the proposed method could provide stable cutting force. Susemihl et al. [210] developed a mobile robotic system in large component machining. They presented an approach of stereo camera based on the position of robot which can open new possibilities of improving the real time processing. It was shown that the developed mobile robotic system offers an automated and efficient application for large-scale components machining. Hao et al. [211] demonstrated the stability predictions based on ZOA in robotic milling of aluminum. As the robot's dynamic behaviour is shifted greatly during

the operation according to its pose, the effectiveness of ZOA was still under investigation. However, the authors showed that the ZOA can also predict the stability boundaries by conducting several experiments in robotic milling. They also highlighted the low-frequency modes from the robot's structure to show the low-frequency modes have contribution to the error prediction.

To summarise, active control methods are based on supplying or absorbing energy from the system to suppress chatter by measurement of system vibrations by means of sensors. Actuators can be used to change system's natural frequency and damping ratio. Active chatter control can remarkably enhance the damping ratio and suppress the vibrations when the method is applied with the optimum parameters. Otherwise, active control may unstabilise system. As an active control system, direct velocity feedback (DVF), virtual passive absorber (VPA, proportional integral derivative (PID), linear quadratic regulator (LQR), $\mu$-synthesis and $H_\infty$ etc. control systems are implemented by several researchers to improve the chatter stability.

A novel method called robotic-assisted milling [11] where a robot supports the structure while it is machined by a machine tool, provides a promising effect on the productivity since it increases the stiffness and damping ratio of the structure by supporting it during machining. However, the forced and chatter vibrations can still be a limiting factor for the productivity of the robotic-assisted milling. To deal with this potential problem, an active control method can be a solution. Hence, the robotic-assisted milling is extended to consider an actively controlled robot arm to improve the chatter stability in this thesis. In the next section, the robotic-assisted milling will be explained in more detail.

## 2.3 Robotic-assisted milling

### 2.3.1 Introduction

Robots have been used in many machining applications such as drilling, trimming, deburring, and milling recently. Also, they can be attached to a machining system as a moving or fixed support to improve the chatter stability while the workpiece is machined by a machine tool. In this section, a novel machining method which is called robotic-assisted machining will be presented. The robots are used to support the workpiece as a damper, which could be fixed or moving. Especially for aerospace parts and thin-walled structures, the method will be used in large scales in the next decades [212]. The recent robotic-assisted milling applications will be discussed in the following section.

### 2.3.2 Applications

The idea of supporting the thin-walled structure has already been applied to improve dynamic properties of the structures.

During the machining of large flexible workpieces, as the workpiece's stiffness is quite low, vibrations may lead to surface roughness problems. Researchers [123, 213, 214] have tried to overcome this problem by adding more fixed supports or a moving support from the backside of workpiece. For instance, Fei et al. [123] presented a moving damper to increase stability of a process. An auxiliary device was designed as a damper which moves with cutting tool at the same velocity. The frequency response function (FRF) was compared with and without the damper. The results showed that the stability of the process improved significantly. Also, the experimental cutting tests were implemented employing a displacement sensor in order to collect vibration data from the workpiece. However, as the moving damper are fixed to the machine itself, it can be used for only a particular workpiece. Indeed, the vibration of the machine itself may affect the auxiliary device, which can result

in less stable machining operation. Authors also investigated the deformation model for the moving fixture [124] by applying thin-walled shell theory. The predicted results matched with the experimental results. Besides, the moving damper improved the surface quality and decreased form errors due to vibrations.

Ozturk et al. [11] presented a new concept called robotic assisted milling of thin-walled structures. Using a robot for supporting a workpiece provides flexibility and reconfigurability to improve stability of a milling process. Researchers used two types of end effectors which were soft rubber roller and metal castor, to support the workpiece from the back surface. The FRF of the supported system was tested when a Staubli TX90 robotic arm is equipped with a soft rubber roller onto the flexible workpiece. Three different supporting forces were implemented to three points on the workpiece. The support force applied for the machining test was selected considering the FRF results to avoid any excessive loading. The experimental validation results showed that the surface roughness decreased considerably by using a moving support behind the workpiece. Yet, as it is mentioned in the paper, the process was monitored, not controlled. As the stiffness of the workpiece changed due to the material removal, the support force varied during the operation. The contact between the rubber roller and workpiece was affected by the flexibility change along the workpiece. Furthermore, the velocity difference between the cutting tool and rubber roller may have played role on the supporting force.

Sun et al. [215] examined the form error prediction in robotic assisted milling. The error prediction models were introduced using the static deflection, frequency domain and hybrid modelling. They concluded that the hybrid model provided relatively acceptable results with the experimental results. Moreover, effect of the supporting force on the dynamic response of the structure was presented experimentally.

Bo et al. [216] examined the effect of the supporting force using a moving support on machining stability during milling operation of a thin-walled structure. Supporting forces

affect not only the machining stability but also the dynamic behaviour of the workpiece. The machining stability was predicted using full-discretization method. Several hammer test experiments were applied to find the FRF of the structure applying supporting forces from 80 N to 600 N. The most effective force value was determined for the greatest critical limiting the depth of cut. The predicted SLD showed that the critical limiting depth of cut increases until 320 N, as the supporting force increased. Between 320 N and 600 N, there were no significant changes for the critical limiting depth of cut. Verification experiments were done and the results showed that the effective supporting force which been found in the hammer test, maintained a stable cut avoiding excessive deflections on the flexible structure. The researchers also studied the multi support effect [217] and the optimisation of the support location [218]. They concluded that as the number of supports increases, the improvement of the dynamic behaviour increases. Moreover, the profile error was investigated by changing the support location. The surface topography prediction [219] was also examined considering the different support locations.

The real-time compensation of the flexible structure vibration was presented by researchers [220–222]. For instance, Wang et al. [221] studied an approach to compensate deflections in real-time using a laser displacement sensor. The real-time compensation system consists of a machine tool and a supporting manipulator located to other side of the thin-walled structure. The laser sensor which is mounted on the supporting head measures the deflections on the workpiece. Using this data, the position of the cutting tool is adjusted in real-time to provide the targeted axial depth of cut. To minimise the wall thickness errors, the axial depth of cut is adjusted in real-time as a compensation system. The experimental results showed that the proposed real-time compensation system provided an effective compensation system in flexible structure milling.

Recently, collaborative robots have been studied in milling [223–227]. Xiao et al. presented a supporting head and a milling tool which are assembled to collaborative robots. To

maintain a constant wall thickness during milling, the supporting robot follows the milling cutter position from the other side of the structure. They concluded that collaborative robots can minimise the form errors during milling. However, the integration and communication of the robots must be examined to be able to get a stable machining operation and supporting force. The effect of the multi support was presented by Xiao et al. [228] using collaborative robots. The simulation results showed that using multi support has better performance than the single support. As the supporting force is closer to milling force, amplitude of vibration decreases according to simulations. Furthermore, the experimental tests were carried out to verify the simulation results. Using the multi supports provided significantly improved surface quality in milling flexible structure.

Esfandi and Tsao [12] suggested using an industrial robotic manipulator to avoid machining vibrations for turning process of the thin walled cylindrical workpieces. The results encouraged using the manipulator as it provides higher cutting stiffness. Two methods were suggested in the paper. The first one is controlling the force of actuator generated against to robot structure and the other one is the force of actuator is generated against to an added mass. The authors used the first method. The results demonstrated that the control system has significant effect on chatter avoidance, final shape of the part and the surface finish of the workpiece.

Artificial intelligence methods [229, 230] have been applied to the path planning in milling using a moving damper. Also, the machine learning methods [231] have been presented to identify the chatter in milling of the thin walled structure using a moving supporting head.

## 2.4 Summary

The research on chatter has started more than a hundred years ago by Taylor. The aim of the research is to increase the productivity and quality of the machining process. The stability

prediction is an important tool to mitigate chatter. The zero-order approach (ZOA) provides a fast and accurate prediction with high radial immersion cut as an out-of process method. A chatter prediction method is developed for the prediction of the additional lobes which occur at high spindle speeds with a very low radial immersion cut. It is called semi-discretisation method (SDM). However, the method is a complex and time consuming solution which is not preferable for the industrial application. To overcome this, the ZOA method can be extended to a multi-frequency approach (MFA), in order to predict these additional lobes in the frequency domain. By establishing the chatter theory, the chatter suppression methods have been studied by several researchers. All chatter prediction methods are utilised to select the optimum cutting parameters which are the limiting depth of cut and spindle speed using stability lobe diagram (SLD) before the cutting operation as an out-of process method. Alternatively, changing the cutting parameters during the machining can be used to avoid chatter. It is called in-process method which requires chatter detection using the sensors during the machining. Collected data by the sensors are processed to detect the chatter. Nevertheless, the method may cause tool breakage and surface roughness since it is applied in the moment of chatter occurence. Implementing the passive, semi-active and active control methods can also improve the chatter stability by changing the system's dynamic behaviour. In order to suppress the chatter using passive strategy, cutting tool and tool holder can be modified or a damper can be added. Yet, the method may be degraded due to the dynamic properties of the structure change during the machining. The semi-active strategy acts like passive strategy method, and can change the passive properties with an energy input. The difference between passive and semi-active method is that for the passive strategy can only be applied once to change the system's behaviour, but for semi-active strategy the passive properties can be changed many times. However, the semi-active method parameters cannot be adjusted during the machining. Hence, the active control methods provide a better performance since the controller parameters can be adjusted during the machining. The method requires additional

equipments such as an actuator, signal conditioner, sensors, and amplifier.

Robots have been studied in machining recently, since they provide flexibility, improved dynamic response of thin structures, and dexterousness. Robots can be used either as a moving or fixed support to improve the stability of machining system. They provide additional damping to improve the stability of the machining system, as well as quality of the structure. However, the forced and chatter vibrations are still a limiting factor in robotic-assisted milling. To address this problem, researchers have applied some methods such as using multi-supports, controlling the support force, planning/optimising the tool path, and using real-time vibration compensation. Although the mentioned methods can increase the productivity of the robotic-assisted milling, the dynamic milling forces and uncertainty of the machining system can be still potential problems. As the robot moves, its dynamic properties change along the support path. Also, the material removal affects the stiffness and damping ratio of the flexible structure. To deal with these potential problems, active control can be a solution.

The investigation of the benefits of the active control method in robotic assisted milling has remained a research gap in the literature. This thesis therefore investigates the benefits of employing active control methods to improve the chatter stability and critical limiting depth of cut in robotic assisted milling. The aim of the research is to explore how active vibration control can be deployed on a robot arm to support a workpiece during milling operation, to improve chatter stability. This would provide a novel and useful contribution to knowledge compared to the existing machining literature. Six standard active control methods have been implemented for this concept. To predict the stability boundaries, the ZOA method is used for each selected control methods. A numerical optimisation method is utilised to obtain the best performance from controllers. The concept has been validated under real cutting

conditions. The results show that the actively controlled robot arm can significantly improve chatter stability and productivity in robotic assisted milling.

The concept of the actively controlled robot arm will be given in detail in the next chapters of this thesis.

# Chapter 3

# Theoretical Background

## 3.1 Introduction

This chapter presents the theoretical background of machining stability analysis. In Section 3.2, a basic chatter mechanism established by Tobias and Fishwick [4], and Tlusty an Polacek [10] is given considering a single-point cutting operation. The stability lobe diagram concept is also given in this subsection. Section 3.3 shows the milling operation analysis extended by Budak and Altintas [24, 26] using the zero order approach (ZOA). The approach is an analytical model involving the Fourier expansion. The details of the model are presented for two-dof system in this subsection.

## 3.2 Regenerative Chatter Mechanism

The regenerative chatter is a self-excited vibration due to a phase difference caused by waviness of workpiece surface. Depending on the phase difference between two waves, the chip thickness may grow for each cut. The growing chip thickness results in higher cutting forces. Consequently, the amplitude of vibration grows continuously for each pass and the regeneration mechanism causes chatter. The regenerative chatter mechanism was establised

by Tobias and Fishwick [4], and Tlusty and Polacek [10]. Here, it is expained with a turning example that is a single-point cut operation.

The schematic view of the turning operation is shown in Figure 3.1. The rigid workpiece rotates towards a flexible cutting tool. The tool is flexible in the $y$ direction while the $x$ direction is assumed as rigid direction. Assuming an orthogonal cutting operation, the cutting tool generates forces in two directions: tangential cutting force, $F_t$ and normal cutting force, $F_n$, resulting force $F_c$. Assuming the forces are proportinal to cutting coefficient and chip area [232], the force $F_n$ in time domain, which affects the regeneration mechanism, can be written as:

$$F_c(t)\cos(\beta) = F_n(t) = K_n a h(t) \tag{3.1}$$

where $K_n$ is the cutting coefficient in normal direction with in unit $N/m^2$, it is identified for the $y$ direction. $\beta$ is the force angle between $F_c$ and $F_n$. The chip area is multiplication of the chip thickness $h(t)$ and the axial depth of cut $a$. The chip thickness varies due to the phase shift between waves. The instantaneous chip thickness can be written as:

$$h(t) = h_0 + (y(t-\tau) - y(t)) \tag{3.2}$$

where $y(t)$ is the vibration of the tool in current cut whilst $y(t-\tau)$ is the vibration of the previous cut with the time delay $\tau$ due to the rotation of the workpiece.

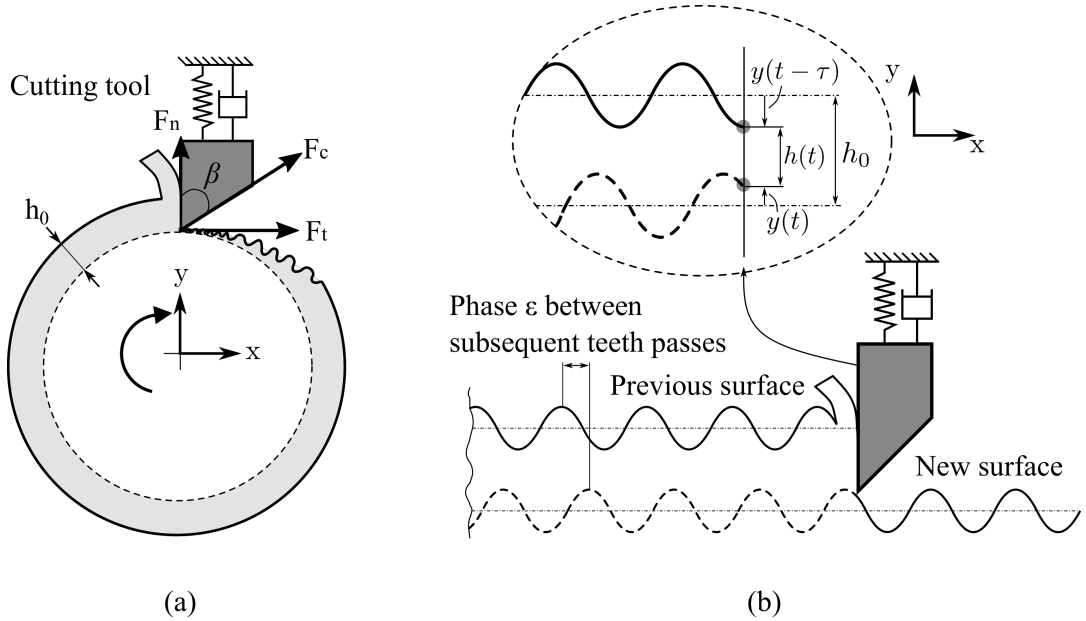


Fig. 3.1 Schematic representation of turning. (a) A single-point of cutting, (b) Phase shift effect on chip thickness

The chatter mechanism can be represented by the block diagram shown in Figure 3.2a in the frequency domain. The vibration of the tool can be written in the frequency domain:

$$Y(s) = F(s)G(s) \tag{3.3}$$

where $F(s)$ is the cutting force and $G(s)$ is the transfer function of the system in Laplace domain. $F(s)$ can be written as:

$$F(s) = K_c a H(s) \tag{3.4}$$

where $K_c$ is the cutting coefficient with in unit $N/m^2$, it is identified for each direction. The dynamic chip thickness in Equation 3.2 can be written in Laplace domain:

$$H(s) = H_0 + (e^{-s\tau} - 1)Y(s) \tag{3.5}$$

Substituting Equation 3.3 to Equation 3.5 yields:

$$H(s) = H_0 + (e^{-s\tau} - 1)K_c a H(s)G(s) \tag{3.6}$$

Using Equation 3.6, the relation between the desired chip thickness and the dynamic chip thickness can be rearranged as:

$$\frac{H(s)}{H_0} = \frac{1}{1 + (1 - e^{-s\tau})K_c a G(s)} \tag{3.7}$$

The stability of Equation 3.7 (a closed-loop transfer function) can be determined by its characteristic equation:

$$1 + (1 - e^{-s\tau})K_c a G(s) = 0 \tag{3.8}$$

The chatter stability can be determined by Equation 3.8. If the characteristic equation roots, $s = \alpha + j\omega_c$, have a positive real part ($\alpha > 0$), then chatter occurs. If the real part is negative ($\alpha < 0$), then chatter vibration is suppressed. Thus, the stability boundary can be identified when the real part is zero ($\alpha = 0$), and in this situation the chatter frequency is given by $s = j\omega_c$. Equation 3.8 can be written as:

$$K_c a_{cr} G(j\omega_c)(1 - e^{-j\omega_c \tau}) = -1 \tag{3.9}$$

where $a_{cr}$ is the critical limiting depth of cut that shows the stability boundary. $\omega_c$ is the chatter frequency which is close to the natural frequency of the system but not equal as the chacteristic equation has additional terms. The phase between the waves can be determined by $\varepsilon = \omega_c \tau$ which will be derived later. Equation 3.9 can be rearranged to determine $a_{cr}$ as:

$$a_{cr} = \frac{-1}{K_c G(j\omega_c)(1 - e^{-j\omega_c \tau})} \tag{3.10}$$

Since $K_c$ and $a_{cr}$ have real and positive values, the term $G(j\omega_c)(1-e^{-j\omega_c\tau})$ needs to be real but negative to cancel the negative sign in Equation 3.10.

$$G(j\omega_c)(1-e^{-j\omega_c\tau}) = 2\Re\mathfrak{e}(G(j\omega_c)) \tag{3.11}$$

This condition can be obtained by a Nyquist plot shown in Figure 3.2b.

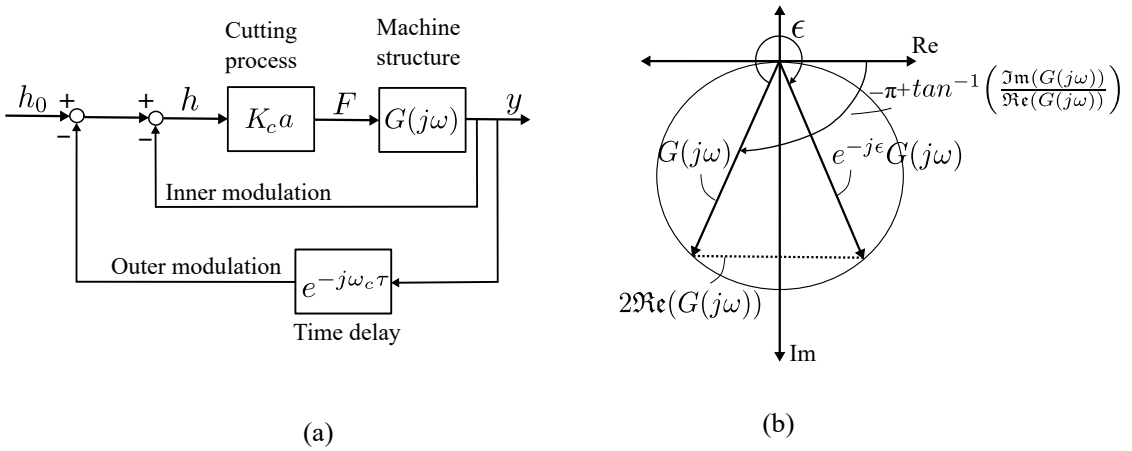


Fig. 3.2 (a) Block diagram of chatter dynamics, (b) Vectorial representation of Equation 3.11 in Nyquist diagram

Equation 3.11 and 3.10 yield:

$$a_{cr} = \frac{-1}{2K_c\Re\mathfrak{e}(G(j\omega_c))} \tag{3.12}$$

where $\Re\mathfrak{e}(G(j\omega_c))$ needs to have a negative sign to obtain a positive depth of cut value.

The dynamic chip thickness is affected by the chatter frequency $\omega_c(rad/s)$ or $f_c(Hz)$ ($\omega_c = 2\pi f_c$) and the spindle speed $n(rev/s)$, the relation between them can be written as:

$$\frac{f_c}{n} = k + \frac{\varepsilon}{2\pi} \tag{3.13}$$

where $k$ is the integer number of waves and $\frac{\varepsilon}{2\pi}$ is the fractional number of waves on the surface, $\varepsilon$ is the phase difference between the inner and outer modulations. If the phase angle is zero or $2\pi$, the chip thickness will be constant and stable, if not, the chip thickness grows

continuously, which means it causes chatter. Also, the phase difference can be derived from the Nyquist diagram in Figure 3.2b, which is:

$$\varepsilon = 2\pi - 2\tan^{-1}\left(\frac{\mathfrak{Re}(G(j\omega_c))}{\mathfrak{Im}(G(j\omega_c))}\right) \tag{3.14}$$

It should be noted that, from Equation 3.12, the cutting stiffness $K_c$ and the real part of the transfer function of the structure $G(j\omega_c)$ are inversly proportional to the axial depth of cut. If the minimum value of negative real part is considered, the critical limiting depth of cut $a_{cr}$ which is the limit value for the stability for any spindle speed, can be calculated. If a harder workpiece that has higher cutting stifness, is selected for the machining operation, then a lower critical limiting depth of cut is obtained. Meanwhile, a more flexible workpiece has lower negative real part value. If it is selected, then a lower critical limiting depth of cut is obtained.

Furthermore, the real part of the structure is a function of chatter frequency $\omega_c$. Selecting different chatter frequencies changes the axial depth of cut. Hence, the stability limit can be obtained selecting a set of chatter frequencies. For different integer number $k$ in Equation 3.13, so-called stability lobe diagram can be illustrated as a function of spindle speed and axial depth of cut shown in Figure 3.3. The chatter occurs above the diagram highlighted in red in Figure 3.3, while the absolute stability can be guaranteed by selecting the axial depth of cut below the $a_{cr}$ for any spindle speed, highlighted in blue.

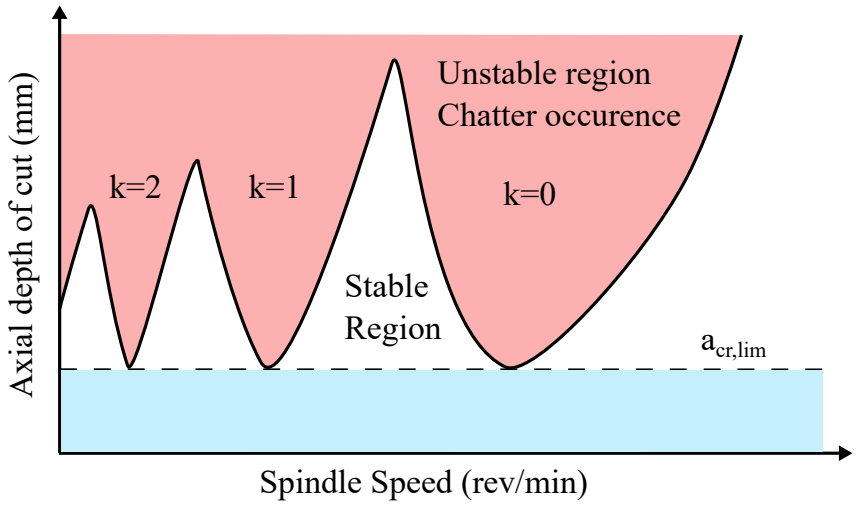


Fig. 3.3 Stability lobe diagram with red region shows the unstable/chatter region while the blue one shows the absolute critical limiting depth of cut border for any spindle speed

The regenerative chatter analysis can be extended for the multiple cutting teeth in milling. The stability of milling will be given in the next section.

## 3.3 Stability of Milling

A stationary workpiece is machined by a rotating cutting tool in milling operations. One or multiple teeth can be in cut in the same time, and the cutting forces vary during the tool rotation. Thus, the more advanced chatter stability analysis is needed to obtain an accurate and sufficent milling model. The regenerative chatter mechanism can be extended for the milling operation. For instance, Sridhar [71] presented a general milling model in 1960s. Yet, an accurate milling model could not been achieved due to the time-periodic force coefficient by the rotating cutting tool. The dynamic milling models were based on average time-varying coefficients [72, 73] or the models depending on time-domain by Tlusty [75, 76], which were not accurate models. Altintas and Budak [24, 26] developed the dynamic milling model called zero-order approach (ZOA) utilising a Fourier expansion, which is an accurate and fast model solved in the frequency-domain. Hence, the ZOA method is used for the milling stability analysis in this thesis.

### 3.3.1 Milling stability analysis

A rotating cutting tool and stationary workpiece are involved in milling operation shown in Figure 3.4a. Due to the tool rotation the cutting forces vary in both directions. The cutting forces $F_r$ and $F_t$ act on the tooth j as shown in Figure 3.4a in radial $(r)$ and tangential $(u)$ directions, respectively. The tool vibrates in $x$ and $y$ directions. As the cutting forces depend on the dynamic chip thickness, the vibration in radial direction $r$ regards to the tool vibration in $x$ and $y$ directions, which can be expressed as:

$$r = -x\sin(\theta_j) - y\cos(\theta_j) \tag{3.15}$$

The desired chip thickness is $h_o = f_t \sin(\theta_j)$ according to tool rotation shown in Figure 3.4b, where $f_t$ is the feed of the milling operation. The total chip thickness consists of the static and dynamic part. Thus, the instantaneous total chip thickness can be calculated as:

$$h(\theta_j) = \Big(f_t \sin(\theta_j) + (r_{j-1} - r_j)\Big) g(\theta_j) \tag{3.16}$$

where, $(r_{j-1} - r_j)$ are the previous and current tool vibration, respectively. The function $g(\theta_j)$ is a unit function which defines the tool is in or out of the cut. It can be written as:

$$g(\theta_j) = \begin{cases} 1, & \theta_s \leq \theta_j < \theta_e \\ 0, & \theta_j < \theta_s, \theta_j > \theta_e \end{cases} \tag{3.17}$$

where $\theta_s$ and $\theta_e$ are the start and exit tool immersion angles, respectively. The static part of the tool vibration $h_o = f_t \sin(\theta_j)$ can be neglected since there is no effect of it to the dynamic chip thickness regeneration mechanism. Substituting the Equation 15 and Equation 16 neglecting the static part of the tool vibration, yields:

$$h(\theta_j) = \Big(\Delta x \sin(\theta_j) + \Delta y \cos(\theta_j)\Big) g(\theta_j) \tag{3.18}$$

where $\Delta x = x_j - x_{j-1}$ and $\Delta y = y_j - y_{j-1}$. $x_j$ and $y_j$ are the present dynamic tool vibration while $x_{j-1}$ and $y_{j-1}$ are the previous dynamic tool vibration. Hence, the tangential $F_t$ and radial $F_r$ cutting forces (assuming they are proportional to the axial depth of cut $a$ and chip thickness $h$), can be expressed as:

$$\begin{aligned} F_{t,j} &= K_t a h(\theta_j), \\ F_{r,j} &= K_r F_{t,j} \end{aligned} \tag{3.19}$$

where $K_t$ and $K_r$ are the cutting coefficients.

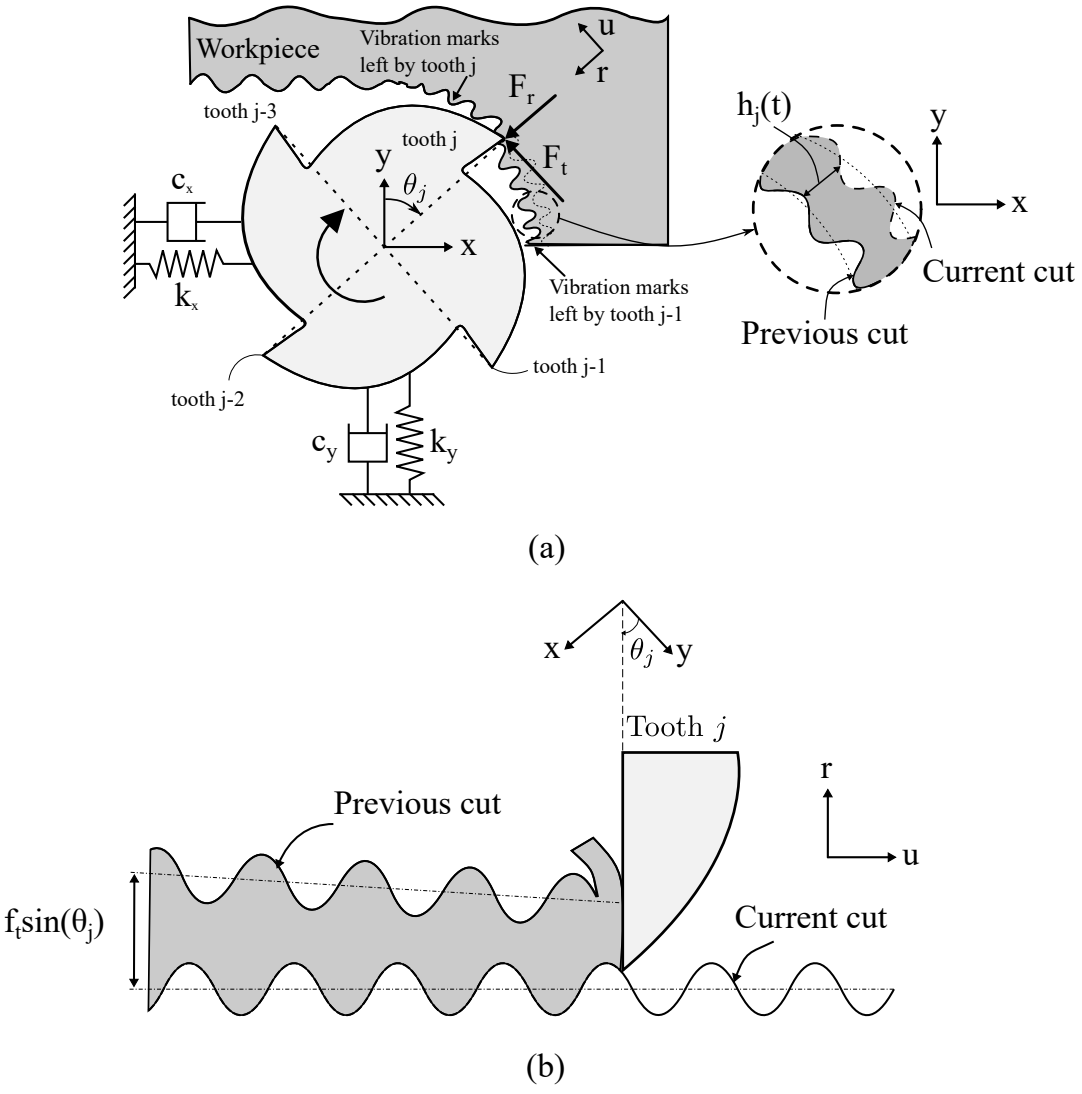


Fig. 3.4 Self-excited vibrations in milling. (a) Schematic view of milling and (b) the desired chip thickness $h_o = f_t \sin(\theta_j)$ according to tool rotation

The cutting forces in $x$ and $y$ directions can be expressed as:

$$\begin{aligned} F_{x,j} &= -F_{t,j}\cos(\theta_j) - F_{r,j}\sin(\theta_j), \\ F_{y,j} &= F_{t,j}\sin(\theta_j) - F_{r,j}\cos(\theta_j) \end{aligned} \tag{3.20}$$

Combining Equation 3.18, Equation 19, and Equation 20, and utilising trigonometric identities, the cutting forces in the $x$ and $y$ directions are:

$$\begin{aligned} F_{x,j} &= -\frac{1}{2}K_t a g(\theta_j)\big[\Delta x\big(\sin(2\theta_j) + K_n(1-\cos(2\theta_j))\big) + \Delta y\big(1+\cos(2\theta_j) + K_n\sin(2\theta_j)\big)\big], \\ F_{y,j} &= -\frac{1}{2}K_t a g(\theta_j)\big[\Delta x\big((1-\cos(2\theta_j)) - K_n(\sin(2\theta_j))\big) + \Delta y\big(\sin(2\theta_j) - K_n(1+\cos(2\theta_j))\big)\big] \end{aligned} \tag{3.21}$$

Here, only one tooth's contribution to the cutting forces is presented. Considering all teeth, the total cutting forces in $x$ and $y$ directions are:

$$\begin{aligned} F_x &= \sum_{j=1}^{N_t} F_{x,j}, \\ F_y &= \sum_{j=1}^{N_t} F_{y,j} \end{aligned} \tag{3.22}$$

where $N_t$ is the total number of teeth.

Forces in $x$ and $y$ direction can be written by summing the forces considering the all teeth in matrix form:

$$\begin{Bmatrix} F_x \\ F_y \end{Bmatrix} = \frac{1}{2}aK_t \begin{bmatrix} \alpha_{xx}(\theta) & \alpha_{xy}(\theta) \\ \alpha_{yx}(\theta) & \alpha_{yy}(\theta) \end{bmatrix} \begin{Bmatrix} \Delta x \\ \Delta y \end{Bmatrix} \tag{3.23}$$

where $F_x$ and $F_y$ are the total forces, the matrix $\alpha$ is the time-varying directional dynamic milling force coefficients, and the terms inside the matrix depend on the direction. This matrix is periodic at the tooth pass frequency. Altintas and Budak [23] proposed to expand it

into a Fourier series and use only the zeroth component to obtain a time-invariant equation term. The matrix $\alpha_0$ becomes:

$$\left[\alpha_0\right] = \frac{N_t}{2\pi}\begin{bmatrix}\alpha_{xx} & \alpha_{xy}\\ \alpha_{yx} & \alpha_{yy}\end{bmatrix} \tag{3.24}$$

where,

$$\begin{aligned}
\alpha_{xx} &= \frac{1}{2}\Big[\cos 2\theta - 2K_r\theta + K_r \sin 2\theta\Big]_{\theta_s}^{\theta_e}\\
\alpha_{xy} &= \frac{1}{2}\Big[-\sin 2\theta - 2\theta + K_r \cos 2\theta\Big]_{\theta_s}^{\theta_e}\\
\alpha_{yx} &= \frac{1}{2}\Big[-\sin 2\theta + 2\theta + K_r \cos 2\theta\Big]_{\theta_s}^{\theta_e}\\
\alpha_{yy} &= \frac{1}{2}\Big[-\cos 2\theta - 2K_r\theta - K_r \sin 2\theta\Big]_{\theta_s}^{\theta_e}
\end{aligned} \tag{3.25}$$

where, $\theta_s$ and $\theta_e$ are the start and the exit tool immersion angles, respectively. $N_t$ is the total number of teeth.

Once the time dependent terms are neglected, the dynamic milling force can be calculated in the frequency domain as:

$$F(\omega) = \frac{1}{2}aK_t[\alpha_0][1 - e^{-j\omega\tau}][G(j\omega)]F(\omega) \tag{3.26}$$

where, $G(j\omega)$ is the transfer function of the structure in frequency domain. If the system is critically stable by vibrating at the chatter frequency $\omega_c$, the roots of the characteristic equation can be written as:

$$\det([I] - \frac{1}{2}aK_t[\alpha_0][1 - e^{-j\omega_c\tau}][G(j\omega_c)]) = 0 \tag{3.27}$$

If we simplify the equation by $[\alpha_0][G(j\omega_c)] = [G_0(j\omega_c)]$, where $[G_0(j\omega_c)]$ is the oriented FRF:

$$\left[G_0(j\omega_c)\right] = \begin{bmatrix} \alpha_{xx}G_{xx}(j\omega_c) & \alpha_{xy}G_{xy}(j\omega_c) \\ \alpha_{yx}G_{yx}(j\omega_c) & \alpha_{yy}G_{yy}(j\omega_c) \end{bmatrix} \tag{3.28}$$

The eigenvalue of the equation can be written as:

$$\Lambda = -\frac{N_t}{4\pi} a K_t [1 - e^{-j\omega_c \tau}] \tag{3.29}$$

The equation becomes,

$$\det([I] + \Lambda[G_0(j\omega_c)]) = 0 \tag{3.30}$$

If only two orthogonal degrees of freedom directions ($x$,$y$) are considered, the equation becomes just a quadratic function as,

$$\alpha_0 \Lambda^2 + \alpha_1 \Lambda + 1 = 0 \tag{3.31}$$

where,

$$\begin{aligned} \alpha_0 =& G_{xx}(j\omega_c)G_{yy}(j\omega_c)(\alpha_{xx}\alpha_{yy} - \alpha_{xy}\alpha_{yx}) \\ \alpha_1 =& G_{xx}(j\omega_c)\alpha_{xx} + G_{yy}(j\omega_c)\alpha_{yy} \end{aligned} \tag{3.32}$$

Then the $\Lambda$ is identified as,

$$\Lambda = -\frac{1}{2\alpha_0}\left[\alpha_1 \pm \sqrt{\alpha_1^2 + 4\alpha_0}\right] \tag{3.33}$$

where $\Lambda = \Lambda_R + j\Lambda_I$. By substituting the eigenvalue and $e^{-j\omega_c T} = \cos\omega_c\tau - j\sin\omega_c\tau$ in Equation 3.31, the critical limiting depth of cut $a_{cr}$ can be calculated as,

$$a_{cr} = -\frac{2\pi}{N_t K_t}\left[\frac{\Lambda_R(1-\cos\omega_c\tau) + \Lambda_I \sin\omega_c\tau}{(1-\cos\omega_c\tau)} + j\frac{\Lambda_I(1-\cos\omega_c\tau) - \Lambda_R\sin\omega_c\tau}{(1-\cos\omega_c\tau)}\right] \tag{3.34}$$

As $a_{cr}$ is a real number, the imaginary part of the equation $\Lambda_I$ needs to be ignored, and it yields,

$$\Lambda_I(1-\cos\omega_c\tau)-\Lambda_R\sin\omega_c\tau=0 \tag{3.35}$$

By substituting,

$$\kappa=\frac{\Lambda_I}{\Lambda_R}=\frac{\sin\omega_c\tau}{1-\cos\omega_c\tau} \tag{3.36}$$

into the real part of the Equation 3.35, we get the chatter free axial depth of cut can be calculated from,

$$a_{cr}=\frac{-2\pi\Lambda_R}{N_tK_t}(1+\kappa^2) \tag{3.37}$$

The spindle speed can be found from Eq. 3.36,

$$\kappa=\tan\psi=\frac{\cos(\omega_c\tau/2)}{\sin(\omega_c\tau/2)}=\tan(\pi/2-(\omega_c\tau/2)) \tag{3.38}$$

where $\psi$ is the phase shift of the eigenvalue, and $\omega_c\tau/2{=}\pi-2\psi+2k\pi$ represents the phase distance in one tooth period $(\tau)$. If $k$ is an integer number and $\varepsilon=\pi-2\psi$ is the phase shift between the current and previous vibration marks,

$$\omega_c\tau=\varepsilon+2k\pi \tag{3.39}$$

Then spindle speed n(rev/min) can be calculated as,

$$n=\frac{60}{N_t\tau} \tag{3.40}$$

Once the system FRF is identified and the cutting coefficients are measured, stability lobe diagram (SLD) can be developed.

The averaged time-invariant term $[\alpha]$ is affected by the milling type which are up and down milling seen in Figure 3.5, and the radial immersion of the tool due to the start $\theta_s$ and exit $\theta_e$ angle changes. ZOA method does not depend on the helix angle as it only reduces the harmonics of the cutting force, not the average of the cutting force [232]. Neverthless, the ZOA method is not accurate for the highly intermittent cutting operations with low radial immersion (up to 10%) due to the increasing harmonics of the cutting force [233]. As high immersion is used for this thesis, the ZOA method is considered for the SLD predictions and the optimisation of the controller gains.

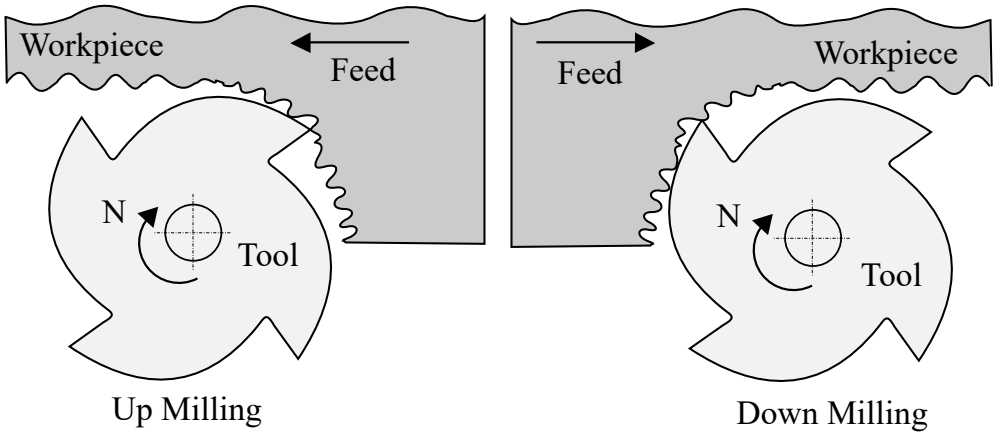


Fig. 3.5 Milling types. (a) Up milling and (b) Down milling

## 3.4 Summary

The theoretical background of the milling stability has been presented in this chapter. Firstly, the regenerative chatter mechanism analysis was explained in detail considering a continuous single-point cutting operation. Then, the stability lobe diagram was presented. Afterwards, the stability analysis was extended to the milling operations which have multiple teeth engagement. The critical limiting depth of cut $a_{cr}$ was derived for a general two-dof milling operation. Finally, the ZOA method accuracy was discussed in terms of low radial immersion and cutting force harmonics due to the cutting parameters.

In this thesis, a tool with 4 teeth is chosen for the down milling with half radial immersion. To predict the stability boundaries, the ZOA method is used. The ZOA method is chosen since it is an accurate and fast model for the predictions using high radial immersion. Then, the predictions are evaluated under real cutting conditions.

# Chapter 4

# Robotic-Assisted Milling Concept

## 4.1 Introduction

The chatter suppression using active control methods has been frequently studied to improve machining stability. However, to the author's knowledge, active control methods have never been utilised in a robotic-assisted milling scenario. It is only applied in turning using an actively controlled robotic arm without experimental verification [12]. Ozturk et al. [11] proposed a method called robotic-assisted milling to increase productivity of milling operation. The authors implement a robot arm to improve the dynamic response of a flexible workpiece, however, they have not applied active control on it. In this chapter, an actively controlled robot arm in milling operation is proposed.

The concept of robotic-assisted active vibration control in milling is illustrated schematically in Figure 4.1. Here, a six-axis industrial robot is used to position an end-effector against a flexible structure which is clamped to the ground. To achieve improved dynamic response of the flexible structure, an end-effector is mounted to the robotic arm, in a similar fashion to previous work [11]. However, unlike previous work the role of end-effector is to transmit dynamic forces upon the flexible structure, by means of a proof-mass (or inertial) actuator, in order to increase the chatter stability during machining. The forces acting at the interface

between the robot, flexible structure, and cutting tool are depicted in Figure 4.1b. It can be seen that the proof-mass actuator force $f_{act}$ will influence the total support force $f_t$, but it should be noted that this total support force can only be positive as the robot is not rigidly attached to the workpiece by the robot-workpiece interface. However, this support force will also be influenced by the preload force provided by the robot itself. Consequently, the dynamic response of the robot and workpiece need to be taken into consideration in order to design the control system for the proff-mass actuator.

The designed concept can be a potential solution to improve the chatter stability, as well as productivity. Increased material removal rate without causing chatter can be obtained by exploring potential benefits of robotic-assisted milling. Meanwhile, the advantage of the concept is that the robot can be positioned to a different point on the flexible workpiece as moving or fixed damper. Also, it can be redeployed to a different machining structure.

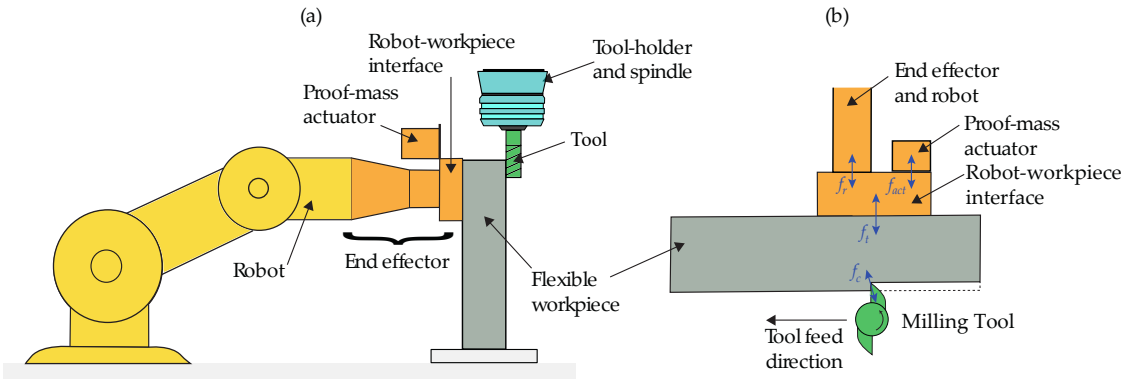


Fig. 4.1 Conceptual illustration of robotic assisted vibration control during milling. (a) side view; (b) top view, showing the cutting force $f_c$, total support force $f_t$, total proof-mass actuator force $f_{act}$ and robot support force $f_r$

To explore the potential benefits of actively controlled robot arm, a representive model for the actuator model is required. The actuator selection criteria are explained in the next section.

### 4.1.1 Actuator selection criteria

Actuators are the controllable auxiliary devices. They can be in many shapes and forms. For selection of an actuator, requirements of the system must be known. The actuator attributes are [1];

1. Actuation Stress: The applied force per unit cross-sectional of an actuator
2. Actuation Strain: The nominal strain produced by an actuator
3. Actuator Modulus: The ratio of a small increment in stress ($\sigma$) to the corresponding small increment in strain ($\varepsilon$) when the control signal to an actuator is held constant
4. Actuator Density: The ratio of mass to initial volume of an actuator
5. Efficiency: The ratio of mechanical work output to energy input during a complete cycle in cylic operation
6. Strain Resolution: The smallest step increment
7. Volumetric Power: The mechanical power output per unit initial volume in sustainable cyclic operation
8. Actuation Bandwidth: The range of actuation bandwidth of the system

The actuator types are given in Table 4.1 [1].

Table 4.1 Actuator Types

| Class of Actuator | Example |
|---|---|
| Electromagnetic | Solenoid, Magnetostriction, Proof-Mass |
| Electromechanical | Linear Drive, MEMS Comb Drives |
| Fluidic | Hyraulics, Pneumatics |
| Piezoelectric | Ceramic, Polymer |
| Smart Materials | Shape Memory Alloy, Bimetallic |
| Hybrid | Piezoelectric and Electromechanical |
| Natural | Human Muscle |

The maximum stroke and maximum force database is presented in Figure 4.2. Muscle has the maximum output force and the maximum stroke.

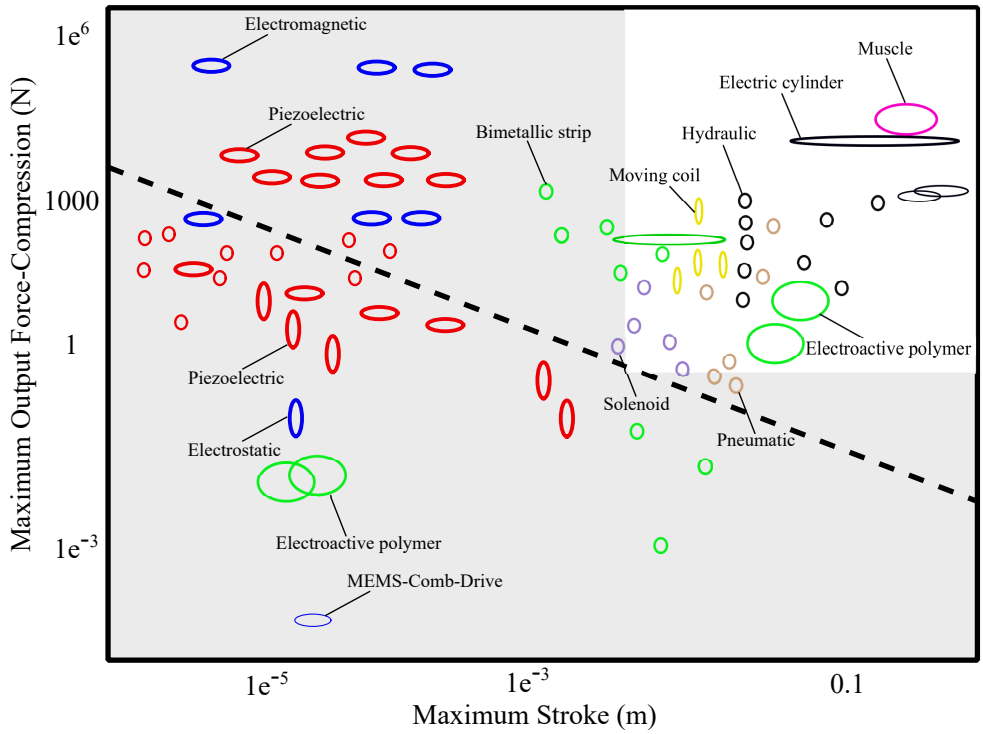


Fig. 4.2 The Maximum Stroke Versus the Maximum Actuator Output Force [1]

The additional requirement of a system is the weight of the actuator. The work capacity of an actuator and weight relation is shown in Figure 4.3. As the work capacity increases, the weight of the actuator increases. The lightest actuator must be selected for required work capacity of a system.

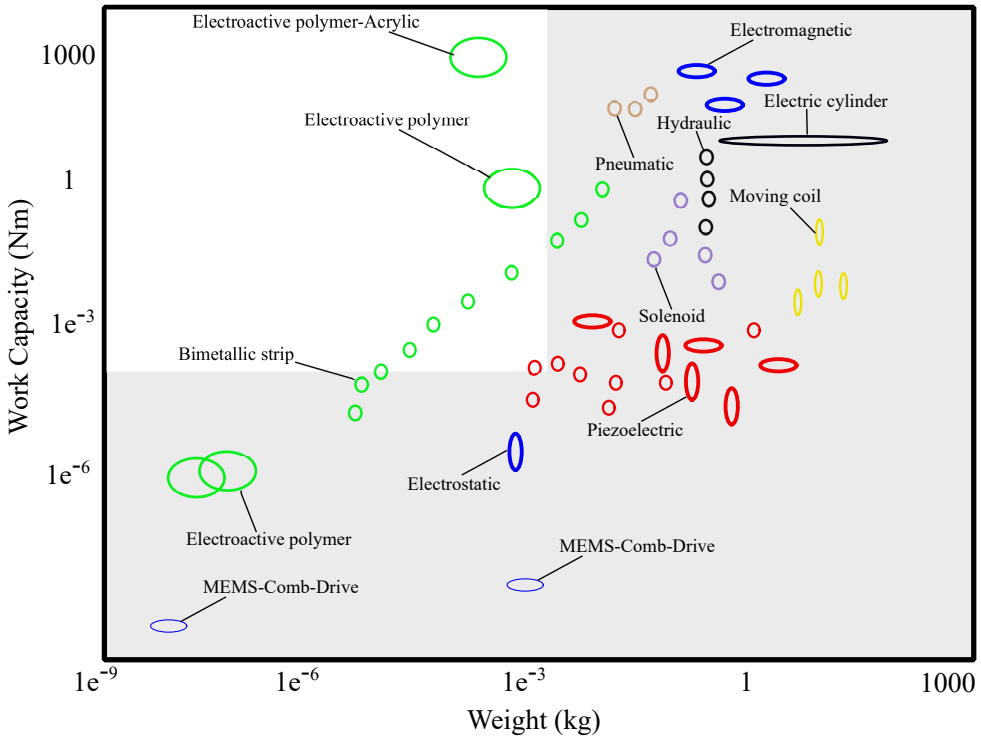


Fig. 4.3 The Maximum Work Capacity Versus the Weight of the Actuator [1]

The figures show that the clear differences between actuator. Also, the power to weight ratio and the efficiency of an actuator can be investigated, as shown in Figure 4.4. The bimetallic and the shape memory actuators have inefficient results even though their characterictics are attractive. Piezo and magnetostrictive actuators can provide high output force and can be cycled at very high frequencies even though they provide small displacements.

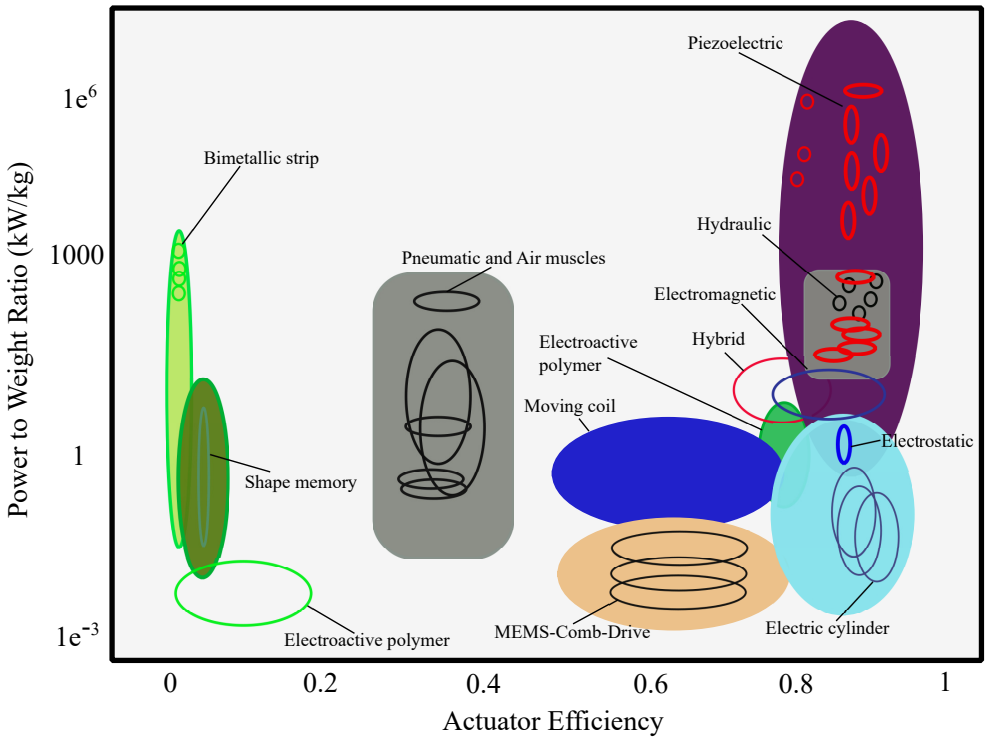


Fig. 4.4 The Power to Weight Ratio and the Efficiency of the Actuator [1]

The frequency of the system requirement is very important as well. The selection of an actuator with the frequency range is given in Figure 4.5. The figure shows that the electrostatic, magnetostrictive and the piezoelectric actuators have the maximum frequency capacity while the magnetostrictive actuator is the heaviest one.

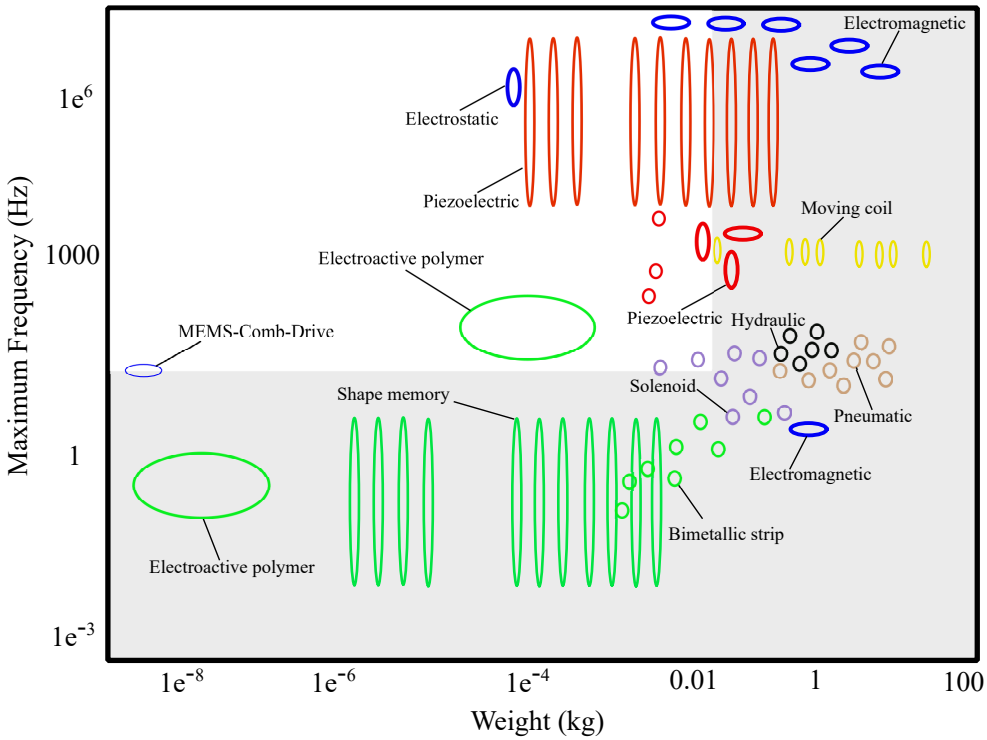


Fig. 4.5 The Maximum Frequency Range and the Weight of the Actuator [1]

Properties of an actuator are very important for applying to a control system. For high output force and frequency application such as machining operations, the piezoelectric and electromagnetic actuators are convenient active devices as shown in Table 4.2. Since the proof-mass actuator which is an electromagnetic actuator, can provide more stroke than piezoelectric actuator, a proof-mass actuator will be implemented in this study to explore the potential improvements in robotic-assisted milling.

Table 4.2 Convenient Actuators Considering the Criteria

| Actuator Selection Criteria | Convenient Actuators |
|---|---|
| Maximum Stroke vs Maximum Force | Muscle and Electric Cylinder |
| Work Capacity vs Weight | Elecroactive Polymer, Shape Memory Piezoelectric |
| Power/Weight vs Efficiency | Piezoelectric, Magnetostrictive, Proof-Mass |
| Max Frequency vs Weight | Piezoelectric, Magnetostrictive, Proof-Mass |

## 4.2 The concept of robotic-assisted active vibration control

The objective of the present contribution is to explore potential solutions to this design problem and assess the potential performance improvements, in terms of increased chatter stability. From a practical perspective, this solution would enable increased productivity from the machining operation, because greater material removal rates could be achieved without causing chatter. Meanwhile, the active controller and its robotic mount could be readily configured to re-deploy the active device, either at different location on the workpiece (e.g. as the machining location is moved), or on different workpiece / machining configurations. The designed concept can be a potential solution to improve the chatter stability, as well as productivity. Increased material removal rate without causing chatter can be obtained by exploring potential benefits of robotic-assisted milling. Meanwhile, the advantage of the concept is that the robot can be positioned to a different point on the flexible workpiece as moving or fixed damper. Also, it can be redeployed to a different machining structure.

### 4.2.1 Robot and actuator specification

To evaluate the feasibility of the proposed concept, representative models of the proof-mass actuator and the robot structure are required. For the present study, STAUBLI TX-90 industrial serial arm robot which is shown in Figure 4.6 is chosen as the representative robot.


Fig. 4.6 STAUBLI TX-90 industrial robot

Meanwhile, to simulate the effect of active vibration control, an inertial actuator specification and dynamic model is required. It should be noted that an inertial actuator is chosen as this approach is easily deployed on the robot's end effector: the actuator can achieve significant dynamic force control of the workpiece, but without changing the static force supplied by the robot manipulator, and without requiring direct rigid connection to an inertial reference frame (i.e. the ground).

A schematic illustration of the actuator frequency response function (FRF) testing setup is shown in Figure 4.7. The actuator is assembled to an aluminium block which is suspended using strings. LMS software connected to a PC is used to drive the actuator. Once the actuator is excited by a harmonic chirp signal, the acceleration of the aluminium block is measured to process the FRF of the actuator. The acceleration data is multiplied with the mass of the aluminium block to calculate the force of the actuator for a specific frequency bandwidth. The FRF of the actuator is illustrated in Figure 4.8(b).

In the present study, the parameters for the actuator are based upon the ADD-45 inertial actuator from Micromega Dynamics [2]. The actuator can be driven up to 9 V and 2000 Hz

according to the user manual. With reference to Figure 4.8(b), this actuator has a mode at 8.4 Hz and is capable of applying up to 3 N/V (max 27 N) supporting force up to 2000 Hz.

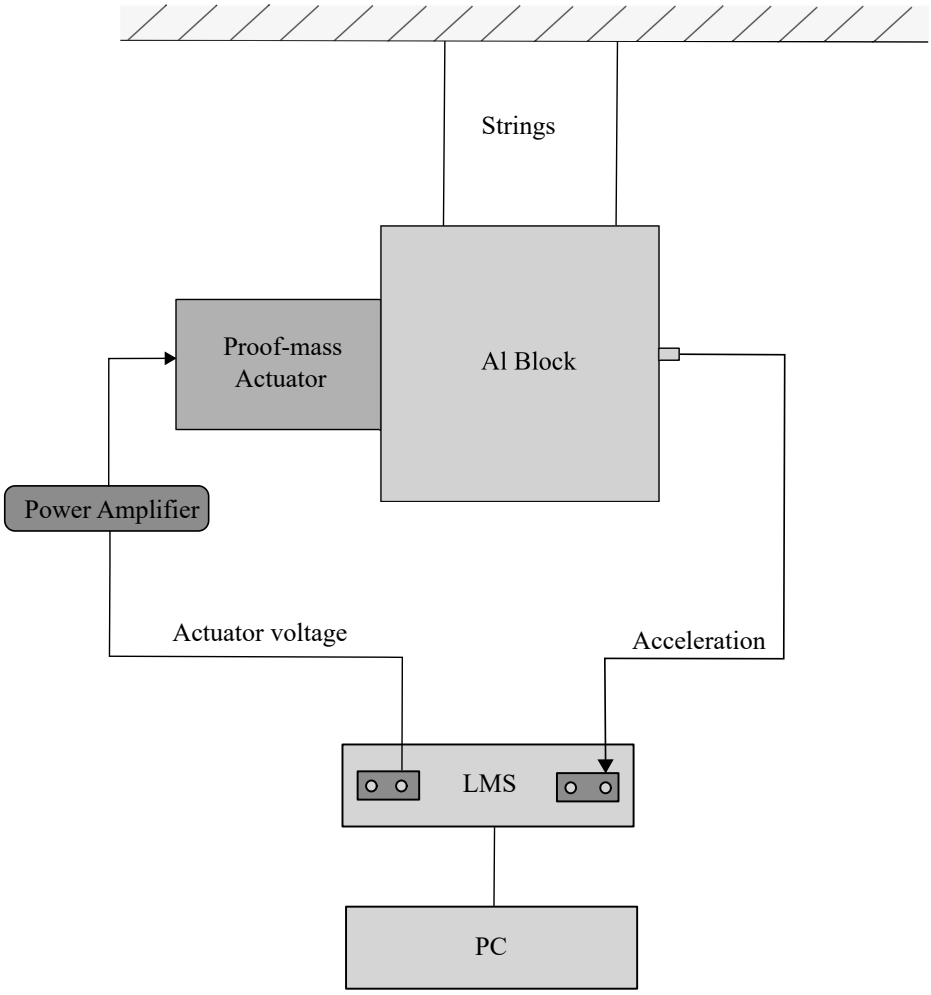


Fig. 4.7 Actuator frequency response function (FRF) test setup

A schematic illustration of an inertial actuator model is shown in Figure 4.8(a).

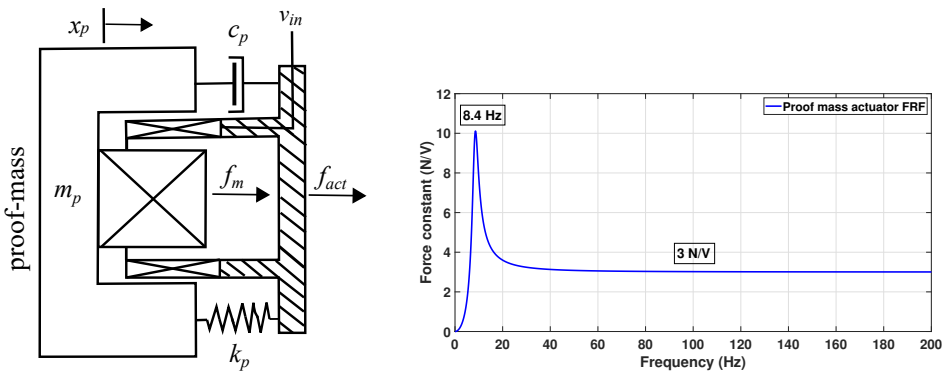

Fig. 4.8 (a) Proof-mass actuator; (b) Frequency response function [2]

The actuator is modelled by a moving mass $m_p$ with a damper $c_p$ and spring $k_p$. The mass is excited by an electromagnetic force $f_m$ pursuant to the voltage input $v_{in}$. The resulting force on the host structure is $f_{act}$. The transfer function between the mass displacement $x_p$ and the voltage input $v_{in}$ can be written as,

$$\frac{X_p(s)}{V_{in}(s)} = \frac{G_1 G_2}{m_p s^2 + c_p s + k_p} \tag{4.1}$$

where $V_{in}$ is the Laplace transform of $v_{in}$, $X_p$ is the Laplace transform of $x_p$, $G_1$ is the electromagnetic gain and $G_2$ is the power amplifier gain [234]. The transfer function between the reaction force $f_{act}$ and the voltage input $v_{in}$ can be written as,

$$\frac{f_{act}(s)}{V_{in}(s)} = \frac{-G_1 G_2 m_p s^2}{m_p s^2 + c_p s + k_p} = g_a \frac{s^2}{s^2 + 2\zeta\omega_p s + \omega_p^2} \tag{4.2}$$

where $\omega_p$ is the natural frequency, $\zeta$ is the damping ratio of the actuator and $g_a = -G_1 G_2$ is the actuator gain [234].

The frequency response function (FRF) of the actuator can be seen in Figure 4.8(b). The actuator transfer function in unit N/V can be written as:

$$\frac{f_{act}(s)}{V_{in}(s)} = 3\frac{s^2}{s^2 + 15.834s + 2785.6} \tag{4.3}$$

### 4.2.2 Simplified model

The simplified model of the robotic-assisted milling concept is explained in this subsection. To evaluate the performance of potential benefits, a test setup is designed as shown in Figure 4.9. Here, a two degree of freedom beam structure which emulates the flexible robot is

pushed against a flexible workpiece. The most flexible two modes of the robot is considered during the design the beam structure. The natural frequencies of the robot are identified as 23 Hz and 47 Hz by tap testing. The FRF of robot is given in Appendix A. The robot and structure parameters were identified, and they are given in Table 4.3. The flexible workpiece is represented using a flexure and Al 7075-T6 block, with natural frequency, damping ratio, an stiffness values of 142.1 Hz, 0.88%, and $2.43\times10^7$ $\mathrm{Nm}^{-1}$, respectively. The robot is pushed against to the workpiece by applying a static preload to avoid any loss-of-contact during cutting. The contact between robot and flexible workpiece is assumed to be rigid. However, the robot is not firmly attacted to the workpiece, the role of contact force is only act on the relative motion between $x_3 - x_2$, with reference to Figure 4.9.

The equation of motion for the structure is:

$$(m_2+m_3)\ddot{x}_2 = -c_2(\dot{x}_2-\dot{x}_1)-c_3\dot{x}_2-c_p(\dot{x}_2-\dot{x}_p)-k_2(x_2-x_1)-k_3x_2-k_p(x_2-x_p)+f_c-f_{act} \tag{4.4}$$

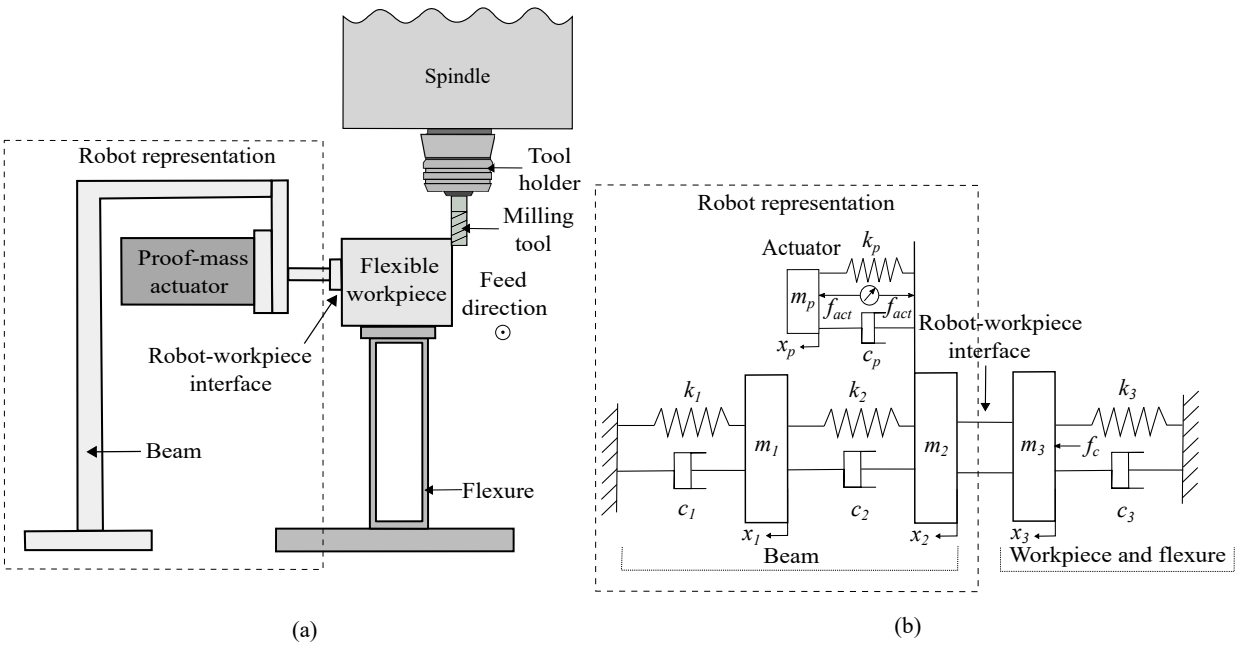


Fig. 4.9 Simplified model of the active vibration problem. (a) Schematic diagram; (b) Lumped parameter representation.

Table 4.3 Structural parameters

| Preloaded Structural Parameters | |
|---|---|
| Natural frequency | 142.1 Hz |
| Damping ratio | 0.88 % |
| Stiffness | $24.3\times10^{6}\ Nm^{-1}$ |
| **Flexible Robot Parameters** | |
| Natural frequency | 23 Hz, 47 Hz |
| Damping ratio | 4.3 %, 2.9 % |
| Stiffness | $0.79\times10^{6}\ Nm^{-1}$, $2\times10^{6}\ Nm^{-1}$ |

## 4.3 Proposed active control systems

The proof-mass actuator can apply any number of active control systems. Although there have been several active vibration control applications in milling scenario in terms of chatter suppression [31, 35, 175, 178], the specific scenario proposed here has not been previously considered. Therefore, the most implemented active control methods in machining are designed for the robotic-assisted milling concept, namely: direct velocity feedback (DVF), virtual passive absorber (VPA), proportional integrated derivative (PID), linear quadratic regulator (LQR), H-infinity ($H_\infty$) and $\mu$ synthesis control.

### 4.3.1 DVF (Direct velocity feedback)

The direct velocity feedback (DVF) control method produces the control force according to the velocity of the controlled structure. The velocity of the structure can be obtained by integrating the acceleration feedback signal. This concept is depicted schematically in Figure 4.10. The approach has been widely proposed by researchers [175, 235, 236] since it is easy

to apply, only one feedback gain must be selected. However, optimisation is required to find the optimal value of feedback gain.

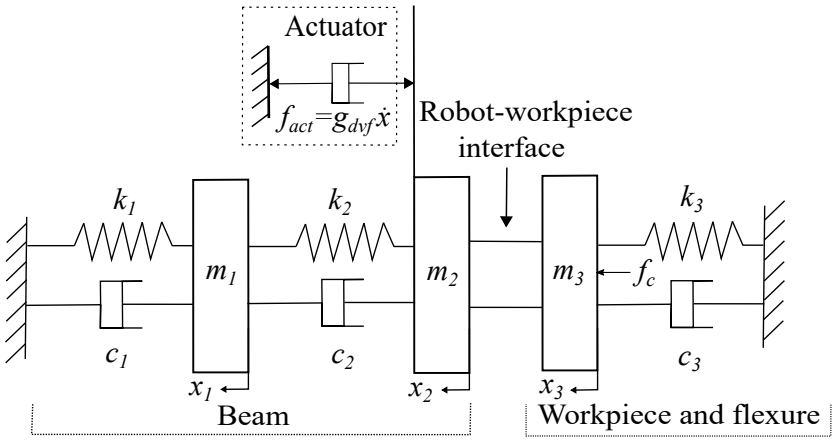


Fig. 4.10 Direct velocity feedback (DVF) control. The dashed box depicts the desired behaviour of the proof-mass actuator.

If the active control force is provided by a proof-mass actuator, the closed-loop characteristic equation of the system with the actuator dynamics can be written as,

$$1 + g_{dvf} s \frac{g_a s^2}{s^2 + 2\zeta \omega_p s + \omega_p^2} G(s) = 0 \tag{4.5}$$

where $\omega_p$, $\zeta$, $g_a$, $g_{dvf}$, $G(s)$ are the natural frequency and damping ratio of the actuator, actuator gain, feedback gain and the the system's transfer function, respectively [234].

### 4.3.2 VPA (Virtual passive absorber)

The Virtual Passive Absorber (VPA) control approach is depicted schematically in Figure 4.11. To choose control system parameters, the dynamic properties of the flexible structure are required. The classical passive vibration absorber method [237, 238] can be used to calculate control parameters. It has been shown that the virtual passive absorber control method can be carried out in order to improve the chatter stability significantly [175]. Den Hartog method [55] is used for VPA control parameter tuning, assuming a single mode of

vibration. Consequently, if the structural parameters to be controlled are changed/shifted dramatically or multiple vibration modes relevant to the chatter stability occur, the controller performance may be degraded.

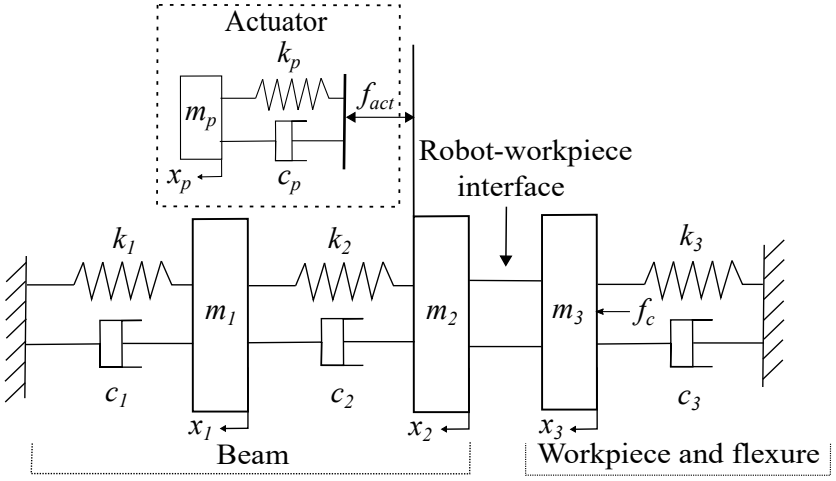


Fig. 4.11 Virtual passive absorber (VPA) control. The dashed box depicts the desired behaviour of the proof-mass actuator

The closed-loop characteristic equation with VPA control can be described as [175],

$$1+\frac{g_a s^2}{s^2+2\zeta\omega_p s+\omega_p^2}\frac{M\mu_c s^2(2\zeta_a\omega_a s+\omega_a^2)}{g_a(s^2+2\zeta_a\omega_a s+\omega_a^2)}G(s)=0 \tag{4.6}$$

Here, $\mu_c$, $\zeta_a$, $\omega_a$ are the mass ratio, the damping ratio and the natural frequency of the absorber, respectively. $M$ is mass of the main structure. To compensate for the actuator gain $g_a$, the control dynamic is multiplied by $g_a^{-1}$. The optimum passive absorber parameters (natural frequency and damping ratio) can be calculated as [55],

$$\frac{w_a}{w_n}=\frac{1}{1+\mu_c} \qquad\qquad \zeta_a=\sqrt{\frac{3\mu_c}{8(1+\mu_c)}} \tag{4.7}$$

where, $\omega_n$ is the natural frequency of the main structure. Optimisation is required to obtain the optimal value of mass ratio $\mu_c$. The mass ratio $\mu_c$ is optimised with the SADE algorithm as described in Section 4.4.3.

### 4.3.3 PID (Proportional-integral-derivative)

PID control is the most widely used control method in industry, with three control parameters [239]. It is well established [240] and one of the successfully implemented control method to suppress the chatter vibrations [153, 241, 242]. The closed-loop characteristic equation with PID control can be written as,

$$1 + (g_{pp} + g_{pv}s + g_{pa}s^2)\frac{g_a s^2}{s^2 + 2\zeta\omega_p s + \omega_p^2}G(s) = 0 \tag{4.8}$$

where $g_{pp}$, $g_{pv}$, $g_{pa}$ are the proportional, integral, derivative control gains, respectively, and optimisation is required to find the optimum control gains.

### 4.3.4 LQR (Linear quadratic regulator)

A linear quadratic regulator (LQR) is an optimal control method which operates a system at minimum cost. In order to design a dynamic system to be controlled by LQR, a quadratic cost function is required. Two weighting matrices are needed to state the cost function [234]. The LQR method has been implemented to suppress the chatter vibrations considerably [243, 244].

Consider a state-variable system

$$\dot{x} = Ax + Bu \tag{4.9}$$

where the $A$ and $B$ are the state space representation of the system. The LQR is a state space control method, which means that the feedback is obtained by multiplying the state vector $x(t)$ with a matrix $K$ [234]:

$$u(t) = -Kx(t). \tag{4.10}$$

To calculate $K$ matrix, the cost function which needs to be minimised can be stated as:

$$J = \frac{1}{2}\int_0^\infty (x^T Q x + u^T R u) dt \tag{4.11}$$

where $Q$ and $R$ are the semi-definite and positive definite weighting martices related to state and control cost, respectively. The weighting parameters are optimised using SADE algorithm. $K$ matrix can be defined as:

$$K = R^{-1} B^T P \tag{4.12}$$

where $P$ is the symmetric positive definite solution of the algebraic Riccati equation:

$$PA + A^T P + Q - PBR^{-1}B^T P = 0. \tag{4.13}$$

### 4.3.5 $H_\infty$ ($H$-infinity)

$H_\infty$ control is a control method which seeks and synthesizes controllers to obtain stabilised guaranteed performance. In order to improve the stability and potential benefits of the $H_\infty$ control, weighting matrices that are defined for the dynamic system and the controller matrix, are required [239]. The control method has been successfully designed and verified in recent studies [164, 167, 178, 199] to improve the machining chatter stability. The approach is summarised in Figure 4.12. Here, $W_{act}$, is the actuator weighting function, $W_{x1}$ is a weighting function defined for the structural vibration, and $G_{act}$ is the actuator transfer function described in the previous section. Single open loop model represents the generalized plant including the weighting functions, external disturbance (cutting force $f_c$) and the error signals $e_1$ and $e_2$ which are the outputs to be tracked to achieve the maximum potential benefits from the controller.

A high-pass filter can be defined for the actuator weighting function:

$$W_{act} = \frac{s^2}{s^2 + 2\zeta w_{hp} + \omega_{hp}^2} \tag{4.14}$$

where $\omega_{hp}$ is $2\pi \times 10$ rad/s; slightly above the natural frequency of the actuator (8.4 Hz).

To penalise the structural vibration, the weighting matrix $W_{x1}$ can be defined as [156]:

$$W_{x1} = G_{st} \frac{\frac{s}{2\pi f_1} + 1}{\frac{s}{2\pi f_2} + 1} \tag{4.15}$$

where $G_{st}$, $f_1$, $f_2$ are the control parameters to be tuned using the SADE algorithm.

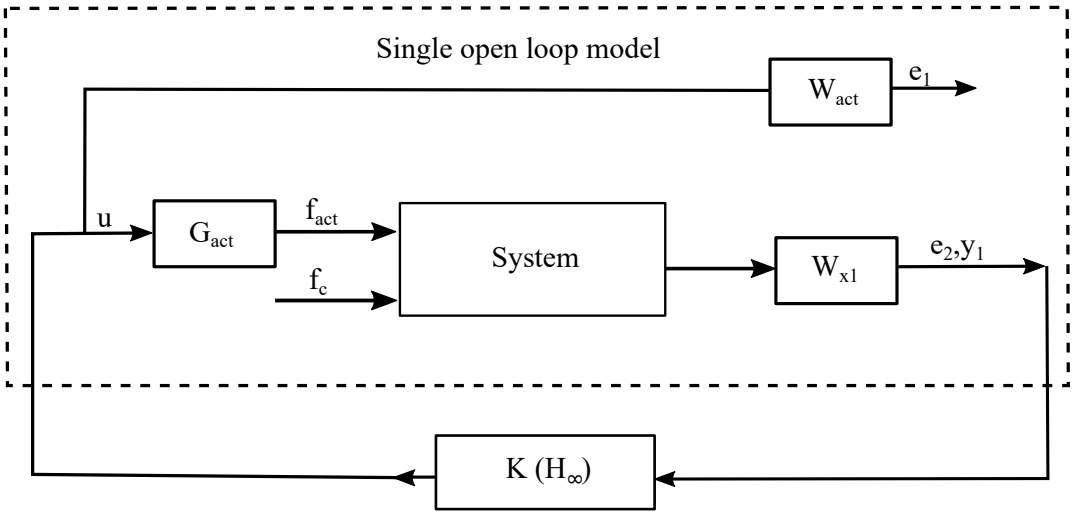


Fig. 4.12 $H_\infty$ control method

### 4.3.6 $\mu$-synthesis control

A control system can be modelled as a robust system to avoid differences between the system model and the real system. The differences called uncertainties can be caused by sensor failure, real system parameters variation, and actuator dynamics [239]. If these uncertainties are not covered by the controller, it may result in detrimental effect on the controller performance and chatter mitigation [245–247]. If a control method considers these

potential uncertainties, the controller is called a robust control system being insensitive the difference between the real system and its model.

The, $\mu$ synthesis control can take into account this controller issue. It has been successfully implemented by researchers [170, 198, 199] to address this issue by covering the potential uncertainties. The $\mu$ synthesis control method could help this potential controller problem by considering the dynamic response variation of the robot, if it is reconfigured during the milling, as well as structural dynamics changes due to the material removal. The $\mu$ synthesis control strategy is shown schematically in Figure 4.13. Here, $\Delta_{act}$ and $\Delta_{sys}$ represent the uncertainties for the actuator and the real system, respectively.

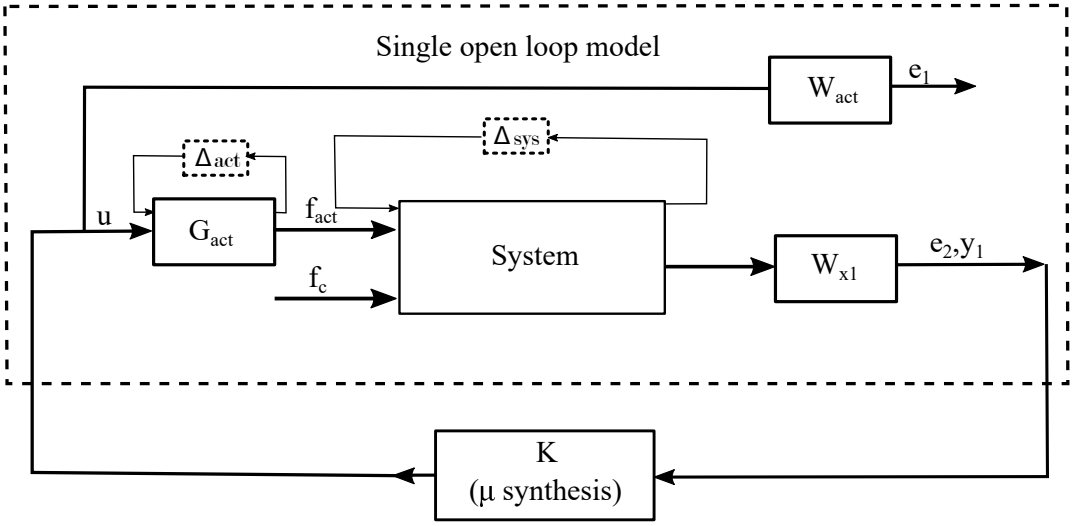


Fig. 4.13 $\mu$ synthesis control method

The robust performance of the controller can be analysed by examining the singular value $\mu$ [239]. The $\mu$ condition is to be sought for a controller which has a reduced singular value, by the $\mu$ synthesis control method iteratively. The $D-K$ iteration approach [248, 249] can be used to find the optimal controller by combining the $H_\infty$ and $\mu$ analysis approach. A convex optimisation problem can be solved by this iterative method. However, the $D-K$ iteration approach can only be used to find a controller which is robust by considering the dynamic uncertainties, $\Delta_{act}$. Therefore, an extended iteration method is required for

the mixed uncertainties. The $D, G-K$ iteration approach [250] can help to obtain robust performance taking into consideration the real and dynamic uncertainties $\Delta_{act}$ and $\Delta_{sys}$ for the robotic-assisted milling concept. Since the approach in general results in a high-order controller, a controller order reduction method can be implemented to able to get a controller for practical applications. Here, the Hankel model [251] is used to reduce the controller order caused by the iteration procedure.

## 4.4 Chatter stability modelling

All the above-mentioned control methods have been successfully applied to improve the chatter stability in milling. However, the robotic-assisted milling concept has not been considered previously. The dynamic properties of the robot and flexible structure, and the potential loss-of-contact between the robot's end-effector and flexible workpiece issues need to be taken into account to implement the active control strategies in robotic-assisted milling concept. Consequently, the present study will benchmark all of these active control methods within this context. To do so, two models of machining chatter will be used.

The first approach is an analytical frequency domain prediction of chatter. Assuming a linear system provides fast computation, yet the accuracy of the results can be reduced. The second approach is time domain modelling. It allows more complex models of the mechanics, and provides more accurate results considering nonlinearities such as actuator saturation. However, the longer computation time results with this modelling approach.

### 4.4.1 Frequency domain model

In the present study, the stability was predicted using Budak and Altintas's method [23]. Details of this approach are explained in detail in Chapter 3 [23, 232]. Active vibration control aims to improve the structural dynamics in order to increase chatter stability. Process

stability can be assessed via the well-known Stability Lobe Diagram (SLD) which plots the stability boundary as a limiting depth of cut for different spindle speeds.

### 4.4.2 Time domain model

A time domain model is required as it allows more complex models of the mechanics, and provides more accurate results considering nonlinearities such as actuator saturation. The model is also needed for the optimisation process of the controller gains.

A Simulink model [3] for simulating robotic-assisted milling is depicted in Figure 4.14. A combination of Simulink [252] and a *c*-program are utilised for the machining process. In order to suppress the vibrations, a feedback control method is carried out. Only one direction ($x$) is controlled although the workpiece is modelled in the $x$ and $y$ directions. The controlled direction is perpendicular to the feed direction as shown in Figure 4.9. The model allows to calculate the cutting force, chip thickness and vibration values in two directions, and the actuator force in controlled direction. The structural behaviour of the workpiece is modelled as a transfer function. To update the cutting tool position, the displacement values along with the feed rate are used. The model calculates the displacement using 4th order Runge-Kutta solver with fixed time steps.

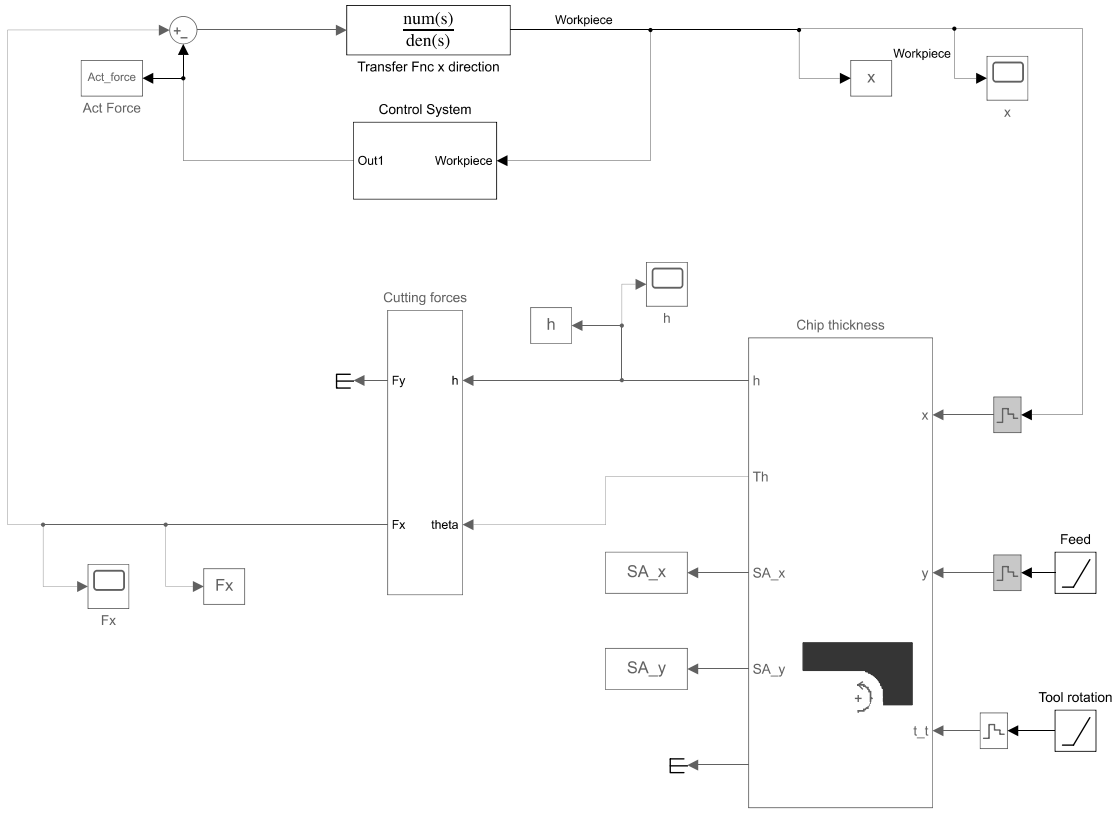


Fig. 4.14 Simulink model for time domain simulation [3]

The time-domain modelling allows the adding nonlinearites such as actuator saturation effects, which enable to compare the different vibration control methods. In the present study, the actuator force saturation point is indicated as 27 N to evaluate the chosen actuator performance. As the computational time is longer with this approach, the stability boundaries cannot be calculated immediately. A suitable chatter criteria needs to be indicated to identify the stability limits within multiple simulations. The nondimensional chip thickness criterion [253] is considered for the stability boundaries. Here, a non-dimensional chatter coefficient, $\eta$, is defined as:

$$\eta = \frac{h_{d,max}}{h_{s,max}} \tag{4.16}$$

where $h_{d,max}$ is the maximum chip thickness during the time-domain simulation, and $h_{s,max}$ is the desired static chip thickness. The threshold of chatter is set at 1.06 as recommended in [253].

### 4.4.3 Machining scenario and controller tuning

In order to investigate the performance of the active vibration control approach, chatter stability analysis and simulations are performed using representative parameters for the cutting conditions. These are summarised in Table 4.4.

Table 4.4 Structural, machining and simulation parameters

| Preloaded Structural Parameters | | Machining Parameters | |
|---|---|---|---|
| Natural frequency | 142.1 Hz | Tool diameter | 16 mm |
| Damping ratio | 0.88 % | Number of teeth | 4 |
| Stiffness | $24.3\times10^6\ Nm^{-1}$ | Tool helix angle | 30° |
| Flexible Robot Parameters | | Material | Al-7075-T6 |
| Natural frequency | 23 Hz, 47 Hz | Cutting stiffness $K_r$ | $205\times10^6\ Nm^{-2}$ |
| Damping ratio | 4.3 %, 2.9 % | Cutting stiffness $K_t$ | $768\times10^6\ Nm^{-2}$ |
| Stiffness | $0.79\times10^6\ Nm^{-1}$, $2\times10^6\ Nm^{-1}$ | Milling type | Down milling |
| Time Domain Simulation Parameters | | Radial depth of cut | Half immersion |
| Iteration per revolution | 512 | Feed per tooth | 0.05 mm |
| Number of tool cycle | 50 | | |
| Sample per iteration | 8 | | |
| Axial tool layers | 30 | | |

In order to evaluate the performance of different control methods and tune controller parameter(s), two problems can be addressed. Taking DVF control method as an example, increasing the controller gain can theoretically improve performance. However, it may result in nonlinear behaviour and suboptimal performance owing to the actuator saturation, reducing the controller's performance at suppressing the chatter vibration. The second problem is that unmodelled modes of the actuator and structure can affect the control performance, leading to instability, as it is widely mentioned in the active vibration control literature.

The first problem is addressed considering the actuator saturation effect to fairly compare the all of the control strategies (in simulations) using a structured approach. Following this, the second problem is addressed by doing experimental frequency response function (FRF) testing to evaluate the vibration suppression performance of the controllers.

To fairly compare the control methods, the controller parameters are optimised using self-adaptive differential evolution (SADE) algorithm. The details of the optimisation algorithm are given in the next section.

### 4.4.4 Self-adaptive differential evolution (SADE) algorithm and tuning approach

The self-adaptive differential evolution (SADE) algorithm is a optimisation algorithm which can adapt its control parameters using a learning period. The differential evolution (DE) algorithm is a straightforward, population-based stochastic search method for solving global optimization problems [254, 255]. Four parameters need to be defined for the traditional DE algorithm, namely; scaling factor F, crossover ratio CR, number of population NP, and the mutation strategy. The convergence time and the performance of the algorithm are considerably affected by all these parameters.

The schematic illustration of the DE algorithm is shown in Figure 4.15. Here, DVF control gain $g_{dvf}$ optimisation process is used as an example. The other control methods' gains are also optimised using the same process. The algorithm seeks the best control parameters which have the best fitness value in a population pool. The initial population is generated by uniformly distributed values from the initial vector which defines the lower and upper boundaries of the controller gains. The generation is updated utilising the mutation and crossover operations, respectively. The mutant vector **V** is generated multiplying by scaling factor **F** in mutation operation. Then, the trial vector **U** from crossover operation, and the target vector **X** chosen randomly from the current generation, are compared to select the parameters which give a better fitness value. The trial vector **U** can be defined as:

$$u^m_{n,G} = \begin{cases} v^m_{n,G}, & if \quad (rand[0,1]) \leq CR \\ x^m_{n,G}, & otherwise \end{cases} \tag{4.17}$$

where CR is the crossover ratio has range between [0,1], and $m = g_{sky}$ as a control parameter to be optimised. $u^m_{n,G}$ is the $n^{th}$ trial vector at generation $G$.

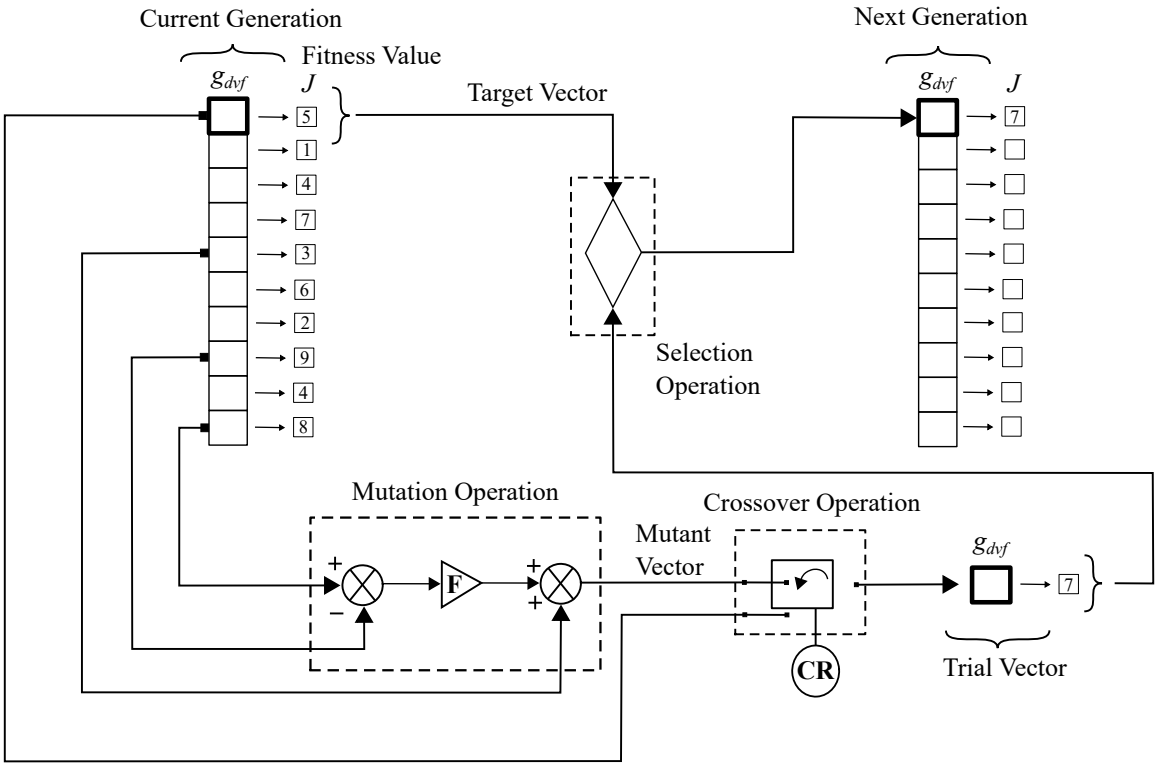


Fig. 4.15 Schematic illustration of the SADE algorithm where the DVF control gain $g_{dvf}$ optimisation process is shown

The SADE algorithm indicates the mutation strategy, crossover ratio CR, and scaling factor F by learning from the previous generation, which allows the appropriate control parameters from not only search space but also other sections in the search space [255]. The mutant vector $\mathbf{V}$ is obtained by four different mutation strategies defined as [256]:

1. rand1: $\mathbf{V}_n = \mathbf{X}_{ra} + F(\mathbf{X}_{rb} - \mathbf{X}_{rc})$
2. current-to-best2: $\mathbf{V}_n = \mathbf{X}_n + F(\mathbf{X}_{best} - \mathbf{X}_n) + F(\mathbf{X}_{ra} - \mathbf{X}_b) + F(\mathbf{X}_{rc} - \mathbf{X}_{rd})$
3. rand2: $\mathbf{V}_n = \mathbf{X}_{ra} + F(\mathbf{X}_{rb} - \mathbf{X}_{rc}) + F(\mathbf{X}_{rd} - \mathbf{X}_{re})$
4. current-to-rand: $\mathbf{V}_n = \mathbf{X}_n + F(\mathbf{X}_{ra} - \mathbf{X}_n) + F(\mathbf{X}_{rb} - \mathbf{X}_{rc})$

where $\mathbf{X}_{ra}, \mathbf{X}_{rb}, \mathbf{X}_{rc}, \mathbf{X}_{rd}, \mathbf{X}_{re}$ are the randomly chosen target vectors whilst $\mathbf{X}_n$ and $\mathbf{X}_{best}$ are the current target and the best target vectors, respectively.

Taking into consideration the success rates of the four mutation strategies, the chosen probabilities of the strategies are updated by the algorithm. The probability of each strategy is equally set initially: $\mathbf{P} = \{0.25, 0.25, 0.25, 0.25\}$. The learning period is stated by recording the number of the successful and discarded trial vectors of each mutation strategy. The probabilities are updated according to the succcess rate of the trial vectors over the first generations. Once the learning period is established, the probabilities are updated for every generation by taking into account the last generation. Similarly, the scaling factor F and crossover ratio CR which are initially taken 0.5, are also updated in the learning period for each mutation strategy since different optimal F and CR values could be indicated for each strategy. The scaling factor F is forced to keep the value between the range [0,2]. In addition, the trial vectors are also checked to keep the mutated values in the given constraint ranges $[\mathbf{X}_{min}, \mathbf{X}_{max}]$.

All controller gains given in Table 4.5, were optimised by SADE algorithm. Different initial values were performed for the lower and upper boundaries. Then, the number of generation was selected when the fitness value was settled, and it did not change. Each case were repeated several times to ensure the best performance achievement was obtained by SADE algorithm. The SADE convergences for each control method are given in Appendix A. The tuning approach and optimised control parameters are explained in the next section.

### Tuning approach

The uncontrolled stability lobe diagram (SLD) is used to illustrate the tuning approach, as shown in Figure 4.16. The SLD is plotted as a function of axial depth of cut and spindle speed. It is shown that the critical limiting depth of cut ($b_{crit}$) is approximately 1 mm: below this value, no chatter can occur at any spindle speed. Meanwhile, there are the higher stability regions, the so-called *lobes*, one of which occurs at around 2100 rpm that is the highest spindle speed of stability lobe diagram. However, around 2100 rpm the excitation frequency is close to the natural frequency of the uncontrolled stucture, which results in much higher forced vibrations.

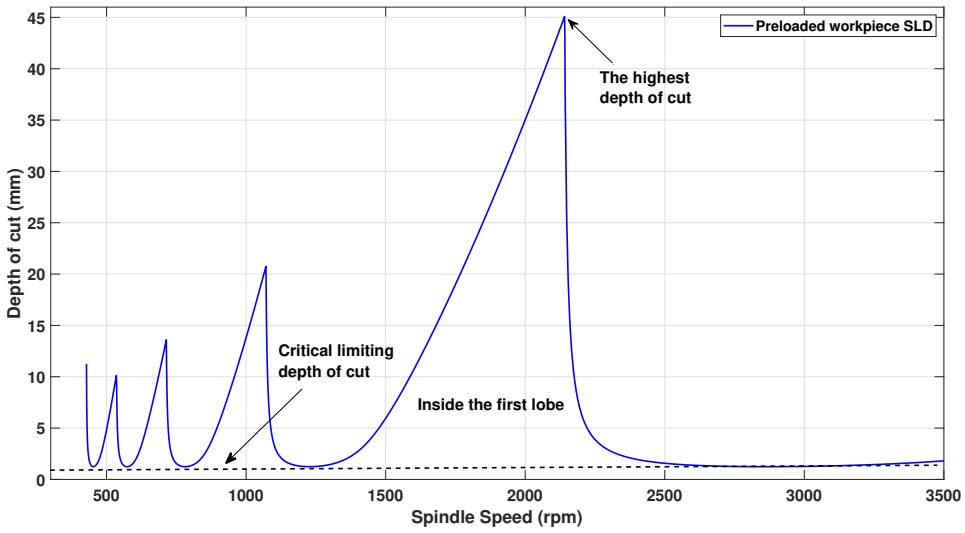


Fig. 4.16 Uncontrolled, preloaded workpiece SLD

The critical limiting depth of cut ($b_{crit}$) and the maximum depth of cut ($b_{max}$) are tuned taking into account two tuning scenarios referred as $b_{crit}$ and $b_{max}$ tuning. In $b_{max}$ tuning, the aim is to maximise the $b_{max}$ value at the spindle speed where the highest depth of cut (around 2100 rpm) illustrated on Figure 4.16 without causing actuator saturation or any instability. It should be noted that the highest spindle speed can be shifted as the controller parameters are tuned. From a practical perspective, utilising the 'lobe' effect in the SLD aims

to maximise the material removal rate. Maximising the $b_{max}$ value is important for rough milling operations where the maximum stable depth of cut is selected in the lobe.

In $b_{crit}$ tuning, the aim is to maximise the critical limiting depth of cut $b_{crit}$ at the spindle speed where the highest depth of cut since the force vibrations are much higher and the actuator saturation more likely occurs. From a practical perspective, the material removal rate is maximised at any spindle speed. Maximising the $b_{crit}$ at the spindle speed where the highest depth of cut (on Figure 4.16) can be considered as a 'worst case' scenario for the onset of saturation. Maximising the $b_{min}$ value is important for finish milling operations where the critical limiting depth of cut is selected for the possible highest spindle speed.

In order to employ this numerical optimisation, the SADE algorithm is used. The numerical optimisation is performed as follows, for two tuning scenarios:

For each candidate, the input to the optimisation problem is the set of controller gains, as summarized in Table 4.5. For example, only the scalar value $g_{dvf}$ is tuned for the direct velocity feedback scenario. The frequency domain analysis is first used to determine the spindle speed where the highest depth of cut and $b_{max}$ (or $b_{crit}$). A time domain simulation is then run at this spindle speed. If saturation is observed (defined as an actuation force exceeding 27N) then this candidate solution is assigned a fitness of zero. If not, the fitness is assigned a value equal to $b_{max}$ (or $b_{crit}$). Consequently, the iterative optimization algorithm will seek the controller gains which provide the maximum value of $b_{max}$ (or $b_{crit}$) without inducing actuator saturation.

The controller tuning process was therefore as follows:

1. Adjust the control parameters to achieve the highest possible stable depth of cut at the spindle speed where the highest depth of cut, without inducing actuator saturation, using the SADE algorithm. Actuator saturation was defined as occurring at 27 N. The process was as follows:

(a) Choose candidate controller gain values from an initial range. The control parameters that were tuned are summarised in Table 4.5.

(b) Perform frequency domain analysis using the candidate controller gains to calculate the spindle speed where the highest depth of cut and $b_{max}$ (or $b_{crit}$).

(c) Perform time domain analysis in the Simulink environment using this spindle speed and the depth of cut from the frequency domain.

(d) Check the actuator saturation occurence. If it occurs, the process starts from step (a) discarding the controller gains and assigning a fitness value of zero.

(e) If not, the fitness is assigned a value equal to $b_{max}$ (or $b_{crit}$).

A flow chart is illustrated in Figure 4.17 for the tuning process.

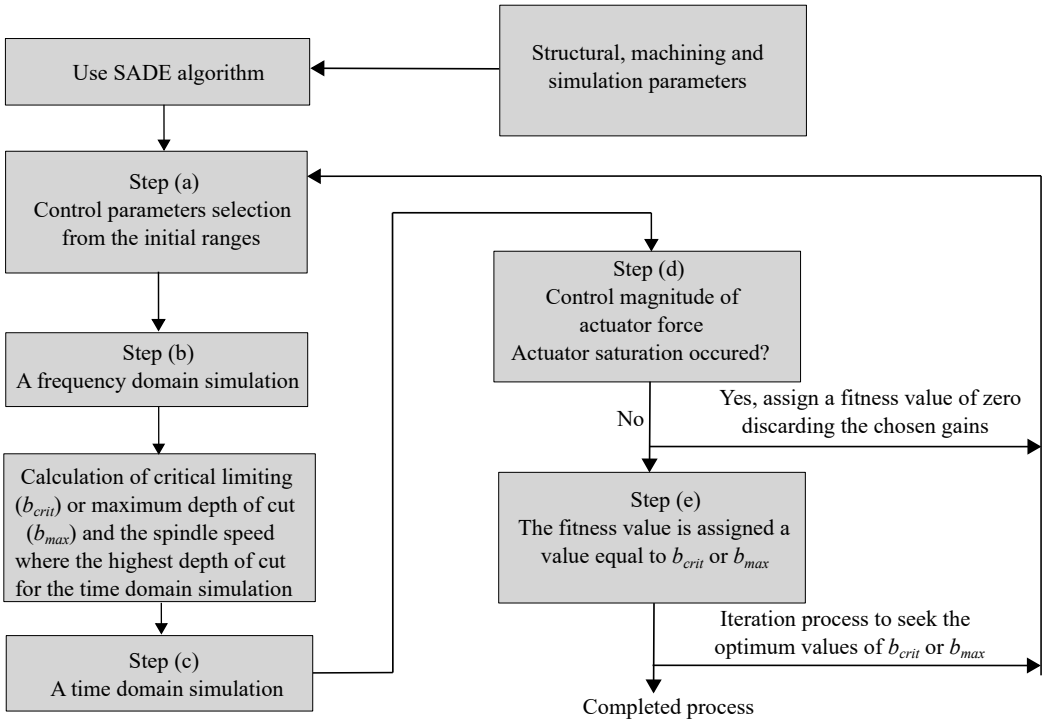


Fig. 4.17 Flow chart to illustrate the optimisation of control parameters for both tuning process

The stability lobe diagram is simulated for the controlled system once the tuning step is completed. In order to detect the actuator saturation effect, the time-domain approach

Table 4.5 Tuning parameters

| Control method | Tuning Parameters |
|---|---|
| Direct Velocity Feedback (DVF) | $g_{dvf}$ |
| Virtual Passive Absorber (VPA) | $\mu_c$ |
| Proportional Integrated Derivative (PID) | $g_a$, $g_v$, $g_p$ |
| Linear Quadratic Regulator (LQR) | $Q$, $R$ |
| $H$ Infinity ($H_\infty$) | $G_{st}$, $f_1$, $f_2$ |
| $\mu$ Synthesis | $G_{st}$, $f_1$, $f_2$ |

is performed as the saturation may occur the spindle speed different to that used for the optimisation process. A spindle speed range from 500 to 3000 rpm is evaluated at 100 rpm intervals, while 0.1 mm intervals are chosen for the depth of cut. In addition to identifying the chatter stability, the onset of actuator saturation is explored using the time-domain approach. The deph of cuts where the actuator saturation first occured were recorded at each spindle speed. Actuator saturation was defined as occurring at 27 N.

## 4.5 Simulated results for chatter stability

The simulated stability lobe diagrams (SLDs) for the $b_{crit}$ tuning scenario are illustrated in Figure 4.18. The objective is to maximise the $b_{crit}$ regardless the spindle speed. The critical limiting depth of cut is increased considerably for all control strategies. Yet, near 2100 rpm where the higher force vibrations occur, all the control methods suffer from actuator saturation. It should be noted that the saturation occurs at the critical limiting depth of cut near 2100 rpm. Consequently, the maximum stable depth of cut is reduced in the lobe region since the actuator cannot provide necessary support force to the flexible workpiece.

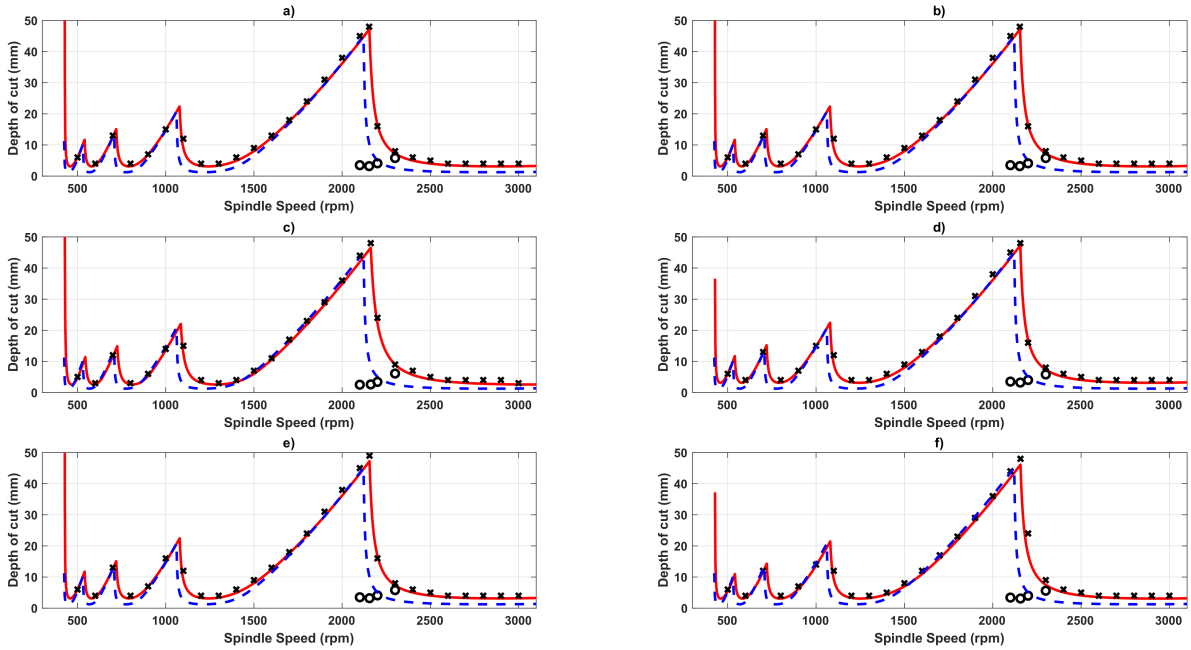


Fig. 4.18 Stability Lobe Diagrams for $b_{crit}$ tuning. Red solid (——) lines show the controlled case and blue dashed (- - -)lines show the uncontrolled case, using the frequency domain chatter prediction. Circles (◯) show the onset of saturation in the controlled case, and cross (×) symbols show the onset of chatter in the controlled case, using the time domain simulation. (a) DVF control, (b) VPA control, (c) PID control, (d) LQR control, (e) $H_\infty$ control, (f) $\mu$-synthesis control.

The predicted stability lobe diagrams (SLDs) for the $b_{max}$ tuning scenario are illustrated in Figure 4.19. The objective is to maximise the highest possible stable depth of cut considering actuator saturation. All controller strategies have similar effect on the maximum stable depth of cut. The $b_{max}$ is improved slightly. However, the improvement at the other spindle speeds is higher, for instance at 3000 rpm the critical limiting depth of cut is increased from 1.3 mm to 2.7 mm. This shows how actuator saturation effects can be very significant when taking into account the active vibration control design for chatter stability improvement.

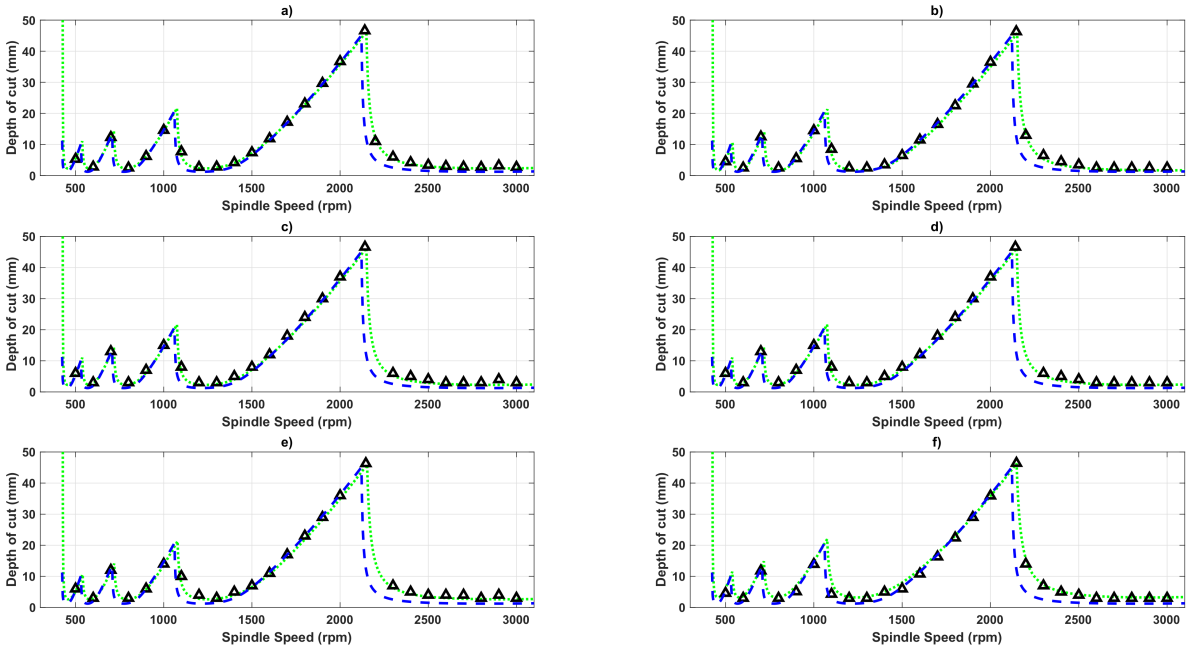


Fig. 4.19 Stability Lobe Diagrams for $b_{max}$ tuning. Green dotted (·····) lines show the controlled case and blue dashed (- - -) lines show the uncontrolled case, using the frequency domain chatter prediction. Triangle (Δ) symbols show the onset of chatter in the controlled case, using the time domain simulation. No actuator saturation usually occurs for this scenario, owing to the controller tuning methodology. (a) DVF control, (b) VPA control, (c) PID control, (d) LQR control, (e) $H_\infty$ control, (f) $\mu$-synthesis control.

To summarise these results, the control effect on the critical limiting and maximum depth of cut is given in Table 4.6, and the optimised parameters are listed in Table 4.7. The tuning scenarios are compared with two benchmarks. The 'base structure' benchmark represents the original workpiece and flexure (as illustrated in Figure 4.9. The 'Uncontrolled' benchmark takes into consideration the interface between the flexible structure and beam, even with no control force applied utilising the proof-mass actuator. The controlled scenarios are presented in Figures 4.18 and 4.19.

Table 4.6 Control effect on critical limiting and maximum depth of cut

| Control method | $b_{crit}$ (mm) | | $b_{max}$ (mm) | |
|---|---|---|---|---|
| Base structure | 0.8 | | 27.2 | |
| Uncontrolled | 1.2 | | 45.1 | |
| | $b_{crit}$ tuning | | $b_{max}$ tuning | |
| | $b_{crit}$ (mm) | $b_{max}$ (mm) | $b_{crit}$ (mm) | $b_{max}$ (mm) |
| DVF | 3.2 | 47.2 | 2.3 | 46.6 |
| VPA | 2.5 | 46.5 | 1.8 | 46.3 |
| PID | 3.2 | 47.3 | 2.3 | 46.6 |
| LQR | 3.2 | 47.2 | 2.3 | 46.6 |
| $H_\infty$ | 3.1 | 46.2 | 2.6 | 46.3 |
| $\mu$ synthesis | 3.1 | 46.7 | 2.6 | 46.7 |

Table 4.7 Control parameters for the critical limiting and maximum depth of cut

| Control method | $b_{crit}$ tuning | $b_{max}$ tuning |
|---|---|---|
| DVF | g=235 | g=135 |
| VPA | $\mu$=0.002, $\zeta$=0.027 | $\mu$=0.0004, $\zeta$=0.013 |
| PID | $g_{pa} = 1x10^{-6}$, $g_{pv} = 236$, $g_{pp} = 1x10^{4}$ | $g_{pa} = 7.52x10^{-5}$, $g_{pv} = 129$, $g_{pp} = 4.25x10^{3}$ |
| LQR | $Q_1 = 6793.3$, $R = 0.024$ | $Q_1 = 9219.8$, $R = 0.065$ |
| $H_\infty$ | $G_{st} = 4.7x10^{5}$, $f_1 = 252.7$, $f_2 = 55.8$ | $G_{st} = 5.3x10^{5}$, $f_1 = 462.8$, $f_2 = 40.6$ |
| $\mu$ synthesis | $G_{st} = 1.9x10^{7}$, $f_1 = 2659$, $f_2 = 4.37$ | $G_{st} = 1.7x10^{7}$, $f_1 = 3035.04$, $f_2 = 3.02$ |

## 4.6 Experimental validation - frequency response function (FRF) testing

The test setup illustrated in Figure 4.20 is designed for the FRF validation experiments. The designed flexible structure is clamped to the ground and a shaker is run to excite the structure by a harmonic chirp signal. The beam is positioned to support the workpiece by a preload force. LMS software is used to process the frequency response of the structure using the data measured by the force and accelerometer sensors. In order to suppress the vibration of the structure, the measured accelerometer is converted velocity/displacement to implement

corresponding controller types using Simulink software. The feedback control system is provided by a multi-channel IO-card (NI PCIe-6321) using a sampling period of 50 $\mu$s. Once the acceleration data is processed by the control system, a control voltage is sent from control PC in real-time to drive the actuator.

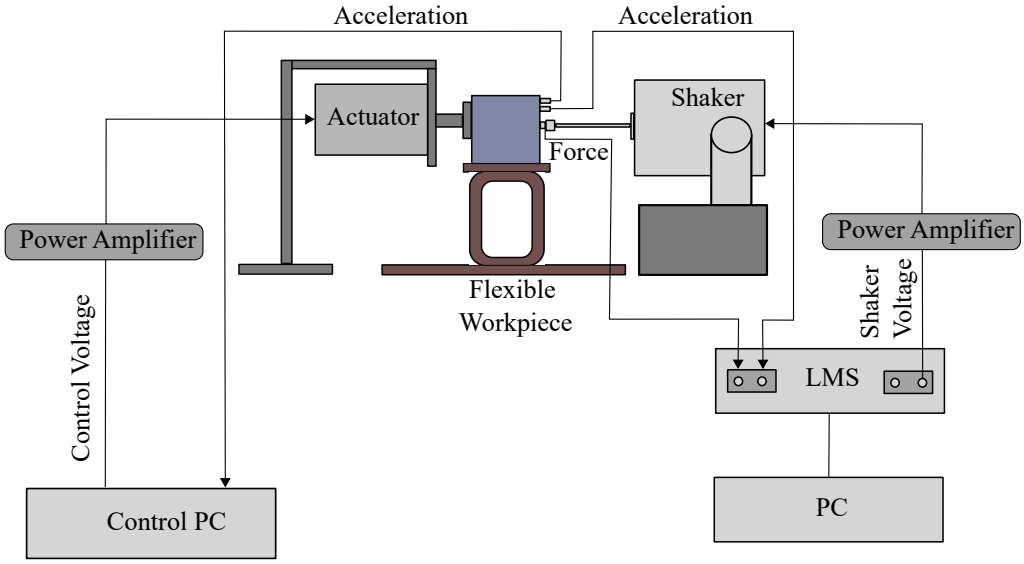


Fig. 4.20 Test setup for the experimental FRF measurement

The resulting performance is compared to the theoretical predictions in Figure 4.21.

All the experimental FRF results match well with the simulated FRF results, although some additional modes of vibration are observed in the experimental data at higher frequencies. These could be associated with unmodelled modes of vibration or actuator dynamics.

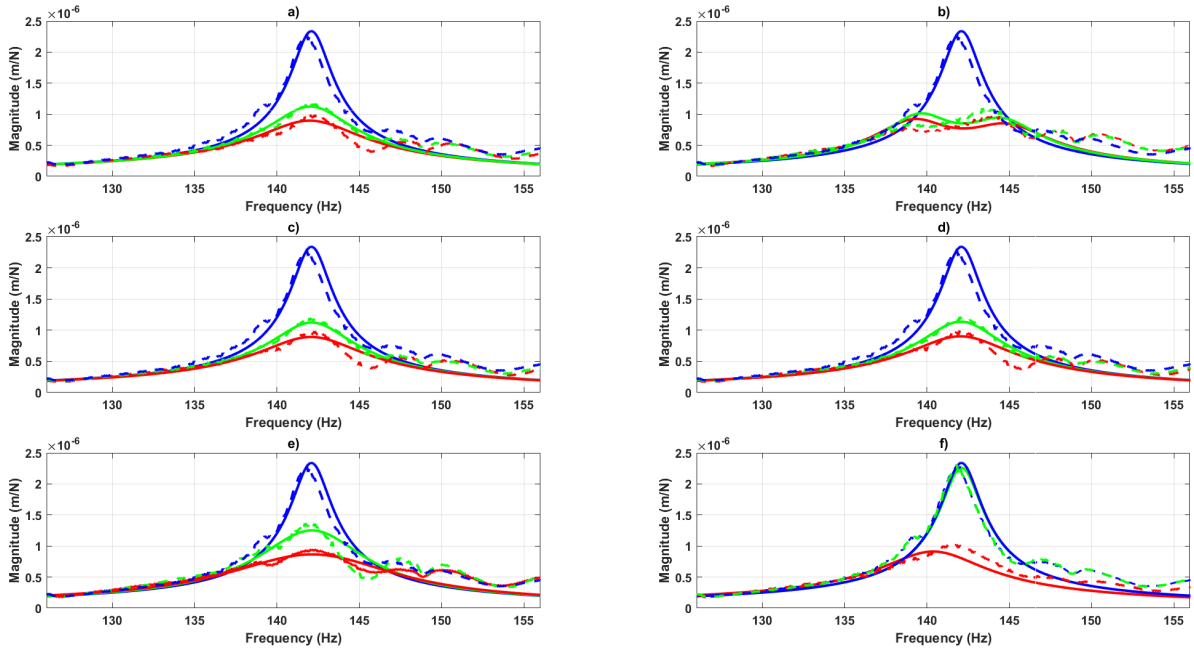


Fig. 4.21 Simulated and experimental FRF results. Red (——) lines show the $b_{crit}$ tuning, green (——) lines show the $b_{max}$ tuning, and blue (——) lines show the uncontrolled case. Solid lines show the theoretical predictions while the dashed lines show the experimental FRFs. (a) DVF control, (b) VPA control, (c) PID control, (d) LQR control, (e) $H_\infty$ control, (f) $\mu$-synthesis control.

## 4.7 Discussion

Some aspects of the results merit further discussion.

### 4.7.1 $\mu$-synthesis control

Robust control using the $\mu$-synthesis method can consider uncertainties in the control model. The uncertainty ($\Delta_{act}$) for the actuator was added as 20% dynamic (frequency-dependent) uncertainty around the natural frequency of the structure. Meanwhile, the structural uncertainty ($\Delta_{sys}$) was added as 20% parametric (real) uncertainty for the modal

parameters of the flexible workpiece. The $\mu$-synthesis method can be beneficial controller as the workpiece dynamics can be changed due to the material removal, also the robot's dynamic variation owing to the robot's posture change during milling. The bode diagram is illustrated in Figure 4.22 showing the models with uncertainties. To calculate the optimum $\mu$ value, $D, G-K$ iteration procedure is utilised as the uncertainties are the frequency-dependent and real uncertainties. $1/\mu$ times uncertainty can be covered by the controller, and the controller can achieve the performance target. The $\mu$-synthesis controller parameters can be selected the same with the $H_\infty$ control adjusting the uncertainty level until the $\mu$ value gets close to 1. Yet, the uncertainty level is kept fixed optimising the controller parameters by SADE algorithm as suggested in the literature [239]. The optimised control parameters were listed in Table 4.7 for both scenarios.

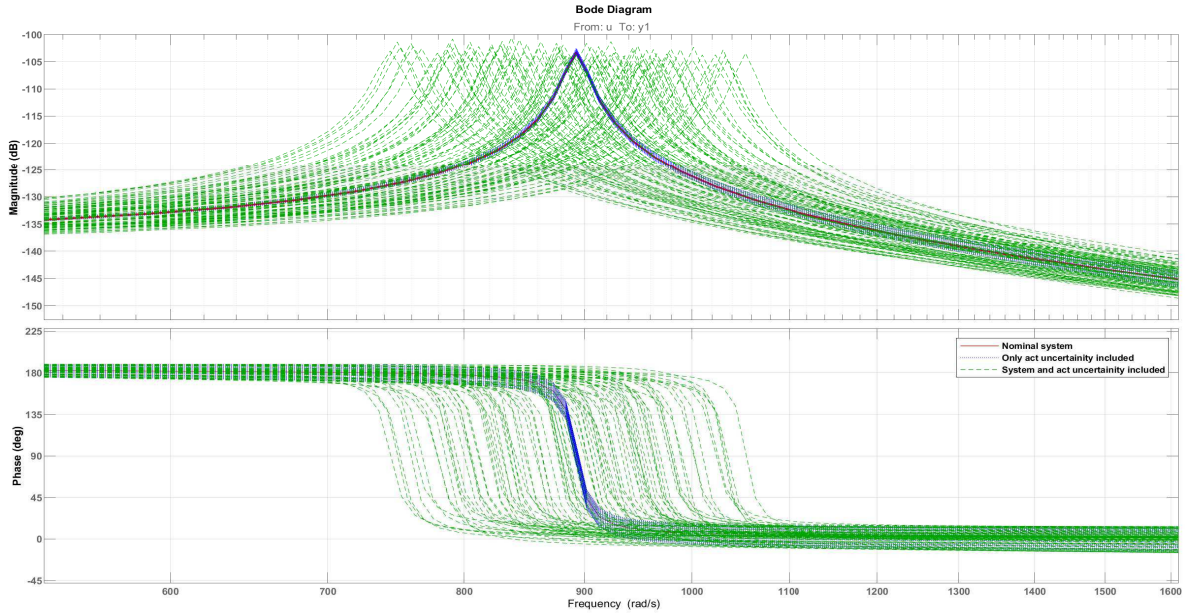


Fig. 4.22 The model with uncertainties. Nominal system (——), only actuator uncertainty included (------), system and actuator uncertainty included (- - -)

### 4.7.2 Practical implementation

A real robot would be required to carry out the robotic-assisted active vibration control concept in practice instead of the simplified beam structure illustrated in Figure 4.9(a). In addition to the modes that were considered for the model and test setup, additional modes could be observed when utilising the real robot. Therefore, further frequency response function (FRF) tests would be needed to make sure these modes of vibration did not destabilise the control system.

However, the contact location between the end-effector and the flexible workpiece could be repositioned by the real robot. This would bring out new possibilities for adaptive control since the real robot moves with the cutting tool along the machining workpiece surface. Controller re-tuning may also be required as material is removed from the workpiece, which also affects the contact location of the tool. The $\mu$ synthesis control system becomes more beneficial when considering the associated uncertainties.

Altintas and Budak's zero-order approach is used to predict the chatter stability boundaries as it is a widely accepted, fast, and accurate method. Although the other chatter models such as semi or full-discretisation methods [35] could be chosen, the same chatter boundaries would be predicted. However, choosing a different prediction method would result in longer computation time for chatter boundary prediction and optimisation of the controller parameters.

The loss-of-contact issue may occur between the end-effector and flexible workpiece. Adjusting the position of the robot can be a solution to provide sufficient static preload force that exceeds the amplitude of the dynamic forces generated by the proof mass actuator. Nonetheless, the force vibrations could also induce the loss-of-contact during the machining operations, which would result in nonlinear behaviour and degrade the performance of the active control system.

The actuator bandwidth is an another limitation to take into account. If the chatter or structure frequencies exceed the actuator bandwidth, the controller cannot improve the chatter stability. Yet, in these scenarios at very low spindle speeds the onset of chatter is less likely due to the process damping phenomenon [257].

Finally, different type of end-effectors could be designed for the proposed method. In the present study, a metallic rigid contact type was chosen. However, alternative contact configurations could be used, a rolling element as a flexible contact could be chosen to provide continuous motion of the end-effector during machining. Such changes would also affect the control system, now that the force transmission between the proof-mass actuator and the flexible structure would be influenced.

### 4.7.3 Actuator saturation

The actuator saturation occurs at the depth of cuts where the force vibrations are higher and do not have constant force profile. The constant force profile is obtained at depth of cut and its multiples [8]:

$$a_{constant} = \frac{\pi d}{\tan(\gamma) N_t} \tag{4.18}$$

where $a_{constant}, d, \gamma, N_t$ are the depth of cut where the constant force profile, diameter of the tool, helix angle, and number of teeth, respectively.

The predicted SLDs for the $b_{crit}$ are illustrated in Figure 4.18. The objective is to maximise the $b_{crit}$ regardless the spindle speed. The $b_{crit}$ is improved significantly for all control strategies. However, all the control methods suffer from actuator saturation near 2100 rpm where the force vibrations are much higher. It should be noted that the saturation occurs at the critical limiting depth of cut near 2100 rpm. The aim is to find the onset of saturation. The simulation is not run for the depth of cuts higher than the depth of cut where the saturation occurs. When the higher depth of cuts are simulated to find the saturation,

saturation islands are found in the first lobe, as illustrated in Figure 4.23. The saturation islands are predicted when the DVF control method is applied. There is a saturation-free region between two large saturation islands. That means there is a region that can be used for the milling without saturation. Using the information of the location of the saturation islands can help to improve the productivity of the machining. That also helps to protect the actuator by choosing the cutting parameters from the saturation-free region. Furthermore, the prediction of saturation islands can be modelled in frequency domain. A saturation prediction model is proposed and explained in detail in Chapter 5.

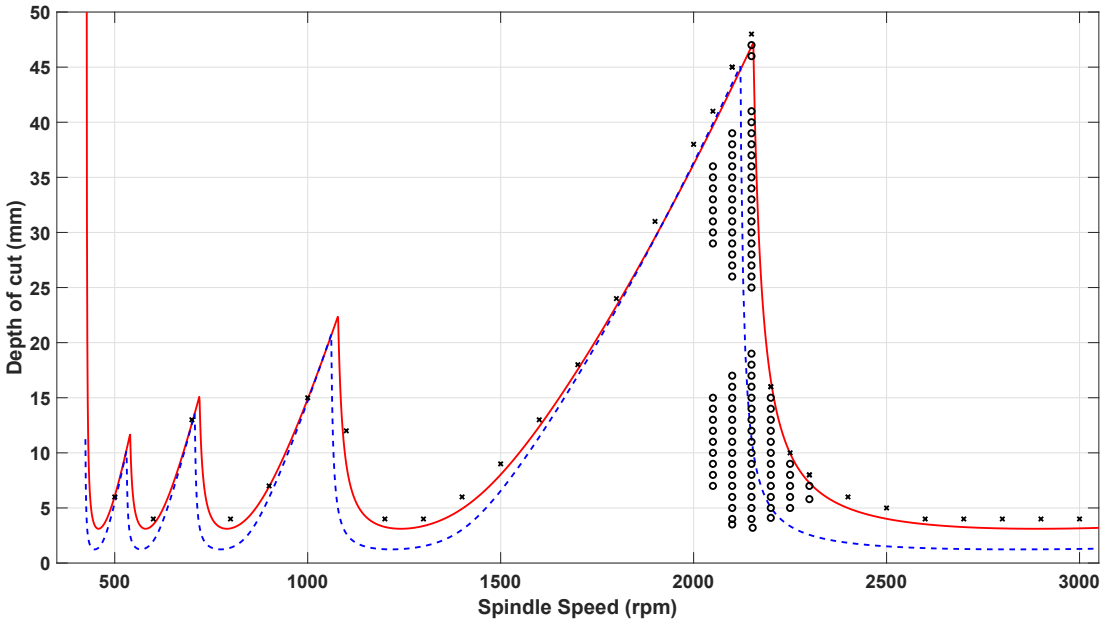


Fig. 4.23 Saturation islands for DVF control. Red solid (——) lines show the controlled case and blue dashed (- - -)lines show the uncontrolled case, using the frequency domain chatter prediction. Circles (◯) show the saturation in the controlled case, and cross (×) symbols show the onset of chatter in the controlled case, using the time domain simulation.

## 4.8 Summary

This chapter introduces the analysis of the concept of the robotic-assisted milling where an actively controlled robotic arm supports a flexible structure while it is machined by a machine tool to suppress and improve the regenerative chatter. Six different control methods which

are direct velocity feedback (DVF), virtual passive absorber (VPA), proportional integral derivative (PID), linear quadratic regulator (LQR), H infinity ($H_\infty$), and $\mu$ synthesis, are applied in robotic-assisted milling. In order to evaluate the feasibility of the method, a proof-mass (inertial) actuator is assembled to a beam which emulates the dynamic behaviour of the robotic arm to improve the dynamic response of a flexible structure. A numerical optimisation method called self-adaptive differential evolution (SADE) algorithm is used to optimise the controller gains to obtain the best performance in terms of chatter suppression ($b_{min}$ and $b_{max}$). Finally, the performance of each controller is evaluated with the experimental frequency response functions (FRFs) and predicted stability lobe diagrams (SLDs) considering a milling scenario. It is shown that the concept can improve the chatter stability and also can increase the criticial limiting depth of cut significantly, comparing to the scenario where the robot has no active control applied.

In this chapter, several objectives of the theses are achieved. Firstly, the performance of the chosen actuator is evaluated numerically. Secondly, a test system is designed to explore the dynamic performance of the actuator employing many standard control methods. Then, the SLDs are predicted to show the improvement of $b_{crit}$ and $b_{max}$ by applying all control methods for a specific milling scenario. Finally, the challenges with the proposed configuration, such as loss-of-contact, end-effector stiffness/damping, robot's dynamic nonlinearity, and the actuator saturation are addressed.

# Chapter 5

# Actuator Saturation Model in Frequency Domain

## 5.1 Introduction

In chapter 4 the robotic-assisted milling concept is explained. Six different control methods are applied to control the vibration of the cutting operation. The controller gains are optimised using SADE algorithm considering the worst case scenario in terms of actuator saturation. The critical limiting depth of cut increased significantly, however, all the controller types suffered from actuator saturation, shown in Figure 4.18. The saturation points were indicated by a time-domain model for each control method. The aim is to find the onset of saturation. The simulation is not run for the depth of cuts higher than the depth of cut where the saturation occurs. When the higher depth of cuts are simulated to find the saturation, saturation islands are found in the first lobe, as illustrated in Figure 4.23. Using the information of the location of the saturation islands can help to improve the productivity of the machining. That also helps to protect the actuator by choosing the cutting parameters from the saturation-free region. In this chapter, an actuator saturation model in frequency-domain is proposed that builds upon the surface location error model by Schmitz [258, 259]. The comparison with

the time-domain model and the details of the frequency-domain model are explained in the next sections.

## 5.2 Frequency-domain solution

The stability lobe diagram (SLD) prediction using the zero-order approach proposed by Budak and Altintas [24, 26] was described in Chapter 3. They analysed the milling model expanding the time-varying force coefficients into Fourier series. Here, an actuator force model in frequency-domain is proposed utilising the Fourier series. The model provides a picture of the role of actuator force saturation islands in active vibration control in milling.

In order to predict the actuator saturation islands using a frequency-domain model, two assumptions are made. First, the actuator force only acts on $y$ direction while the feed direction is $x$. Second, the regeneration effect is neglected in stable machining. Based on the assumptions, the following steps are determined:

1. Calculate the cutting force in $y$ direction in the frequency-domain, $F_y(w)$, using a Fourier series.

2. Determine the displacement $Y(w)$ in $y$ direction in the frequency-domain, multiplying $F_y(w)$ by the structure FRF in $y$ direction.

3. Apply inverse fourier transform to $Y(w)$ in order to calculate the $y(t)$, vibration in time-domain.

4. Find the voltage value implemented by the control method using the $y(t)$. For instance, calculate the velocity of the structure using $y(t)$, then multiply the velocity by the gain $g_{dvf}$ to find the voltage for the DVF control.

5. Calculate the actuator force utilising the voltage value.

### 5.2.1 Fourier force model

The tangential $F_t$ and normal $F_n$ cutting forces can be expressed as:

$$\begin{aligned} F_t(\theta) &= K_t b h(\theta) + K_{te} b \\ F_n(\theta) &= K_n b h(\theta) + K_{ne} b \end{aligned} \tag{5.1}$$

where $K_t$, $K_{te}$, $K_n$, and $K_{ne}$ are the tangential, tangential edge, normal, and normal edge cutting coefficients, respectively. $b$ and $h$ represent the axial depth of cut and chip thickness.

The cutting force in $y$ direction, $F_y(\theta)$ can be expressed as:

$$\begin{aligned} F_y(\theta) = -b\Bigg[ &\frac{-K_t f_t}{2} \sum_{j=1}^{N_t} g(\theta_j)(1-\cos(2\theta_j)) + \frac{K_n f_t}{2} \sum_{j=1}^{N_t} g(\theta_j)(\sin(2\theta_j)) \\ &- K_{te} \sum_{j=1}^{N_t} g(\theta_j)\sin(\theta_j) + K_{ne} \sum_{j=1}^{N_t} g(\theta_j)\cos(\theta_j) \Bigg] \end{aligned} \tag{5.2}$$

where $f_t$ and $N_t$ are the feed per tooth and total number of teeth, respectively. $g(\theta_j)$ is the switching function which is previously defined in Eq. 3.17. The angle of each tooth, $j$, at any instant in time is $\theta_j = \omega t + \frac{2\pi}{N_t}(j-1)$, (rad), where $\omega$ is the spindle rotation frequency (rad/s).

The cutting force in $y$ direction, $F_y$, can be written using the equivalent Fourier series once the Fourier coefficients, $a_n$ and $b_n$, are calculated.

$$F_y(\theta) = \sum_{j=1}^{N_t} \left[ a_0 + \sum_{j=1}^{\infty} (a_n \cos(n\theta_j) + b_n \sin(n\theta_j)) \right] \tag{5.3}$$

The $a_0$ term can be calculate using Eq. 5.4, where the full revolution of the cutting tool is divided into three parts. $\theta_1$ represents the entry angle in down milling or exit angle in up milling.

$$a_0 = \frac{1}{2\pi}\int_0^{2\pi} F_y(\theta)\,d\theta = \frac{1}{2\pi}\left[\int_0^{\theta_1} F_y(\theta)\,d\theta + \int_{\theta_1}^{\pi} F_y(\theta)\,d\theta + \int_{\pi}^{2\pi} F_y(\theta)\,d\theta\right] \tag{5.4}$$

If a down milling operation is considered, only the middle integral term is nonzero in Eq. 5.4 according to the tool engagement, and after the integration process is performed, Eq. 5.5 is obtained. Otherwise, in up milling, only the first integral term is nonzero, and the integration limits become zero to $\theta_1$ in Eq. 5.5.

$$a_0 = -\frac{bN_t}{2\pi}\left[-\frac{K_t f_t \theta}{2} + \frac{K_t f_t}{4}\sin(2\theta) - \frac{K_n f_t}{4}\cos(2\theta) + K_{te}\cos(\theta) + K_{ne}\sin(\theta)\right]_{\theta_1}^{\pi} \tag{5.5}$$

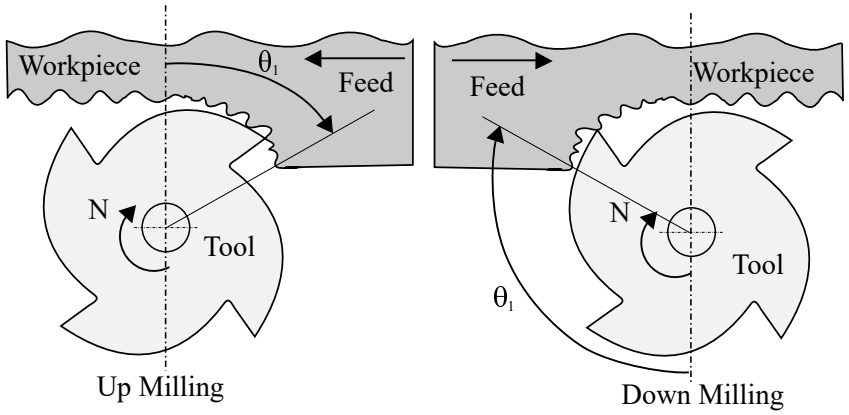


Fig. 5.1 Angles for the integrals considering the milling type

The coefficients $a_n$ and $b_n$ can be determined as:

$$a_n = \frac{1}{\pi}\int_0^{2\pi} F_y(\theta)\cos(n\theta)\,d\theta \tag{5.6}$$

$$b_n = \frac{1}{\pi}\int_0^{2\pi} F_y(\theta)\sin(n\theta)\,d\theta \tag{5.7}$$

Similar to Eq. 5.4, the integrals can be partitioned for the $\theta$ and $\pi$ angles. Following the same recursive patterns of the integration, the equations can be determined for $n = 3,4,5,....$ The Fourier series coefficients $a_1, a_2, a_3, ...$ and $b_1, b_2, b_3, ...$ are given in Appendix B.

In order to represent the milling forces taking into account the helix angle $\gamma$, the tool can be sectioned into $A$ axial slices. Each slice is assumed to have a zero helix angle, and the slices are rotated relatively to the another slice by the angle $\chi = \frac{2db\tan(\gamma)}{d}$, (rad), where $db$ and $d$ are the slice height and the tool diameter, respectively. Then, the Fourier series can now be expressed as:

$$F_y(\theta) = \sum_{i=1}^{A}\sum_{j=1}^{N_t}\left[a_0 + \sum_{n=1}^{\infty}(a_n\cos(n\theta_j) + b_n\sin(n\theta_j))\right] \tag{5.8}$$

where $\theta_j = \omega t + \frac{2\pi}{N_t}(j-1) - \chi(i-1)$. The force can be accurately determined by the higher number of slices.

## 5.3 Frequency-domain actuator saturation islands

The five steps explained in section 5.2 to find the actuator saturation islands are followed for each controller type. Since all the control methods suffer from actuator saturation around the spindle speed where the highest depth of cut, the spindle speed range between 1700 rpm and 2200 rpm is selected to determine the saturation effect on the stability improvement. The spindle speed range is scanned with 50 rpm intervals while the axial depth of cut interval is 0.5 mm from zero to the stability boundary, highlighted with a dashed box in Figure 5.2.

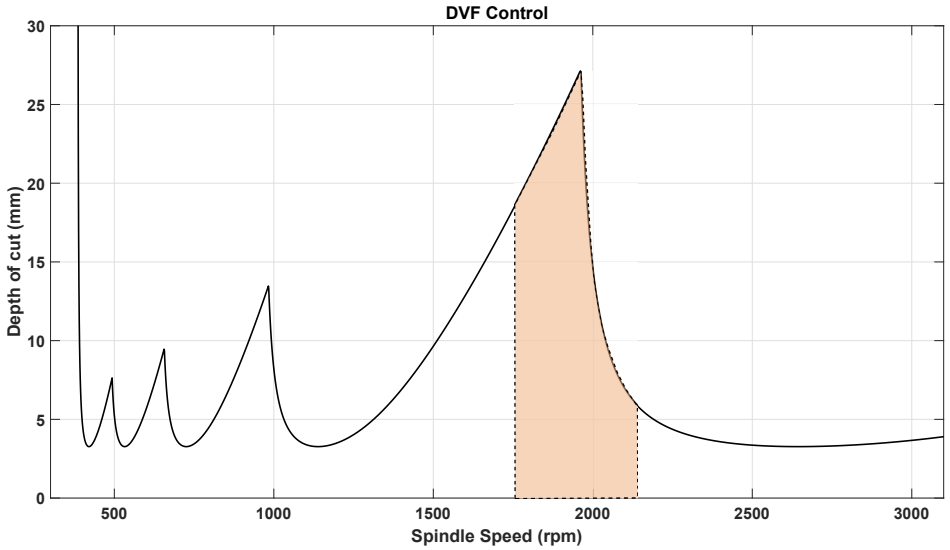


Fig. 5.2 Actuator saturation island target on SLD, DVF controlled system

The structural parameters are shown in Table 5.1. All the controller parameters are optimised utilising the $b_{crit}$ tuning method explained in section 4.4.3.

Table 5.1 Structural, machining and simulation parameters

| Preloaded Structural Parameters | | Machining Parameters | |
|---|---|---|---|
| Natural frequency | 128.1 Hz | Tool diameter | 16 mm |
| Damping ratio | 1.48 % | Number of teeth | 4 |
| Stiffness | $1.13\times10^{7}\ Nm^{-1}$ | Tool helix angle | 30° |
| Flexible Robot Parameters | | Material | Al-7075-T6 |
| Natural frequency | 23 Hz, 47 Hz | Cutting stiffness $K_r$ | $180\times10^{6}\ Nm^{-2}$ |
| Damping ratio | 4.3 %, 2.9 % | Cutting stiffness $K_t$ | $660\times10^{6}\ Nm^{-2}$ |
| Stiffness | $0.79\times10^{6}\ Nm^{-1}$, $2\times10^{6}\ Nm^{-1}$ | Milling type | Down milling |
| Simulation Parameters | | Radial depth of cut | Half immersion |
| Iteration per revolution | 512 | Feed per tooth | 0.05 mm |
| Axial tool layers | 30 | | |

The saturation islands in frequency-domain for each control method are illustrated in Figure 5.3. The actuator saturation occurs at the depth of cuts where the force vibrations are higher and do not have constant force profile. The constant force profile is obtained at depth of cut and its multiples [8]:

$$a_{constant} = \frac{\pi d}{\tan(\gamma) N_t} \tag{5.9}$$

where $a_{constant}, d, \gamma, N_t$ are the depth of cut where the constant force profile, diameter of the tool, helix angle, and number of teeth, respectively.

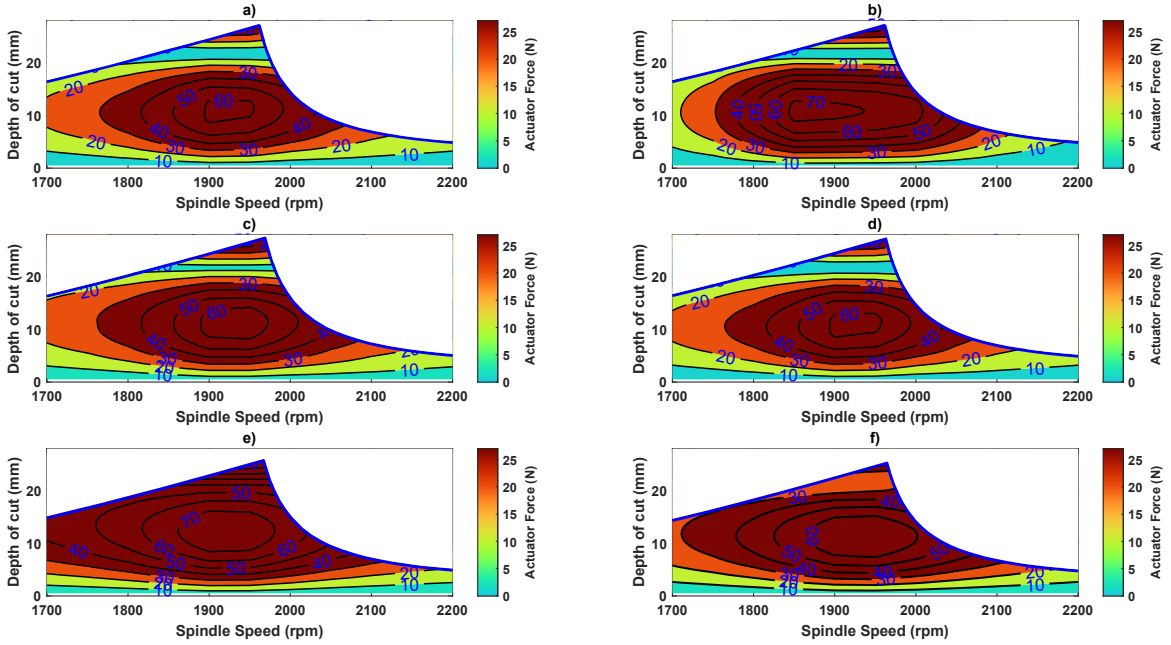


Fig. 5.3 Actuator saturation islands in frequency-domain for each control method. (a) DVF control, (b) VPA control, (c) PID control, (d) LQR control, (e) $H_\infty$ control, (f) $\mu$-synthesis control.

The saturation islands in time-domain for each control method are illustrated in Figure 5.4. To indicate the saturation islands in time-domain, the Simulink model which is used for the optimisation process of the controller parameters and depicted in Figure 4.14, is utilised. The same spindle speed range is scanned with 50 rpm intervals while the depth of cut interval is 0.5 mm from zero until the chatter occurence. Also, a simulation is run at the spindle speed where the highest depth of cut to find saturation occurs. The depths of cut where the saturation occurs, are indicated by circles ($\circ$), and cross ($\times$) symbols show the onset of chatter.

Table 5.2 The saturation occurence depths of cut at the spindle speed (around 1970 rpm) where the highest depth of cut

| Control method | Frequency-domain (Proposed method) | Time-domain |
|---|---|---|
| DVF | 3.4 | 3.3 |
| VPA | 2.9 | 2.8 |
| PID | 3.4 | 3.4 |
| LQR | 3.4 | 3.3 |
| $H_\infty$ | 3 | 3.2 |
| $\mu$ synthesis | 3 | 3.4 |

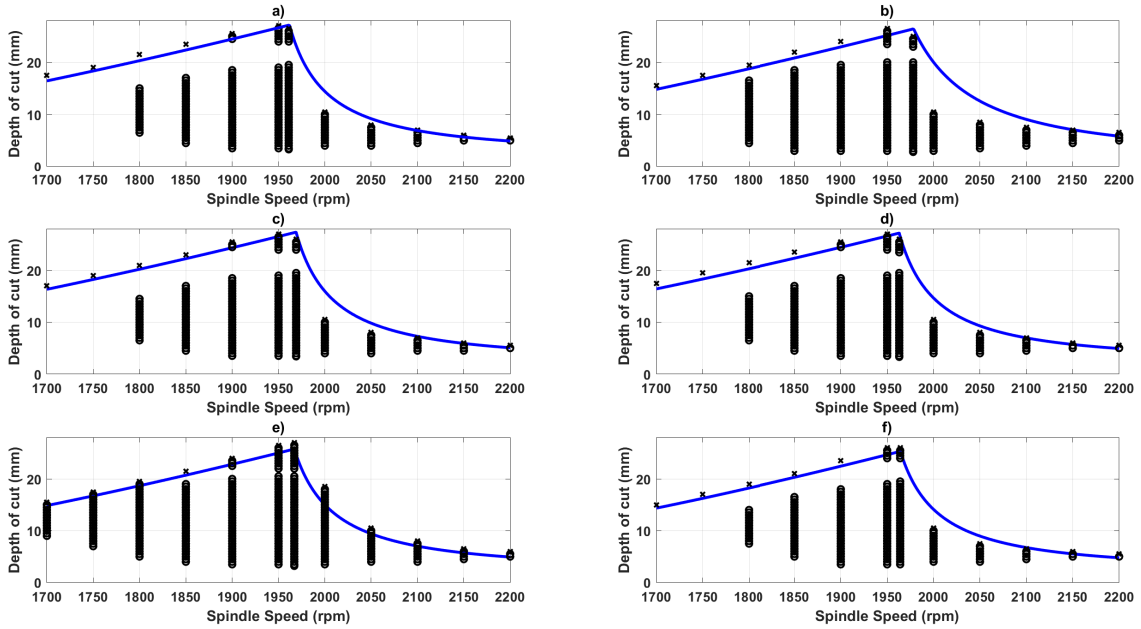


Fig. 5.4 Actuator saturation islands in time-domain for each control method. (a) DVF control, (b) VPA control, (c) PID control, (d) LQR control, (e) $H_\infty$ control, (f) $\mu$-synthesis control.

The saturation occurence depths of cut for the frequency and time-domain methods are shown in Table 5.2. The table shows the depth of cut where the saturation starts at the spindle speed (around 1970 rpm) where the highest depth of cut. It is seen that the saturation islands in frequency-domain match with the time-domain results. Since the frequency-domain predictions neglect the regeneration, only stable conditions are predicted considering the forced vibrations.

## 5.4 Discussion

It is seen that the saturation islands in frequency-domain match with the time-domain results in Table 5.2. However, the actuator saturation occurs until a point in the lobe and then it occurs again until the stability boundary. For instance, the actuator saturation occurence starts around 3.4 mm until around 18.5 mm at the spindle speed where the highest depth of cut, DVF controlled structure. There is an unsaturated stable area between 18.5 mm and 25 mm, where the actuator force is under 27 N. The second saturation island starts from 25 mm until the stability boundary. Since the total tool length does not engage with the cut at the same instant due to the helix angle, which affects the cutting process according to the type of the milling, the saturation islands occur for a specific spindle speed range and depth of cut. This occurs as the saturation islands are determined by the time dependent vibration in the controlled direction. Therefore, since the time dependent vibration varies due to the helix angle of the tool, the saturation islands occurs according to this pattern.

The vibration difference (between max and min value) islands are shown in Figure 5.5. It can be seen that the saturation islands determined by the time dependent vibration value and follow the same pattern. Also, the surface location errors are shown in Figure 5.6. It can be seen that it does not follow the same pattern with the saturation islands. The surface location errors are determined by the tool vibrations at the same instant, however, the actuator saturation islands have only a relation with the vibration difference between maximum and minimum values at the time instant. Figure 5.5 shows the relation with the saturation islands.

Considering the saturation islands, the cutting parameters can be selected in order to improve the material removal rate and the productivity of the cutting operation.

The computation times for both method are compared. When 5 and 10 terms of Fourier force model are used for frequency domain method, less computation time is computed by a factor of 4.6 and 2.9 comparing to time domain model, respectively. Using higher terms of Fourier force model result in more computation time for frequency domain method.

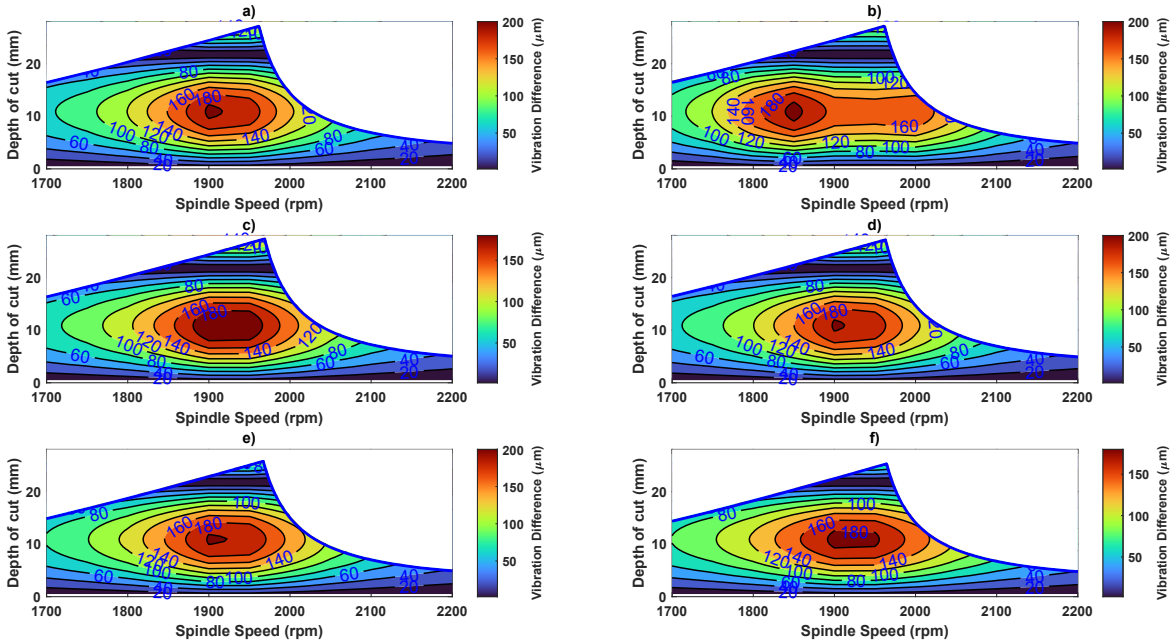


Fig. 5.5 Vibration difference islands in freq-domain for each control method. (a) DVF control, (b) VPA control, (c) PID control, (d) LQR control, (e) $H_\infty$ control, (f) $\mu$-synthesis control.

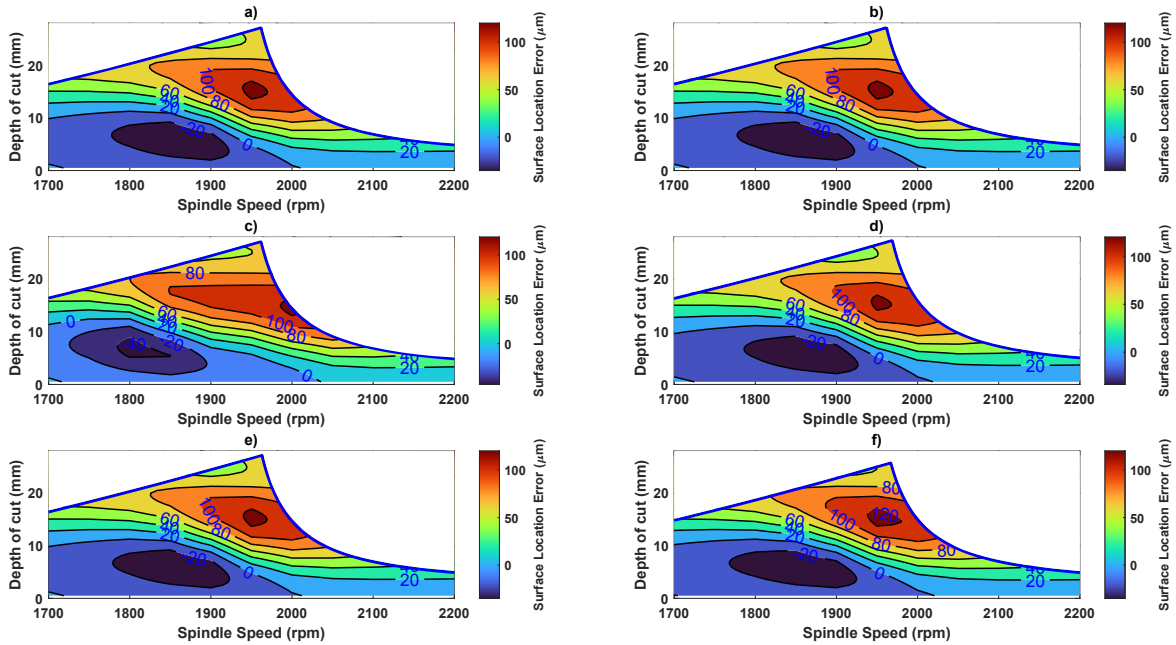


Fig. 5.6 Surface location errors in freq-domain for each control method. (a) DVF control, (b) VPA control, (c) PID control, (d) LQR control, (e) $H_\infty$ control, (f) $\mu$-synthesis control.

### 5.4.1 The effect of helix angle on saturation islands

The effect of the helix angle is considered as the cutting force profile is affected according to the helix angle of cutting tool. It is evaluated using zero and 45 degree helix angles for DVF control method. The same control parameters are utilised for the comparison of the saturation islands. Yet, It should be noted that it would be relatively higher $b_{crit}$ obtained for the tools with higher helix angle. For example, the $b_{crit}$ is improved to 3.6 mm using the tool with 45 degree helix angle.

Actuator saturation islands in frequency-domain are illustrated in Figure 5.7 and Figure 5.8 for DVF controlled structure with the same control parameters using 45 degree and zero helix angle, respectively. The number of saturation islands, their locations, and actuator forces are affected due to the helix angle which affects the delay of the cutting process. Two saturation islands occured while using the tool with 45 degree helix angle since the helix angle reduces the forced vibrations in the controlled direction and affects the delay of the cutting process. Although the same number of islands occured using 30 and 45 helix angle, the location of the islands is different. Since the forced vibrations are higher in the controlled direction while using the tool with zero helix angle, only one large saturation island is occured. That means when the saturation occurence starts, it continues until the stability boundary without any saturation free zone.

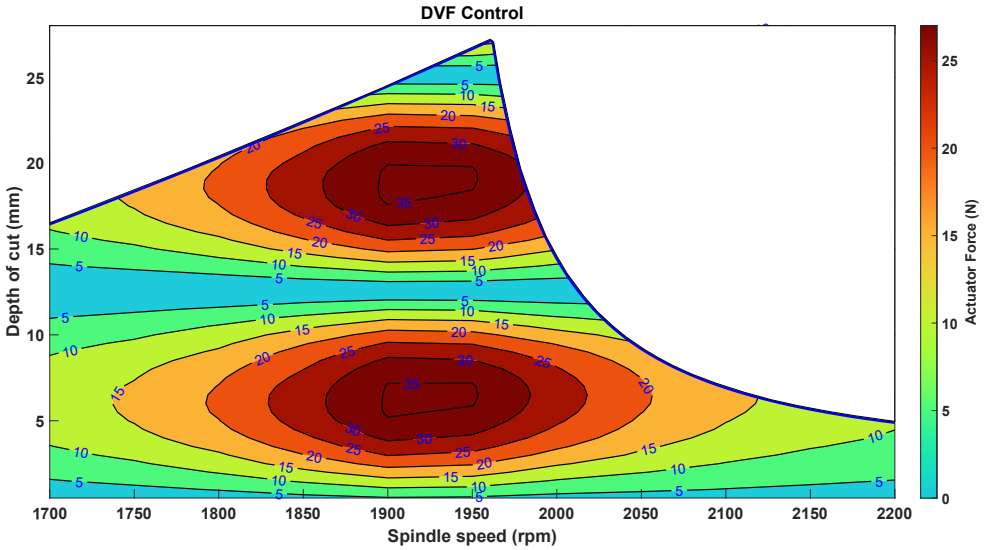


Fig. 5.7 Actuator saturation islands in frequency-domain, DVF controlled, 45 helix angle

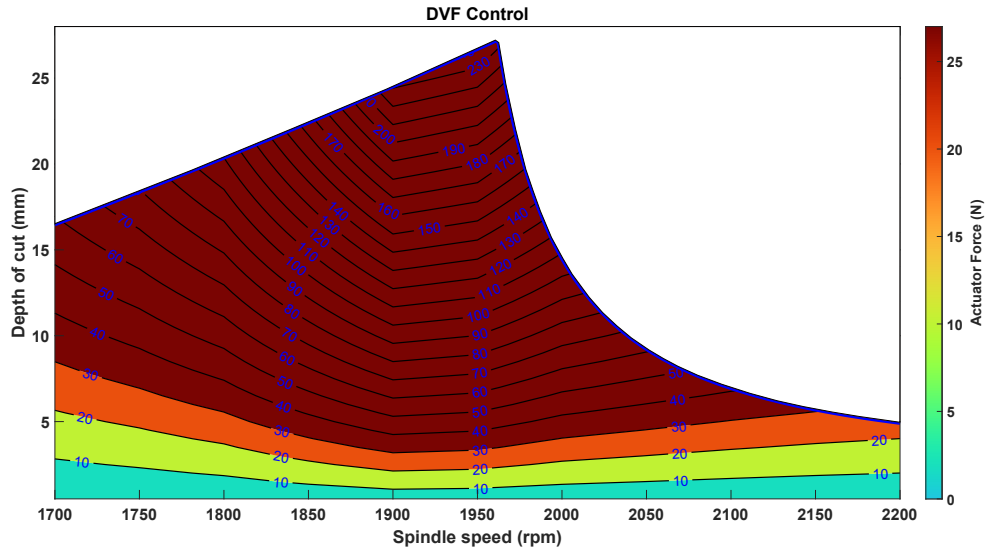


Fig. 5.8 Actuator saturation islands in frequency-domain, DVF controlled, zero helix angle

## 5.5 Summary

In this chapter, an actuator saturation model in frequency-domain is proposed by updating the surface location error model by Schmitz [258]. The regeneration effect is neglected in the model, only forced vibrations are taken into account. Fourier force model is utilised for the saturation islands considering the type of the milling. The saturation islands between 1700

rpm and 2200 rpm, where the all controllers suffer from saturation, are determined up to the stability boundary for each control method. The comparison table shown in Table 5.2 for the frequency and time-domain actuator saturation islands is presented. The table shows the depth of cut where the saturation starts at the spindle speed (around 1970 rpm) where the forced vibrations are much higher. It is seen that the saturation islands in frequency-domain (proposed method) match with the time-domain results. Besides, the effect of the helix angle on the saturation islands is presented. It is shown that the helix angle influences the location of the saturation islands, and the actuator forces since the delay of the process is affected by the helix angle of the cutting tool.

The predicted saturation islands using a cutting tool with 45 degree helix angle, are validated experimentally. The experimental results match well with the predictions. The experimental results are presented in the next chapter.

# Chapter 6

# Machining Experiments

## 6.1 Introduction

This chapter presents the machining experiments to verify the robotic-assisted concept with the real cutting conditions. Firstly, the dynamic response of the flexible structure is explored by impact hammer tests with preload provided by a beam that represents the robot's dynamic behaviour. Then, the real cutting experiments are conducted to verify the controlled SLD for each control method.

The FRF and milling experiments are presented in the next sections.

## 6.2 Frequency response function (FRF) test

To verify the effect of active vibration control, an inertial actuator specification and dynamic model are required. The FRF of the actuator is explored in section 4.2.1. A schematic illustration of the actuator frequency response function (FRF) testing setup is shown in Figure 4.7.

The simplified model of the robotic-assisted milling concept is explained in section 4.2.2. To evaluate the performance of potential benefits, a test setup is designed shown in Figure 6.1.

In order to explore the dynamic response of the structure, the impact hammer Dytran 5800B2 and and the accelerometer PCB 353B18 are used. The flexible workpiece is represented using a flexure and Al 7075-T6 block, with natural frequency, damping ratio, an stiffness values of 129.3 Hz, 1.34%, and $1.34\times10^7$ Nm$^{-1}$, respectively. The dynamic properties differ from the workpiece explained in Chapter 4 due to the clamping conditions in different work tables. The contact between robot and flexible workpiece is assumed to be rigid. Yet, the robot is not firmly attacted to the workpiece, the role of contact force is only act on the relative motion between the flexible workpiece and the robot.

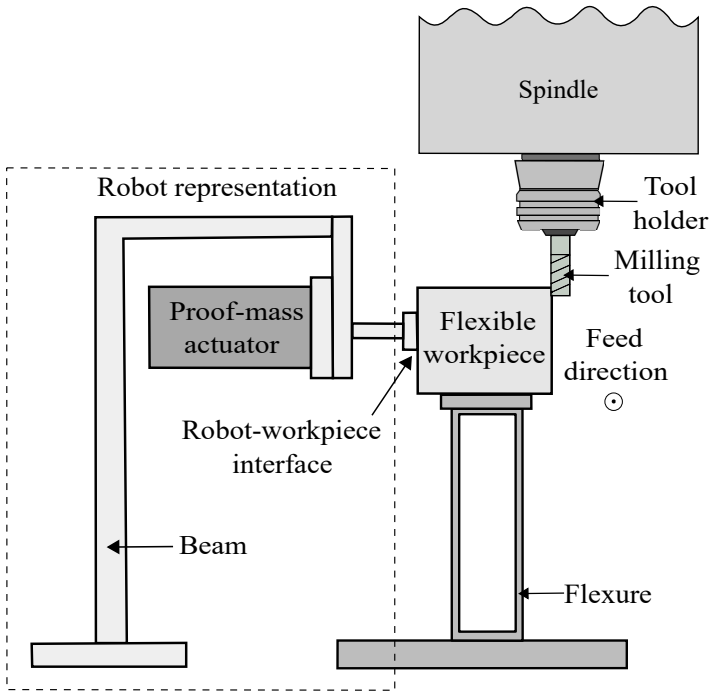


Fig. 6.1 Simplified model of the active vibration control system.

All the controller gains are optimised considering the dynamic response of the workpiece when it is supported by the robot and fixed to the CNC table. The $b_{crit}$ tuning method explained in section 4.4.3, is utilised for the optimisation process. The optimised controller gains are shown in Table 6.1

The experimental FRFs for each control method are illustrated in Figure 6.2.

Table 6.1 Tuning parameters for machining experiments

| Control method | Controller Parameters |
|---|---|
| Direct Velocity Feedback (DVF) | $g_{dvf} = 253$ |
| Virtual Passive Absorber (VPA) | $\mu_c = 0.0061$ |
| Proportional Integrated Derivative (PID) | $g_a = 9.97\times10^{-4}$, $g_v = 256$, $g_p = 2.88\times10^{4}$ |
| Linear Quadratic Regulator (LQR) | $Q = 8262.4$, $R = 0.028$ |
| $H$ Infinity ($H_\infty$) | $G_{st} = 9.92\times10^{5}$, $f_1 = 59.12$, $f_2 = 9.95$ |
| $\mu$ Synthesis | $G_{st} = 2.2\times10^{7}$, $f_1 = 4553.84$, $f_2 = 4.29$ |

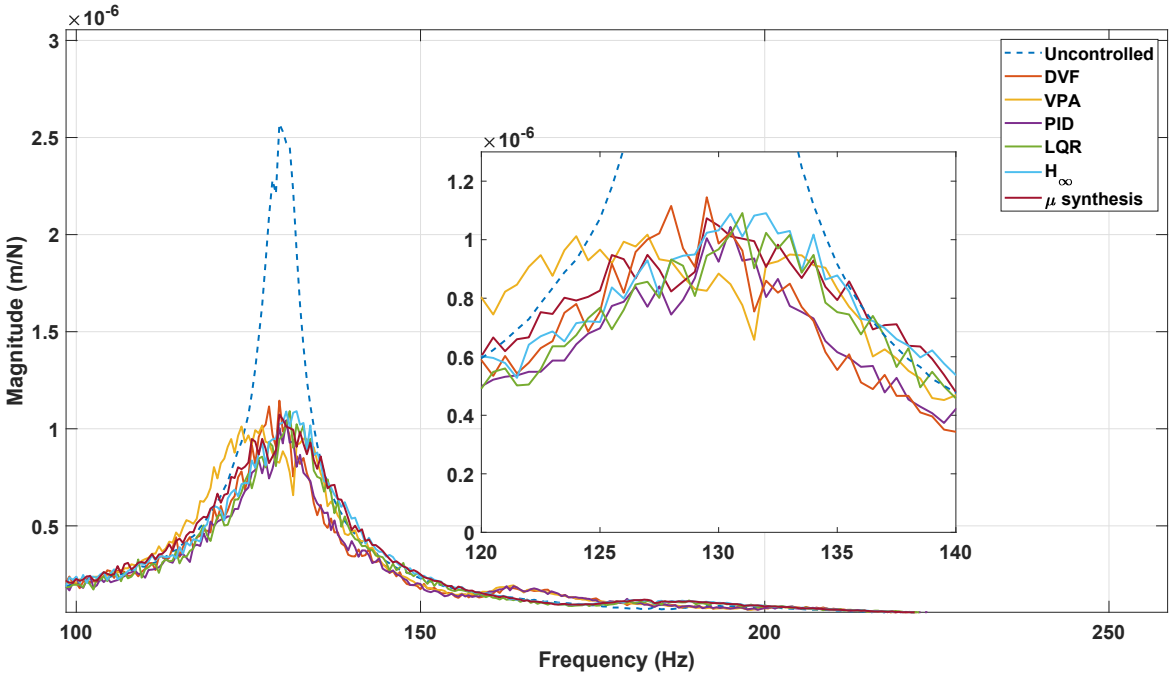


Fig. 6.2 Experimental FRFs for each control method.

## 6.3 Milling stability experiments

The chatter stability performance is evaluated experimentally. The controller gains are optimised using the dynamic response of the flexible structure when it is fixed to the CNC table. The cutting stiffnesses which are required to predict the chatter stability boundaries, were identified. Finally, several cutting tests were carried out for each control method to validate the SLDs experimentally. The details of the experiments are presented in the next sections.

### 6.3.1 Identification of the cutting force coefficients

The cutting force coefficients were identified for the milling tests. An Aluminium alloy block (40x20x150) mm, which is the same material for the verification tests, was fixed to a Kistler 9257B dynamometer to measure the cutting forces in $x$ and $y$ directions. A half immersion and down milling operation was selected for the cutting stiffness identification tests. A cutting tool with 16 mm diameter was used for the 1 mm axial depth of cut, 0.05 mm/tooth constant feed rate at 1500 rpm spindle speed.

Tool runout was determined from the cutting force results. Hence, the cutting force coefficient identification was made utilising time-domain simulation [258], instead of utilising different feed rates for the identification [232]. The cutting force coefficients in tangential ($K_t$) and radial ($K_r$) directions were indicated taking into consideration the cutting tool runout as 660 $N/mm^2$ and 180 $N/mm^2$, respectively. The time-domain simulation used for the cutting force coefficient identification is shown in Figure 6.3.

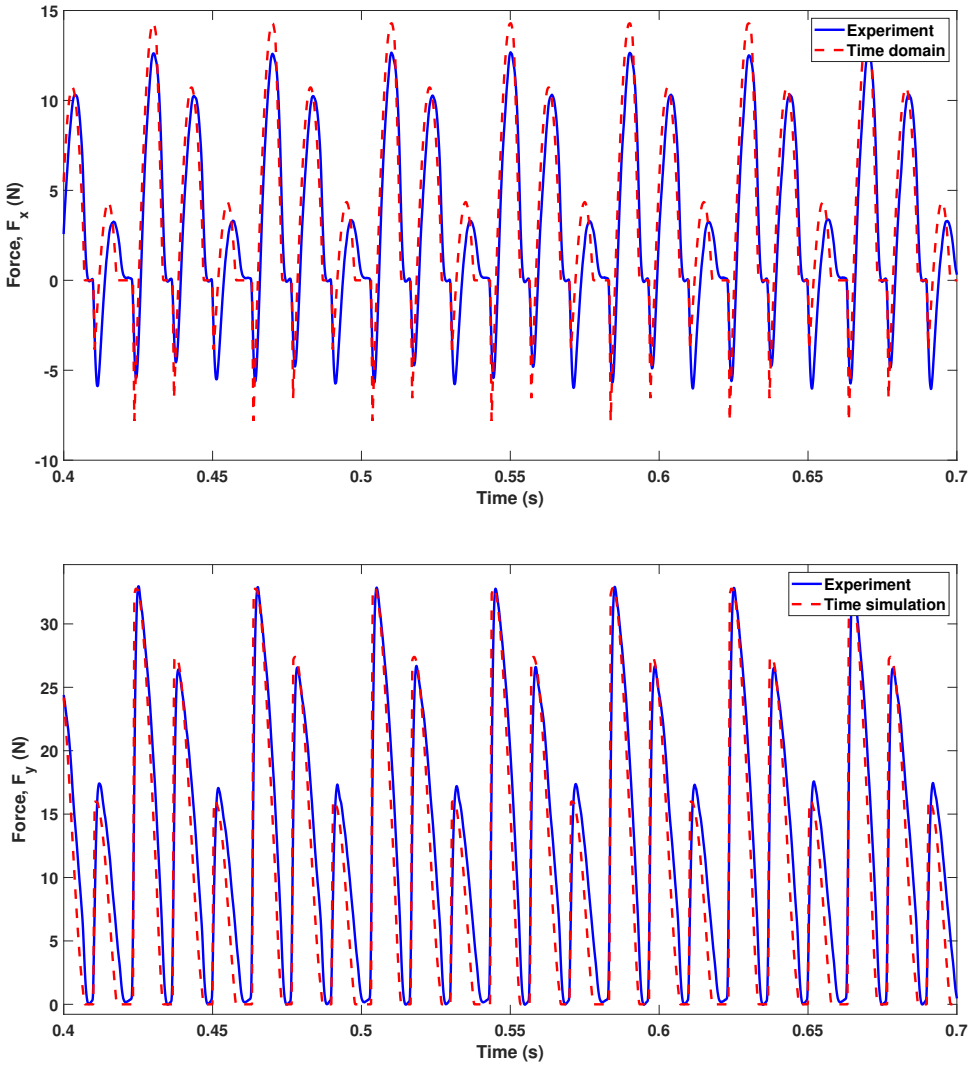


Fig. 6.3 The cutting forces by the dynamometer in both directions for half immersion, down milling operation with the axial depth of cut of 1 mm at 1500 rpm spindle speed. The simulation and experimental cutting forces are compared considering the tool runout.

### 6.3.2 Milling tests

The flexible structure was fixed to the CNC table and the experimental setup is illustrated in Figure 6.4 and 6.5. The beam and actuator (as robot representation) were attached to the Aluminium alloy block (Al 7075-T6) to control the vibration in the flexible direction $y$. The acceleration of workpiece and beam was measured using the accelerometer PCB 353B18. A

hall-effect sensor was utilised to identify the one revolution of the spindle speed by fixing the sensor close to the tool holder. The voltage change of the hall-effect sensor owing to the two slots on the tool holder was recorded while the spindle was rotating. To acquire the all data from the experiments, NI DAQ USB-4431 was used.

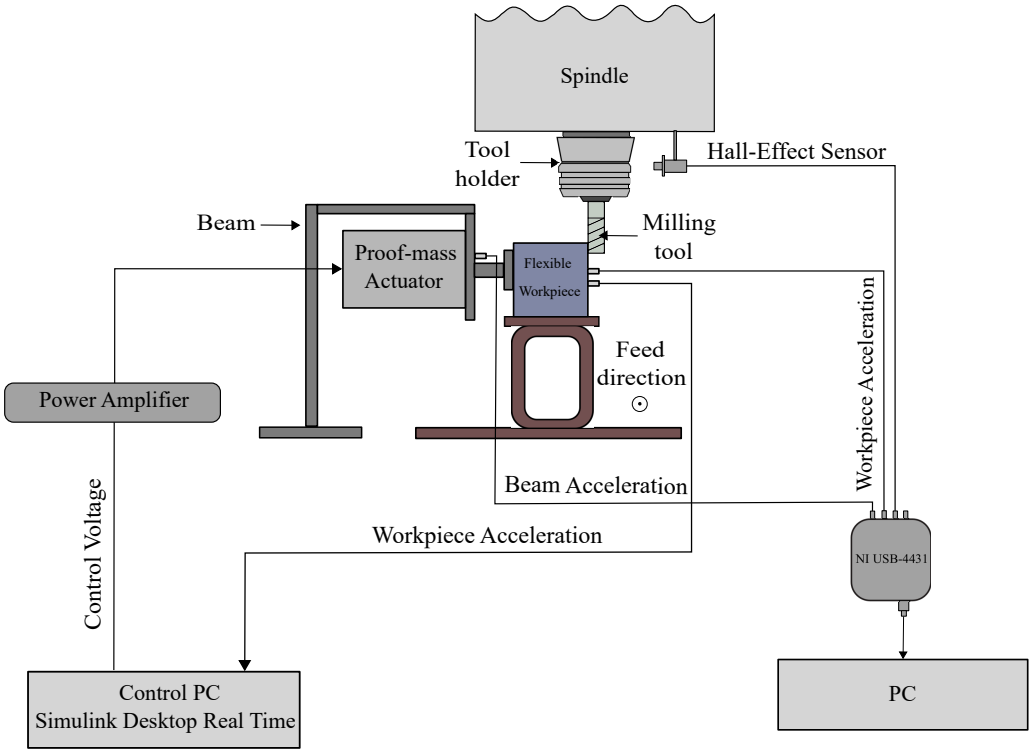


Fig. 6.4 Experimental setup for the milling tests

Fig. 6.5 An image for the milling test setup

The milling parameters and the tool properties are given in Table 6.2. The Aluminium block dimension was 100x100x300 mm and the cutting operations were carried out the opposite side the location of the beam. The cutting length was indicated as 100 mm and 8 mm (half) radial immersion for the set of axial depht of cuts. The feed direction of the cutting tool was out of the page.

Table 6.2 Milling parameters for the cutting tests

| Machining Parameters | |
|---|---|
| Tool diameter | 16 mm |
| Number of teeth | 4 |
| Tool helix angle | 45° |
| Material | Al-7075-T6 |
| Cutting stiffness $K_r$ | $180\times10^6\ Nm^{-2}$ |
| Cutting stiffness $K_t$ | $660\times10^6\ Nm^{-2}$ |
| Milling type | Down milling |
| Radial depth of cut | Half immersion |
| Feed per tooth | 0.05 mm |

Table 6.3 The critical limiting depth of cuts

| Control method | $b_{min}$ (mm) |
|---|---|
| Uncontrolled | 1.2 |
| DVF | 3.5 |
| VPA | 2.9 |
| PID | 3.4 |
| LQR | 3.4 |
| $H_\infty$ | 3.3 |
| $\mu$ synthesis | 3.4 |

### Chatter detection methods

The once per revolution sampling and FFT spectrum are the most utilised chatter detection methods [50, 51]. It is expected that the measured signal will be periodic at the tooth passing frequency $f_{tp} = N_t N/60$ (where $N$ and $N_t$ are the spindle speed (rpm) and the total number of the tool teeth, respectively) and its harmonics if the operation is with non-zero runout. If the runout occurs during the cutting operation, the spindle rotation frequency, $f_s = N/60$, appears in the FFT spectrum [260]. The other frequencies in FFT spectrum are determined as chatter [261]. Thus, the FFT spectrum can be used to detect the onset of the chatter.

The once per revolution sampling is based on synchronised sampled data points in cutting operation [51, 262]. A Poincaré plot which is showing the motion of the cutting tool in both directions for each revolution, was presented by Davies et al. [262]. The motion of the cutting tool was sampled once per revolution for a stable cut, this should show the same tool position in each revolution. In the case of chatter, the tool position varies for each revolution. Thus, the method can be used to detect the chatter observing the tool position by sampling the data points for each revolution. Alternatively, the tool position in both directions can be used by plotting them against each other, namely the Poincaré map. In case of stable cut, a small cluster of the data appears while a distributed cluster is observed for the chatter case.

The once per revolution sampling and FFT spectrum methods are utilised in order to detect the chatter phenomena in this thesis. Once the each cut is conducted, both techniques are employed using the acceleration data of the flexible structure. Once per revolution sampling method is employed for the Poincaré map and time-domain plot for each cut.

### Milling results

The experiments were conducted to verify the chatter stability of the flexible structure applying each control method. As an example, the experimental results implementing the DVF control illustrated in Figure 6.6. The milling experiments were carried out to verify the

chatter stability for the uncontrolled and controlled cases. Also, the loss-of-contact problem was detected comparing the acceleration values of the beam and flexible workpiece. Since the controller parameters were optimised focussing on maximising the critical limiting depth of cut ($b_{min}$), the actuator saturation occurred around the spindle speed where the highest depth of cut, as shown in Figure 6.6. It should be noted that the actuator saturation did not occur below the critical limiting depth of cut ($b_{min}$) value. The details of the tuning method is explained in section 4.4.3. The predicted actuator saturation points in time-domain were compared with the experimental results.

Initially, the milling experiments were conducted for the uncontrolled structure. For instance, the results when point A (2800 rpm, 0.5 mm depth of cut (doc)) and point B (2800 rpm, 1.5 mm doc) parameters were selected, showed the stable and chatter cuts, respectively. It can be seen from Figure 6.7 (A), concentrated data points for Poincaré plot were obtained. Also, only tooth-pass and run-out frequencies were observed in the FFT spectrum, which indicates a stable cut. For point B, an eliptical shape was obtained at Poincaré plot and a chatter frequency additional to tooth-pass and run-out frequencies was observed in the FFT spectrum, which indicates a chatter cut. The predictions for the uncontrolled case were verified experimentally. It should be considered that the critical limiting depth of cut was 1.2 mm for the uncontrolled flexible structure.

For the controlled case, the same spindle speed was chosen to show the control effect on the chatter stability. A stable cut was observed with Point C (2800 rpm, 2.5 mm doc) parameters while the control was on. To verify the chatter case with control, 4 mm doc was selected at 2800 rpm, however the cut was stable. It was not expected according to the controlled SLD. Thus, the depth of cut was increased to point D (2800 rpm, 5.5 mm doc), however, here the loss-of-contact issue was confronted. The issue was detected by comparing the acceleration data of the beam and the flexible structure. Also, the loss-of-contact problem can be detected using the FFT spectrum. Several frequencies additional to the tooth-pass

and run-out frequencies were appeared in the FFT spectrum as shown in Figure 6.7 (D), it is explained in detail in section 6.3.3. The once-per-revolution samples, Poincaré map and the FFT spectrum plots for Point A, B, C, D parameters are illustrated in Figure 6.7. In order to validate a chatter cut for the controlled case, the spindle speed was changed. Therefore, Point E (2700 rpm, 4 mm doc) cutting parameters were carried out and a chatter case was observed with the control.

Besides, the saturation issue was evaluated around 2000 rpm where the saturation occured according to the time-domain results. Point F (2000 rpm, 5 mm doc) was selected as the parameters were also in the first lobe even there was no control. As it was expected, a stable cut was obtained with control since the chosen parameters were in the uncontrolled SLD, altough the actuator could not provide sufficient control force and saturated for point F parameters. The parameters between two SLDs were also performed considering the actuator saturation. Point G (2100 rpm, 5 mm doc) and point H (2100 rpm, 6 mm doc) were conducted, a marginal and a chatter cut were detected now that the actuator could not generate adequate control force as it was saturated according to the time-domain simulation results. In addition, a stable cut (2100 rpm, 4 mm doc) with control can be seen just under the saturation point (2100 rpm, 4.5 mm doc). That means, the time-domain results for the actuator saturation detection match with the experimental results. The once-per-revolution samples, Poincaré map and the FFT spectrum plots for Point E, F, G, H parameters are illustrated in Figure 6.8.

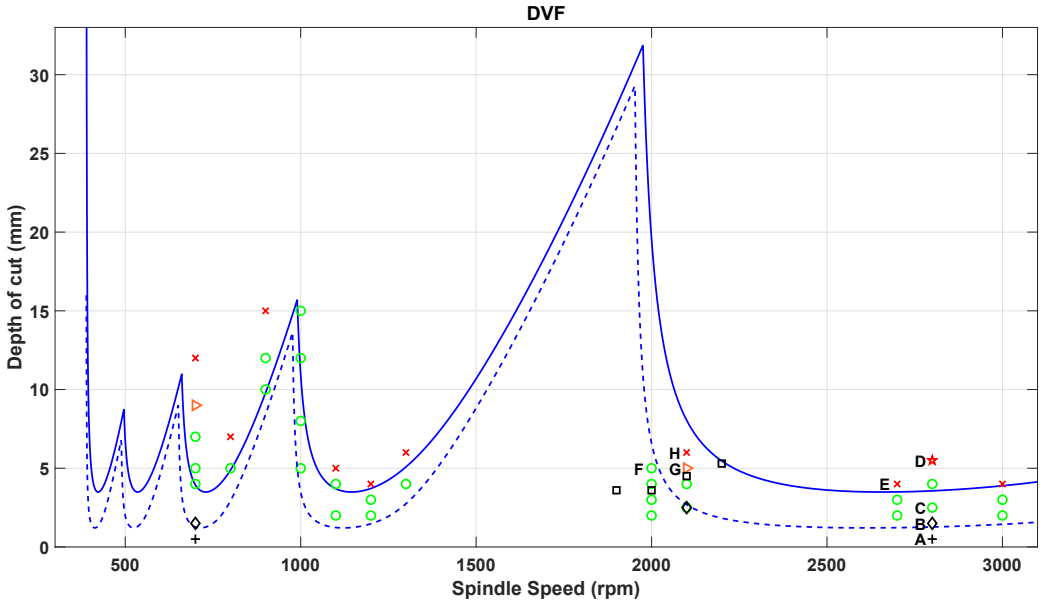


Fig. 6.6 Stability lobe diagram with experimental results for DVF control method. DVF controlled SLD (——), uncontrolled SLD (- - -), uncontrolled stable cut (+), uncontrolled chatter (◊), controlled stable cut (○), controlled marginal cut (▷), controlled chatter (*x*), controlled loss-of-contact (⋆), onset of actuator saturation in time-domain simulation (□).

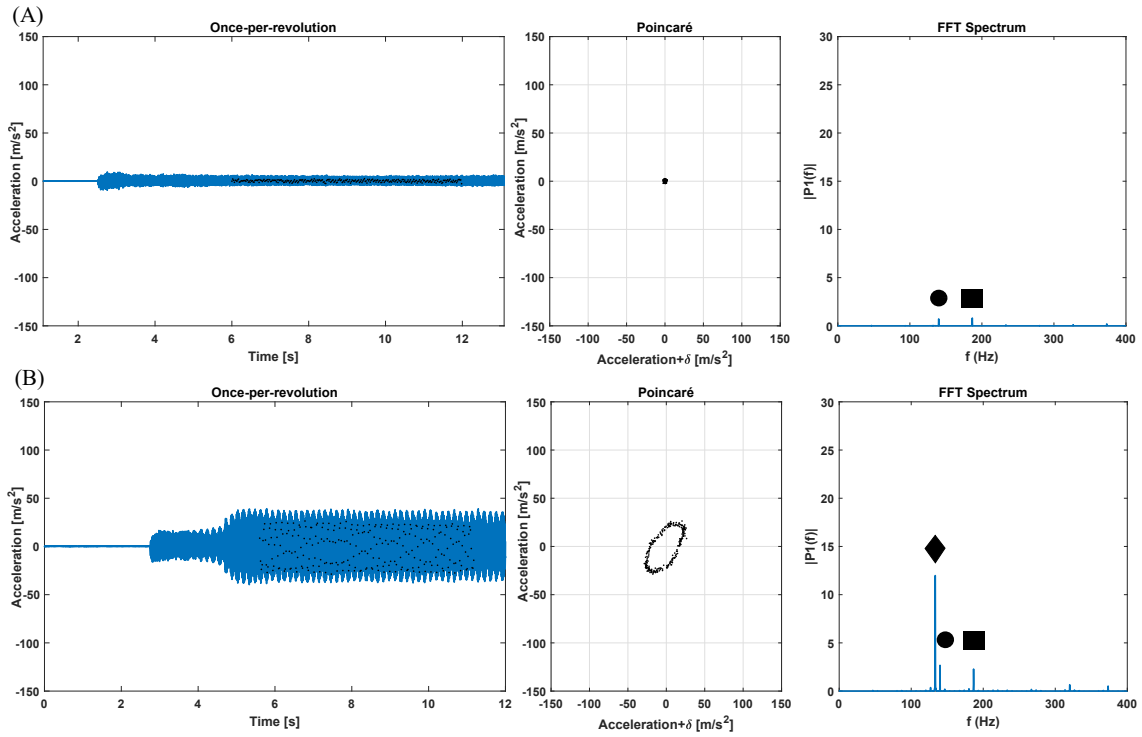

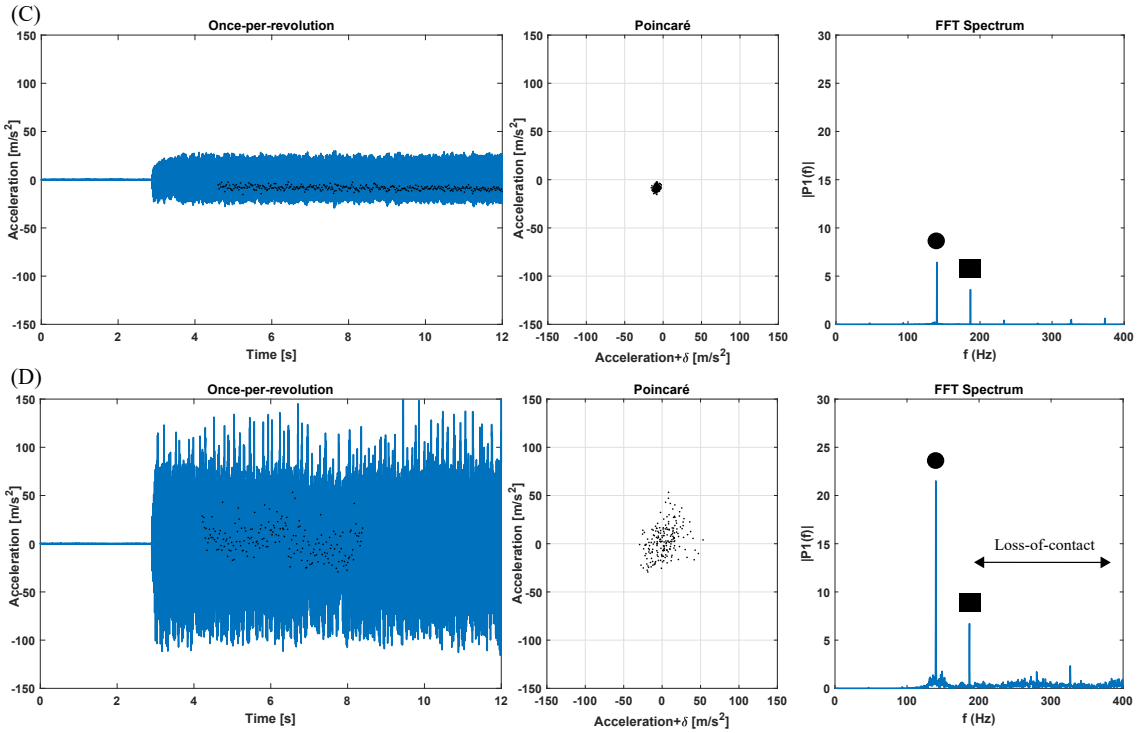


Fig. 6.7 Once per revolution samples, Poincaré map and the FFT spectrum for stable cut A (2800 rpm, 0.5 mm), chatter cut B (2800 rpm, 1.5 mm), stable cut C (2800 rpm, 2.5 mm), loss-of-contact cut D (2800 rpm, 5.5 mm). Spindle frequency (runout) (●), tooth passing frequency (■), chatter frequency (♦)

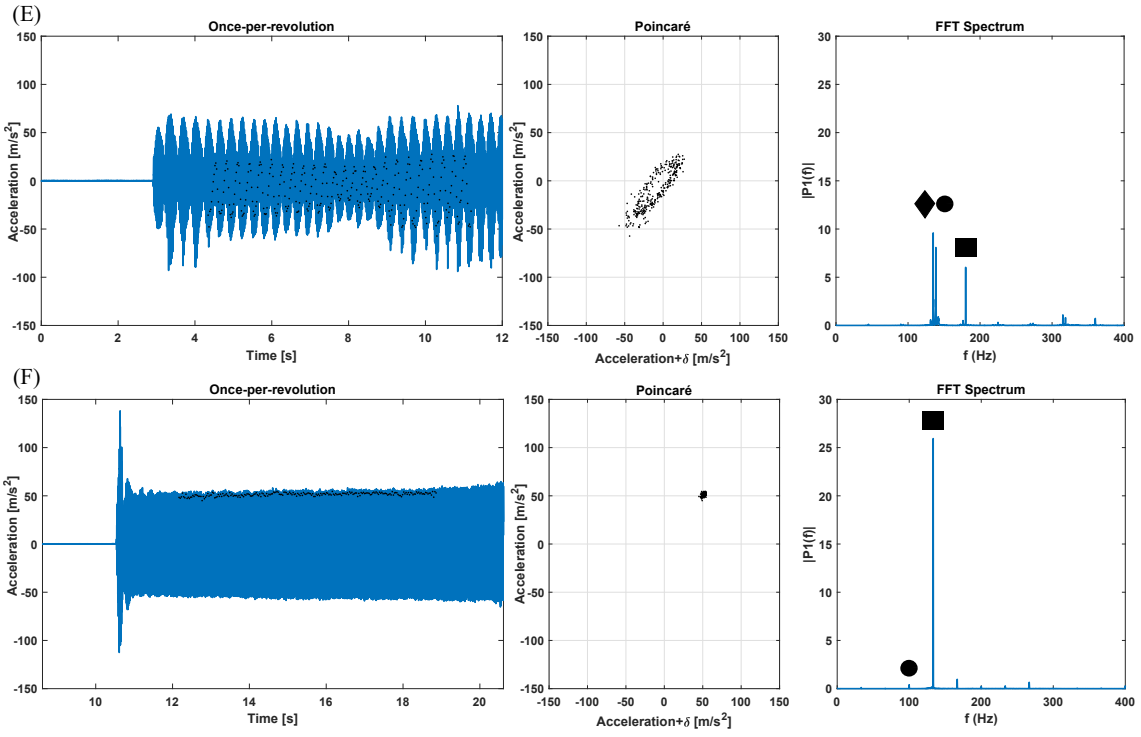

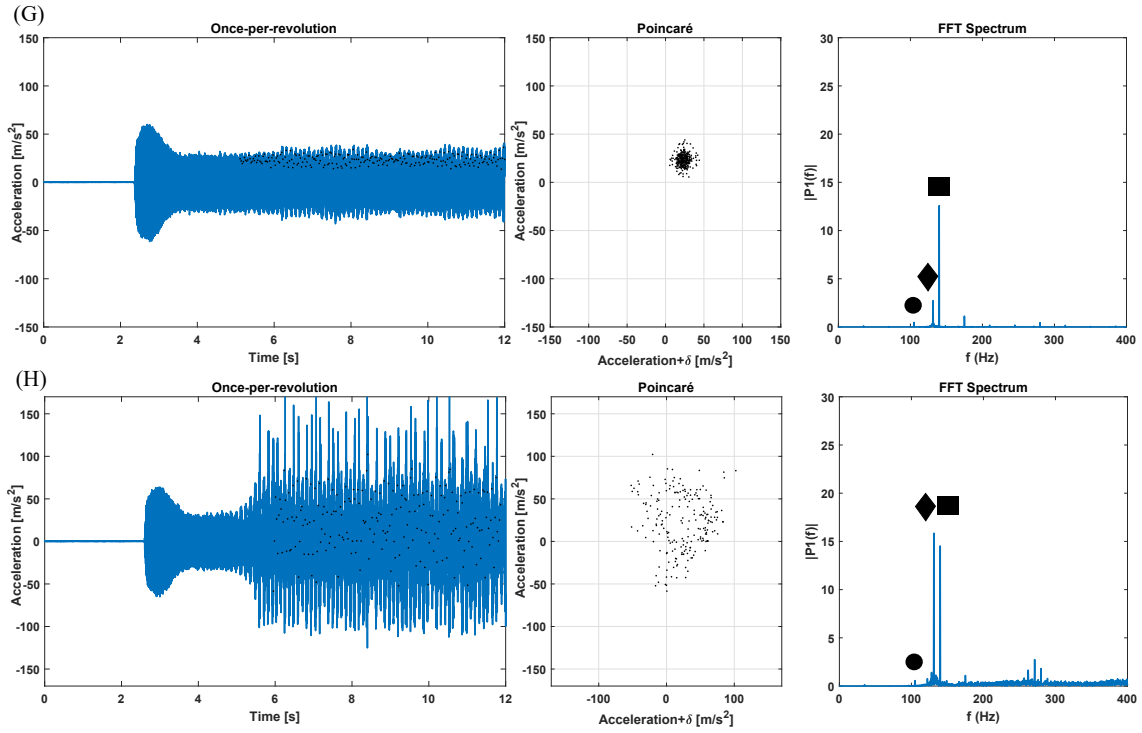


Fig. 6.8 Once per revolution samples, Poincaré map and the FFT spectrum for chatter cut E (2700 rpm, 4 mm), stable cut F (2000 rpm, 5 mm), marginal cut G (2100 rpm, 5 mm), chatter cut H (2100 rpm, 6 mm). Spindle frequency (runout) (●), tooth passing frequency (■), chatter frequency (⧫)

Once per revolution samples, Poincaré map and the FFT spectrum are shown in Figure 6.9 when DVF control is on and off at 2100 rpm, 2.5 mm doc. Red and blue color represent the chatter and stable cut cases, respectively.

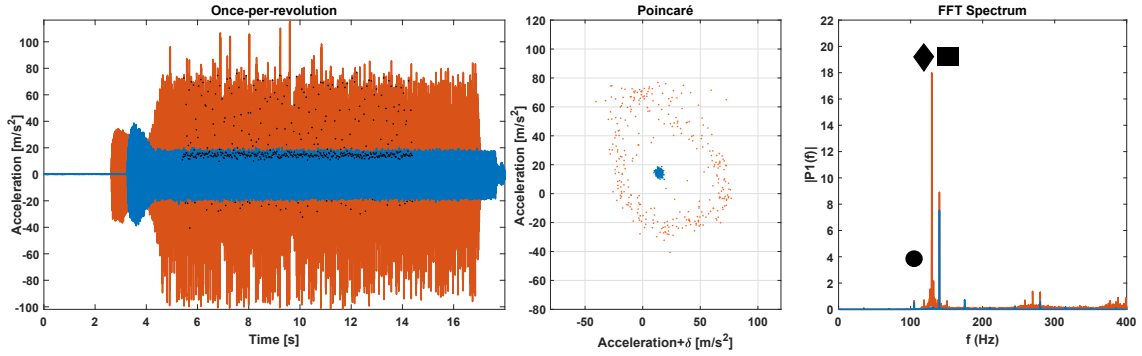


Fig. 6.9 Once per revolution samples, Poincaré map and the FFT spectrum when DVF control was on and off at 2100 rpm, 2.5 mm doc. Red and blue color represent the chatter and stable cut cases, respectively. Spindle frequency (runout) (●), tooth passing frequency (■), chatter frequency (⧫)

The chatter marks can be seen in Figure 6.10 for the parameters, 2900 rpm, 5 mm doc with DVF control. While the control is on, there is no chatter mark observed since it is a stable cut. The chatter marks are seen on the cut surface when the control is switched off. Also, the once per revolution samples, Poincaré map and the FFT spectrum plots are illustrated in Figure 6.11 for the related cuts. It was expected that a chatter case for the parameters 2900 rpm, 5 mm doc according to the SLD with DVF control, yet, it was a stable cut. The structural nonlinearties such as contact, clamping conditions, or the beam nonlinearities might had been experienced.

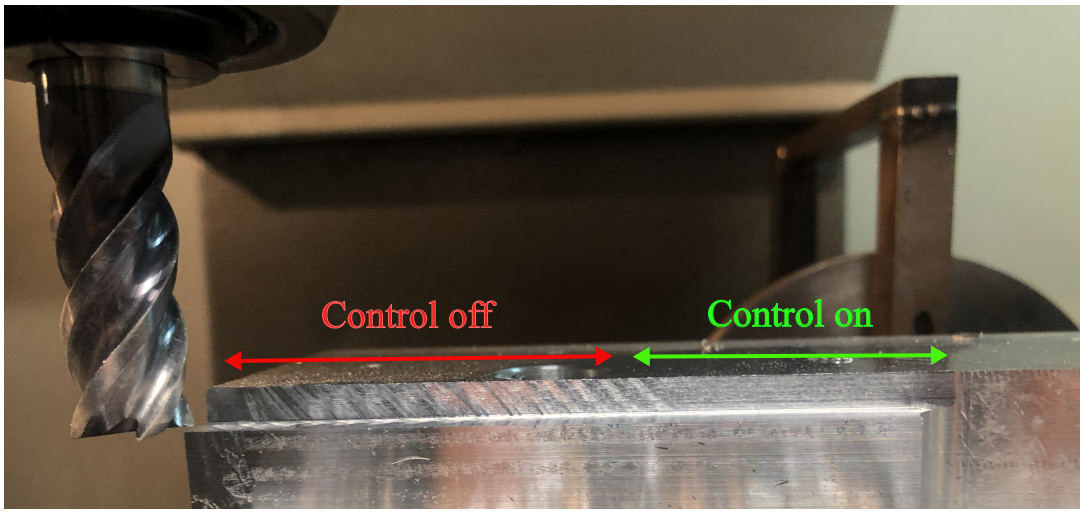


Fig. 6.10 The chatter marks when the control is on and off with the parameters 2900 rpm, 5 mm doc for DVF controlled structure.

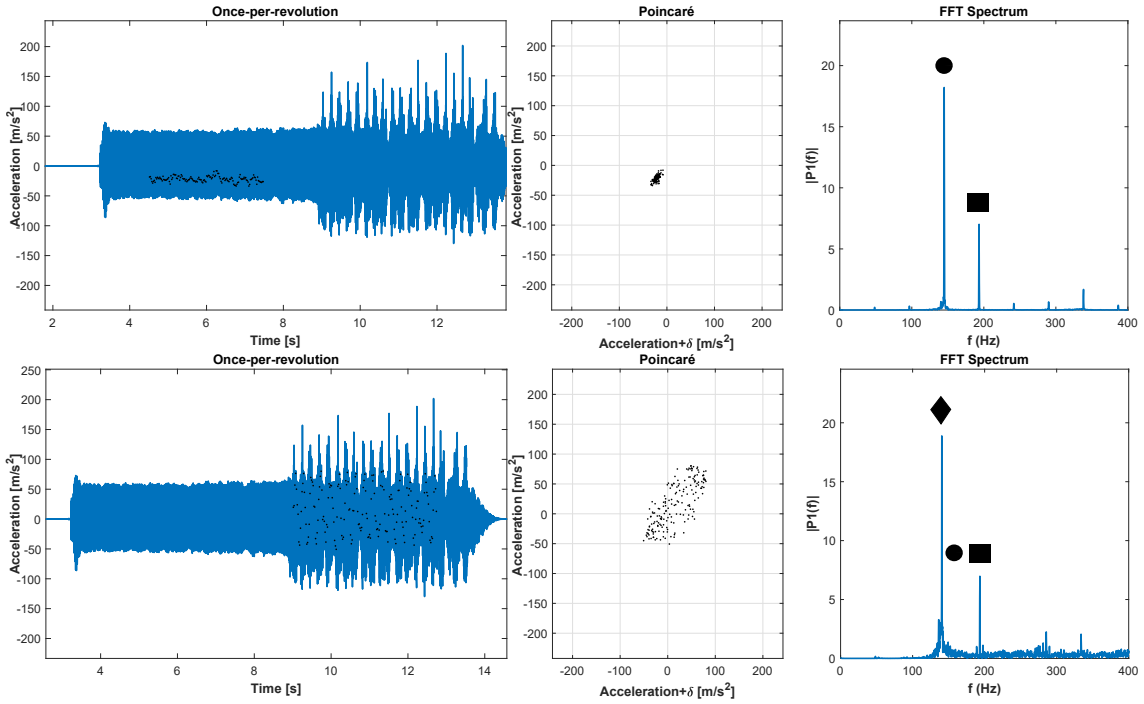


Fig. 6.11 The chatter marks when the control is on and off with the parameters 2900 rpm, 5 mm doc for DVF controlled structure. Spindle frequency (runout) (●), tooth passing frequency (■), chatter frequency (♦)

Experimental results for six different control methods are shown in Figure 6.12. It can be seen that the loss-of-contact issue was experienced for all control methods for the same spindle speed, 2800 rpm. That means higher forced vibrations and the nonlinearity of the structure were confronted for this spindle speed. Also, it can be deduced from the milling experiments, the loss-of-contact issue is irrelevant to the controller type, it is related with the dynamic properties of the structure and the cutting parameters. The milling test results for the other control methods are given in Appendix C.

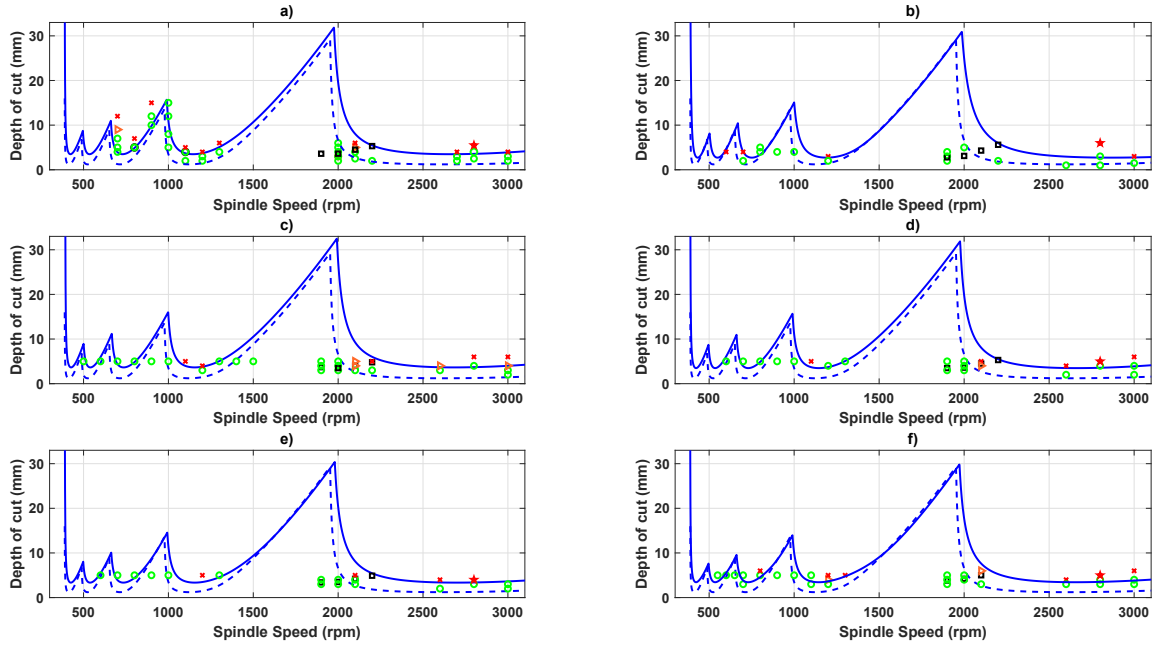


Fig. 6.12 Stability lobe diagrams with experimental results for (a) DVF control, (b) VPA control, (c) PID control, (d) LQR control, (e) $H_\infty$ control, (f) $\mu$-synthesis control. Controlled SLD (——), uncontrolled SLD (- - -), controlled stable cut (○), controlled marginal cut (▷), controlled chatter ($x$), controlled loss-of-contact (⋆), onset of actuator saturation in time-domain simulation (□).

The loss-of-conctact detection is explained in the next section.

### 6.3.3 Loss-of-contact detection

The loss-of-contact issue was encountered for the parameters at the point D (2800 rpm, 5.5 mm doc) in Figure 6.7. In order to detect the issue the acceleration data was recorded from the flexible structure and the beam. If the contact between the structure and beam is rigid and no loss-of-contact is faced, the acceleration data should be close to each other, otherwise, they will be different and disturbed value. The acceleration data of the workpiece and beam are plotted against each other for a stable (2800 rpm, 3 mm doc) and loss-of-contact (2800 rpm, 5.5 mm doc) case in Figure 6.13. They are also illustrated against time, and FFT spectrums from the workpiece acceleration data. When the loss-of-contact issue is observed, the beam acceleration (blue in Figure 6.13) is far away being close to the workpiece acceleration.

Besides, the different frequencies than runout and tooth pass frequencies can be seen in FFT spectrum due to the loss-of-contact issue.

The loss-of-contact issue was experienced for all control methods for the same spindle speed, 2800 rpm. That means higher forced vibrations and the nonlinearity of the structure were faced for this spindle speed. Also, it can be deduced from the milling experiments, the loss-of-contact issue is irrelevant to the controller type, it is related with the dynamic properties of the structure and the cutting parameters.

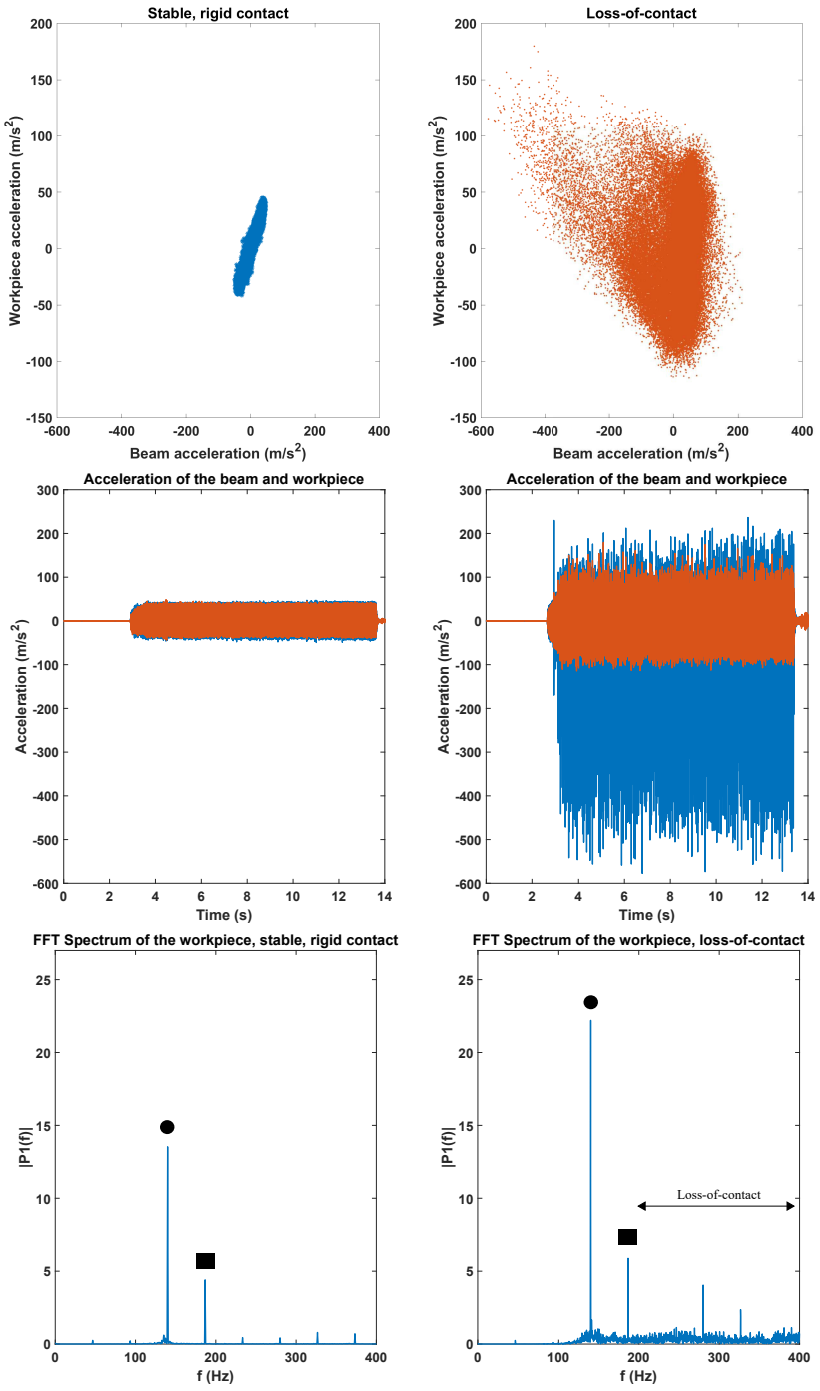


Fig. 6.13 Loss-of-contact detection, acceleration of the workpiece and beam, FFT spectrums for each scenario. Spindle frequency (runout) (●), tooth passing frequency (■)

### 6.3.4 Verification of actuator saturation islands

In this subsection, the proposed actuator saturation model in frequency model explained in chapter 5, will be validated experimentally. The predicted saturation islands between 1700 rpm and 2200 rpm were chosen for the cutting trials. The experiments were conducted using a tool with constant 45 degree helix angle for DVF control method. The predicted saturation islands in time-domain, in frequency-domain and the experimental actuator forces which were collected through machining tests are illustrated in Figure 6.14. The actuator forces are added to the location of the chosen cutting parameters in SLD. The saturation islands are encircled with a red dashed line. The location of the saturation islands is matched well in experiments.

The saturation occurs just above 3 mm doc around 1950 rpm according to the frequency and time-domain predictions. Then, the actuator saturated until 10 mm doc in experiments. It can be seen that there is a saturation-free region between the predicted saturation islands. Also, the second saturation island (higher docs) is obtained around 20 mm doc as predicted in both models.

Furthermore, between two SLDs, chatter and marginal cuts with actuator saturation were observed since the chosen depth of cuts were above the predicted saturation points and the actuator could not provide sufficient force. There is a slight difference between the frequency and time-domain predictions especially between 2050 rpm and 2200 rpm now that the frequency-domain predictions are based on only forced vibrations. The experimental results correlate with the time-domain predictions between these spindle speeds.

It can be seen from the comparison figure, the predicted saturation islands in frequency domain are matched considerably with the experimental results.

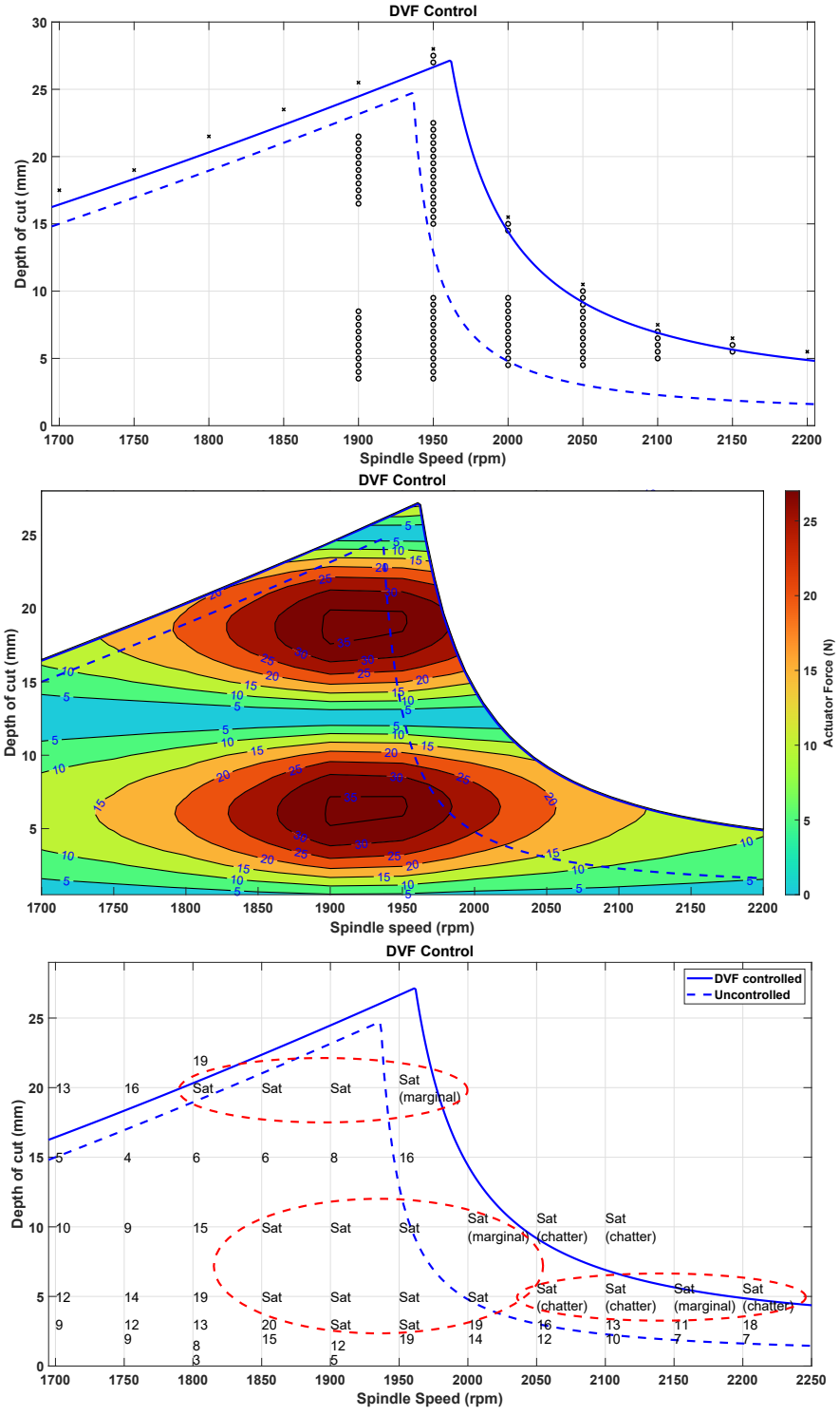


Fig. 6.14 The predicted saturation islands (a) in time-domain ,(b) in frequency-domain, and (c) experimental actuator forces for DVF controlled system. Controlled SLD (——), uncontrolled SLD (- - -).

### 6.3.5 Discussion

The experimental results showed that the actively controlled robot arm could effectively improve the chatter stability and critical limiting depth of cut. It provides a very close performance to the stability boundary obtained from impact hammer test for each control method. That means the proposed system can be utilised and it is a feasible method for the milling operations.

The FRF results are nearly the same for each controller type. However, the stability limits are slightly different as the dynamics of each controller is sligtly different. The chatter boundaries are predicted using a tool with 30° helix angle. However, a tool with 45° helix angle was used in experiments as the chatter stability is not affected by the helix angle. The chatter boundaries were validated using this tool since the boundaries are not affected by the helix angle. It only affects the actuator force as it is produced by processing the vibration of the workpiece. The higher helix angle reduces the vibration of the workpiece slightly. Thus, the location of the saturation islands are compared with the predictions for the milling scenario using a tool with 45° helix angle. The proposed actuator saturation model in frequency model explained in chapter 5, was validated experimentally. The location of the predicted saturation islands is matched well in experiments.

The cutting force coefficients were identified using time-domain simulation method instead of utilising different feed rates for the identification given that a runout was determined from the cutting force results.

The loss-of-contact issue was experienced for parameters at point D (2800 rpm, 5.5 mm) as illustrated in Figure 6.13. In order to detect the issue, the acceleration of the workpiece and beam were compared. A considerable difference was observed when the issue was occured. Also, the issue was noticed in the FFT spectrum that had several frequencies other than the FFT spectrum plotted for a stable cut. It should be noted that the issue was not faced at depth

of cut that was below the critical limiting depth of cut. The forced vibrations and structural nonlinear effects may be a factor for the loss-of-contact occurence.

## 6.4 Summary

This chapter evaluated the predicted SLDs of the robotic-assisted milling concept. The concept was first tested considering the FRF results for each control method. It was shown that the concept can effectively improve the dynamic response of the flexible structure. Then, the concept was examined under the real milling conditions. The experimental results showed that the chatter stability and the critical limiting depth of cut ($b_{min}$) were considerably improved. In order to examine the experimental results, once per revolution samples, Poincaré map and the FFT spectrum plots were utilised. Yet, some differences were observed at the spindle speed around 2800 rpm. The structural nonlinearites were experienced around this spindle speed and resulted in loss-of-contact. Besides, the predicted time-domain saturation points were tested. The results showed that the saturation points were successfully explored with the experimental verification tests.

The proposed actuator saturation model in frequency model explained in chapter 5, was validated experimentally. The predicted saturation islands between 1700 rpm and 2200 rpm were chosen for the cutting trials. The experiments were conducted with a tool with constant 45 degree helix angle for DVF control method. The predicted saturation islands in time-domain, in frequency-domain and the experimental actuator forces are compared. The results show that the predicted saturation islands in frequency domain are considerably matched with the experimental results.

# Chapter 7

# Conclusions

## 7.1 Summary of thesis

Chapter 2 introduced the literature review of machining and robotic-assisted milling applications. The machining stability prediction using the methods of zero-order approach (ZOA), semi-discretisation method (SDM), and multi-frequency approach (MFA) were reviewed in the part of machining literature. Then, the chatter mitigation and suppression methods were presented including the passive and active control methods. In the robotic-assisted milling literature, the concept and additional support system were presented. Its applications and details were introduced including the support force and contact type.

Chapter 3 presented the theoretical background of the milling stability analysis. A basic chatter mechanism considering a single-point cutting operation was given. Then, the stability lobe diagram was presented. Afterwards, the chatter stability analysis was extended using ZOA for the milling which is an intermittent cutting operation due to a rotating cutting tool. The method is based on expanding the time-varying dynamic cutting coefficients into Fourier series to obtain averaged constant term (zeroth order) of the series. The critical limiting depth of cut $a_{cr}$ was derived for a general two-dof milling operation. Finally, the ZOA method

accuracy was discussed in terms of low radial immersion and cutting force harmonics due to the cutting parameters.

Chapter 4 introduced the analysis of the concept of the robotic-assisted milling where a robot supports a flexible structure while it is machined by a machine tool to suppress and improve the regenerative chatter. Six different control methods which were direct velocity feedback (DVF), virtual passive absorber (VPA), proportional integral derivative (PID), linear quadratic regulator (LQR), H infinity ($H_\infty$), and $\mu$ synthesis, were applied in robotic-assisted milling. In order to evaluate the feasibility of the method, a proof-mass (inertial) actuator was assembled to a beam which emulates the dynamic behaviour of the robotic arm to improve the dynamic response of a flexible structure. A numerical optimisation method called self-adaptive differential evolution (SADE) algorithm was used to optimise the controller gains to obtain the best performance in terms of chatter suppression ($b_{min}$ and $b_{max}$). Finally, the performance of each controller was evaluated with the experimental frequency response functions (FRFs) and predicted stability lobe diagrams (SLDs) considering a milling scenario. It was shown that the concept can improve the chatter stability and also can increase the criticial limiting depth of cut significantly, comparing to the scenario where the robot has no active control applied.

In Chapter 5, an actuator saturation model in frequency-domain was proposed by extending the surface location error model by Schmitz [258]. The regeneration effect was neglegted in the model, only forced vibrations were taken into account. Fourier force model was utilised for the saturation islands considering the type of the milling. The saturation islands between 1700 rpm and 2200 rpm where the all controllers suffer from saturation, were determined up to the stability boundary for each control method. The comparison table shown in Table 5.2 for the frequency and time-domain actuator saturation islands was presented. The table

shows the depth of cut where the saturation starts at the spindle speed where the highest depth of cut. It was seen that the saturation islands in frequency-domain (proposed method) match with the time-domain results. Besides, the effect of the helix angle on the saturation islands was presented. It was shown that the higher number of helix angle can affect the location of the saturation islands and actuator force now that the forced vibrations were reduced in the controlled direction and the delay of the process was affected due to the helix angle of the cutting tool.

Chapter 6 evaluated the predicted SLDs of the robotic-assisted milling concept. The concept was first tested considering the FRF results for each control method. It was shown that the concept can effectively improve the dynamic response of the flexible structure. Then, the concept was examined under the real milling conditions. The experimental results showed that the chatter stability and the critical limiting depth of cut ($b_{min}$) were considerably improved. In order to examine the experimental results, once per revolution samples, Poincaré map and the FFT spectrum plots were utilised. The structural nonlinearites were experienced and resulted in loss-of-contact. Besides, the predicted time-domain saturation points were tested. The results showed that the saturation points were successfully explored with the experimental verification tests. The proposed actuator saturation model in frequency model were validated experimentally. The location of the saturation islands is slightly shifted in experiments. It can be seen from the comparison figure, the predicted saturation islands in frequency domain are considerably matched with the experimental results.

Conclusions and the main contributions to knowledge will be discussed in the following section.

## 7.2 Conclusions and original contributions

The conclusions and main contributions from this research that can be drawn are:

- A new approach for active vibration control in milling is presented. A novel configuration of the robotic-assisted milling has been proposed to improve the chatter stability implementing standard active control methods (DVF, VPA, PID, LQG, $H_\infty$ and $\mu$ synthesis).

- The critical limiting depth of cut $b_{crit}$ can be increased by a factor of 2.9 compared to a system with no active control, and by a factor of 4.4 compared to a system with no robotic assisted supporting system.

- The maximum depth of cut $b_{max}$ was not significantly improved compared to $b_{crit}$. The actuator saturation limited the performance of the supporting system due to the high amplitude forced vibrations in milling. Therefore, actuator saturation needs to be considered for tuning process of the controller parameters.

- The practical performance of each controller has been evaluated using a simplified model and by verification experiments. The predicted stability boundaries matched well with the experimental results.

- The onset of actuator saturation in the time-domain has been validated experimentally. The predictions of the saturation point between uncontrolled and controlled SLDs matched well with the experimental results.

- A new predictive model for the actuator saturation is presented. The actuator saturation island model in frequency-domain has been proposed in milling. The model only considers the forced vibrations. The saturation islands in frequency model (proposed method) match with the time-domain results. Then, the islands were validated experimentally. Afterwards, the effect of the helix angle was also evaluated. It was shown

that higher helical angles affect the location of the saturation islands and the actuator force as the milling process was influenced owing to the helix angle of the cutting tool.

These contributions to knowledge have been disseminated in the conferences, and journal papers. The list of research papers are given in Appendix D.

## 7.3 Discussion and future works

The experimental results show that the actively controlled robot arm can considerably improve the chatter stability and critical limiting depth of cut. The experiments were conducted using a simplified beam that an inertial actuator assembled on. The robot is represented by a beam using the most flexible modes of the real robot. However, this robot can exhibit additional modes of the vibration. Consequently, further FRF tests would be required to avoid the destabilisation of the machining system.

Since the position of the robot affects the contact point, the dynamic response of the workpiece may vary. Also, the dynamic response of the structure may be influenced by the material removal during cutting. The re-tuning of controller parameters would be required to ensure the optimised controller performance. This could be overcome by employing $\mu$ synthesis control to cover the associated uncertainties. It can be more beneficial for the robotic assisted milling concept.

The loss-of-contact issue may be confronted between the robot and the structure. Adjusting the position of the robot could be a solution so that the additional supporting system is always in contact during the operation by ensuring the static pre-load force that is higher than the control force produced by the actuator. Yet, the force vibrations or the structure nonlinearities may also be a factor for the loss-of-contact occurence which may degrade the performance of the control system.

Different types of contact between the robot and the workpiece could be chosen for the robotic assisted milling. In this thesis, a rigid metallic contact was used. However, a rolling contact using soft/hard rubber could be an alternative contact. Such changes would also influence the system as the actuator force transmission would be changed by the contact type.

The actuator saturation islands were determined and validated experimentally. A cutting tool with 45 degree helix angle was used for the experiments. The effect of the helix angle was identified in the simulation work. Thus, the validation of the saturation islands predicted using the tool that has a different helix angle than 45 degree, has remained as future work to demonstrate in practice.

The potential limitations of the system for a different scenario can be listed as follows:

1. Rough/gentle cutting conditions (e.g., higher feed rates).
    - It can be degraded, for 3 times higher feed per tooth, the $b_{crit}$ 1.96 mm, g=88, DVF control.
2. High speed machining (>12000 rpm, instead of <3000 rpm).
    - The spindle speed is increased up to 20000 rpm, the actuator performance is not degraded.
3. Multiple vibration modes (e.g., bending and torsion, instead of only bending).
    - The actuator performance is not degraded when it is tuned for all modes.
4. Low/high natural frequencies (e.g., 1500 Hz instead of 142 Hz).
    - For 15 times higher natural freq (142 Hz), the $b_{crit}$ 3.4 mm, g=17, DVF control. The actuator performance is not degraded, however, the feedback gain should be optimised according to the new natural frequency.
5. Different machining materials (e.g., Steel and Ti alloy) harder than Aluminum.

- The cutting coefficient is increased 3 times higher than Aluminum material, the $b_{crit}$ improvement is not degraded, the same improvement ratio is achieved.

To conclude, the proposed approach has been shown to be a feasible method for improving the stability of milling based upon robotic-assisted milling concepts. Further work is needed to demonstrate using a real robot in practice.

# Appendix A

# Robot FRF and SADE convergences for each control method

The FRF of robot for different postures is illustrated in Figure A.1. The most flexible modes which are 23 Hz and 47 Hz, are considered to desing the beam as robot representation in the experimental setup.

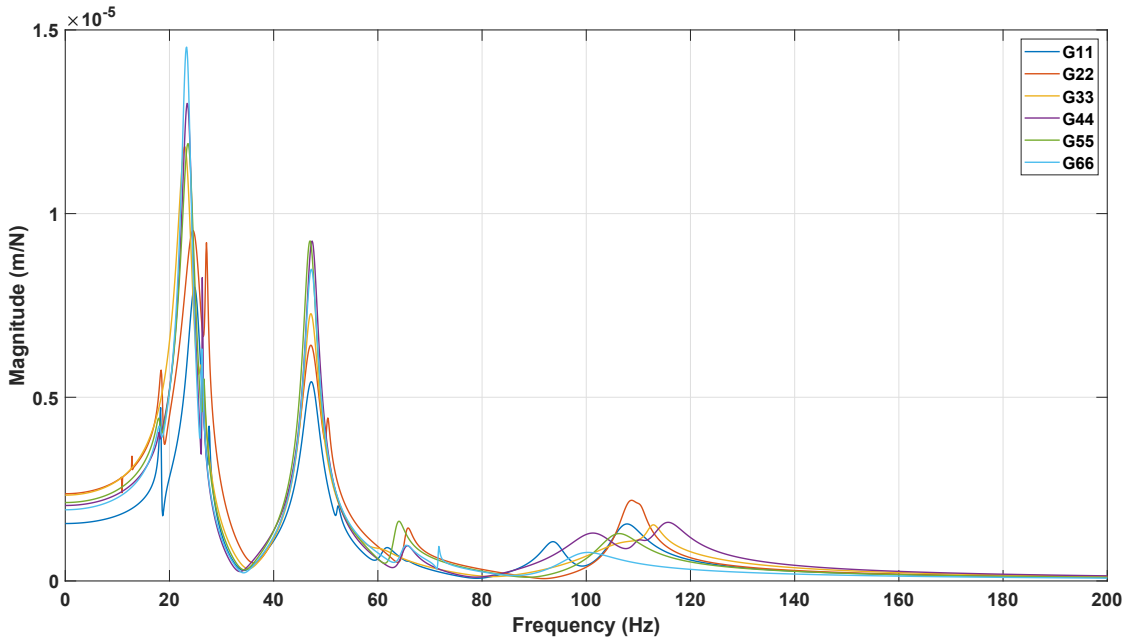


Fig. A.1 The FRF of robot.

The objective values ($b_{min}$) for each control method are illustrated in Figure A.2. The results were obtained performing SADE algorithm several times.

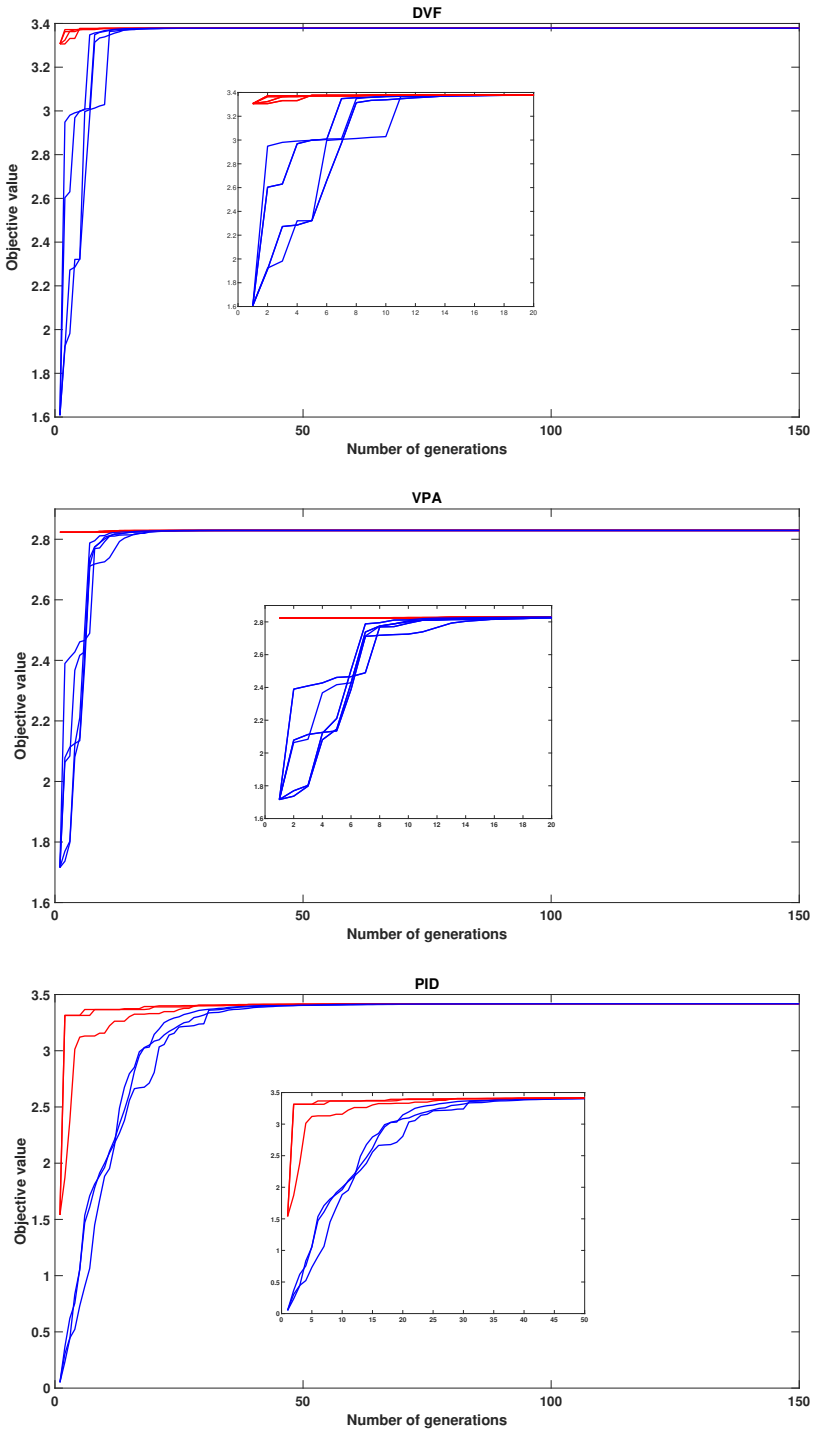

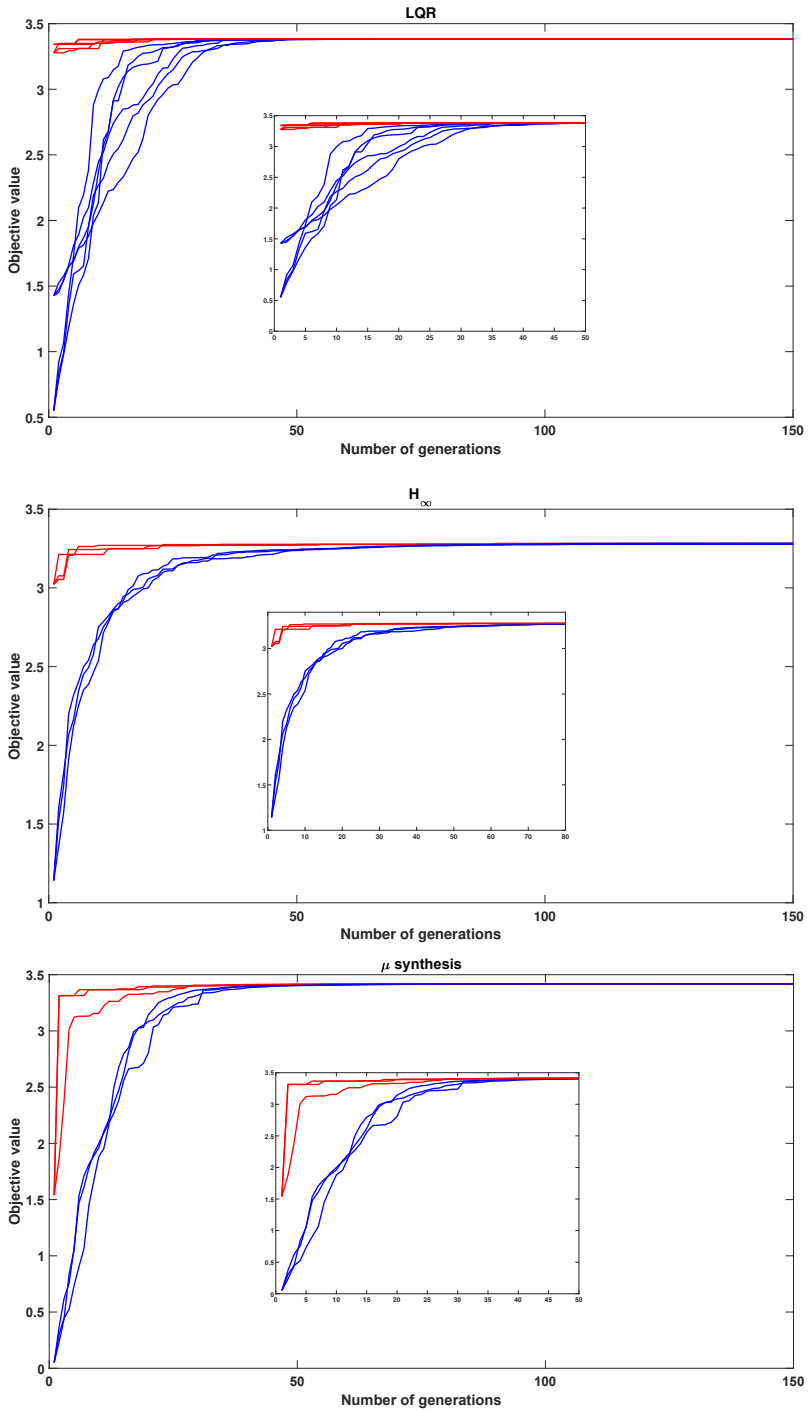


Fig. A.2 Converge studies for SADE for each control method.

# Appendix B

# The Fourier series coefficients

The Fourier coefficients, $a_n$ and $b_n$, for $y$ direction force series:

$$F_y(\theta) = \sum_{i=1}^{A} \sum_{j=1}^{N_t} \left[ a_0 + \sum_{n=1}^{\infty} (a_n \cos(n\theta_j) + b_n \sin(n\theta_j)) \right] \tag{B.1}$$

where $\theta_j = \omega t + \frac{2\pi}{N_t}(j-1) - \chi(i-1)$. The force can be accurately determined by the higher number of slices.

The terms in equations B.2 through B.7 are determined using equations 5.6 and 5.7. Considering the down milling operation, the integration limits become from $\theta_1$ to $\pi$, otherwise zero to $\theta_1$.

$$a_1 = -\frac{bN_t}{\pi} \left[ K_t f_t \left( -\frac{1}{4}\sin(\theta) + \frac{1}{12}\sin(3\theta) \right) + K_n f_t \left( -\frac{1}{4}\cos(\theta) - \frac{1}{12}\cos(3\theta) \right) \right.$$
$$\left. + K_{te} \left( \frac{1}{4}\cos(2\theta) \right) + K_{ne} \left( \frac{1}{2}(\theta) + \frac{1}{4}\sin(2\theta) \right) \right]_{\theta_1}^{\pi} \tag{B.2}$$

$$a_1 = -\frac{bN_t}{\pi}\left[K_t f_t\left(\frac{1}{4}(\theta) - \frac{1}{4}\sin(2\theta) + \frac{1}{16}\sin(4\theta)\right) + K_n f_t\left(-\frac{1}{16}\cos(4\theta)\right)\right.$$
$$\left. + K_{te}\left(-\frac{1}{2}\cos(\theta) + \frac{1}{6}\cos(3\theta)\right) + K_{ne}\left(\frac{1}{2}\sin(\theta) + \frac{1}{6}\sin(3\theta)\right)\right]_{\theta_1}^{\pi} \quad \text{(B.3)}$$

$$a_n = -\frac{bN_t}{\pi}\left[K_t f_t\left(-\frac{1}{2n}\sin(n\theta) + \frac{1}{4(n-2)}\sin((n-2)\theta) + \frac{1}{4(n+2)}\sin((n+2)\theta)\right)\right.$$
$$+ K_n f_t\left(\frac{1}{4(n-2)}\cos((n-2)\theta) - \frac{1}{4(n+2)}\cos((n+2)\theta)\right)$$
$$+ K_{te}\left(-\frac{1}{2(n-1)}\cos((n-1)\theta) + \frac{1}{2(n+1)}\cos((n+1)\theta)\right)$$
$$\left. + K_{ne}\left(-\frac{1}{2(n-1)}\sin((n-1)\theta) + \frac{1}{2(n+1)}\sin((n+1)\theta)\right)\right]_{\theta_1}^{\pi}, n = 3,4,.. \quad \text{(B.4)}$$

$$b_1 = -\frac{bN_t}{\pi}\left[K_t f_t\left(\frac{3}{4}\cos(\theta) - \frac{1}{12}\cos(3\theta)\right) + K_n f_t\left(\frac{1}{4}\sin(\theta) - \frac{1}{12}\sin(3\theta)\right)\right.$$
$$\left. + K_{te}\left(-\frac{1}{2}(\theta) + \frac{1}{4}\sin(2\theta)\right) + K_{ne}\left(-\frac{1}{4}\cos(2\theta)\right)\right]_{\theta_1}^{\pi} \quad \text{(B.5)}$$

$$b_2 = -\frac{bN_t}{\pi}\left[K_t f_t\left(\frac{1}{4}\cos(2\theta) - \frac{1}{16}\cos(4\theta)\right) + K_n f_t\left(\frac{1}{4}(\theta) - \frac{1}{16}\sin(4\theta)\right)\right.$$
$$\left. + K_{te}\left(-\frac{1}{2}\sin(\theta) + \frac{1}{6}\sin(3\theta)\right) + K_{ne}\left(-\frac{1}{2}\cos(\theta) - \frac{1}{6}\cos(3\theta)\right)\right]_{\theta_1}^{\pi} \quad \text{(B.6)}$$

$$b_n = -\frac{bN_t}{\pi}\left[K_t f_t\left(\frac{1}{2n}\cos(n\theta) - \frac{1}{4(n-2)}\cos((n-2)\theta) - \frac{1}{4(n+2)}\cos((n+2)\theta)\right)\right.$$
$$+ K_n f_t\left(\frac{1}{4(n-2)}\sin((n-2)\theta) - \frac{1}{4(n+2)}\sin((n+2)\theta)\right)$$
$$+ K_{te} f_t\left(-\frac{1}{2(n-1)}\sin((n-1)\theta) + \frac{1}{2(n+1)}\sin((n+1)\theta)\right)$$
$$\left. + K_{ne} f_t\left(-\frac{1}{2(n-1)}\cos((n-1)\theta) - \frac{1}{2(n+1)}\cos((n+1)\theta)\right)\right]_{\theta_1}^{\pi}, n = 3,4,.. \quad \text{(B.7)}$$

# Appendix C

# Milling test results

## C.1 VPA

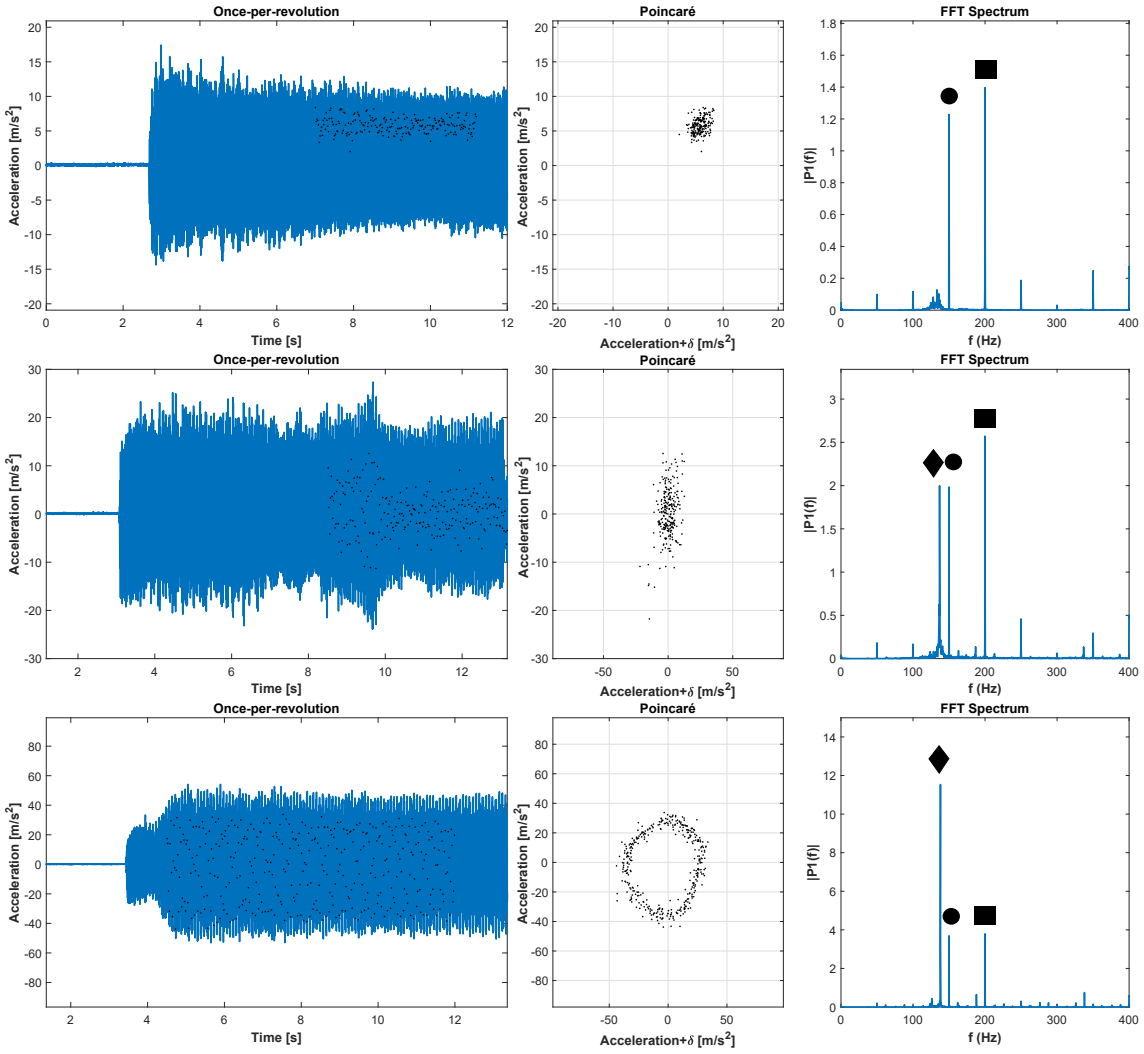

Fig. C.1 Once per revolution samples, Poincaré map and the FFT spectrum for stable cut (3000 rpm, 1 mm), marginal cut (3000 rpm, 2.5 mm), chatter cut (3000 rpm, 3 mm), respectively. Spindle frequency (runout) (●), tooth passing frequency (■), chatter frequency (♦)

## C.2 PID

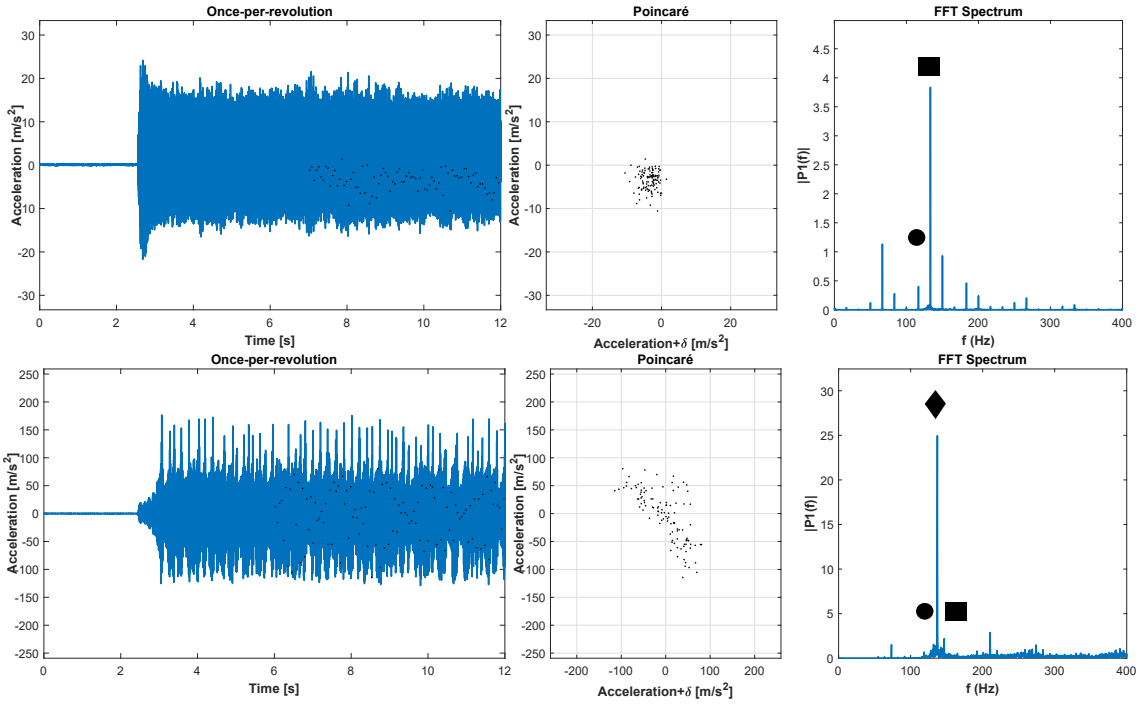

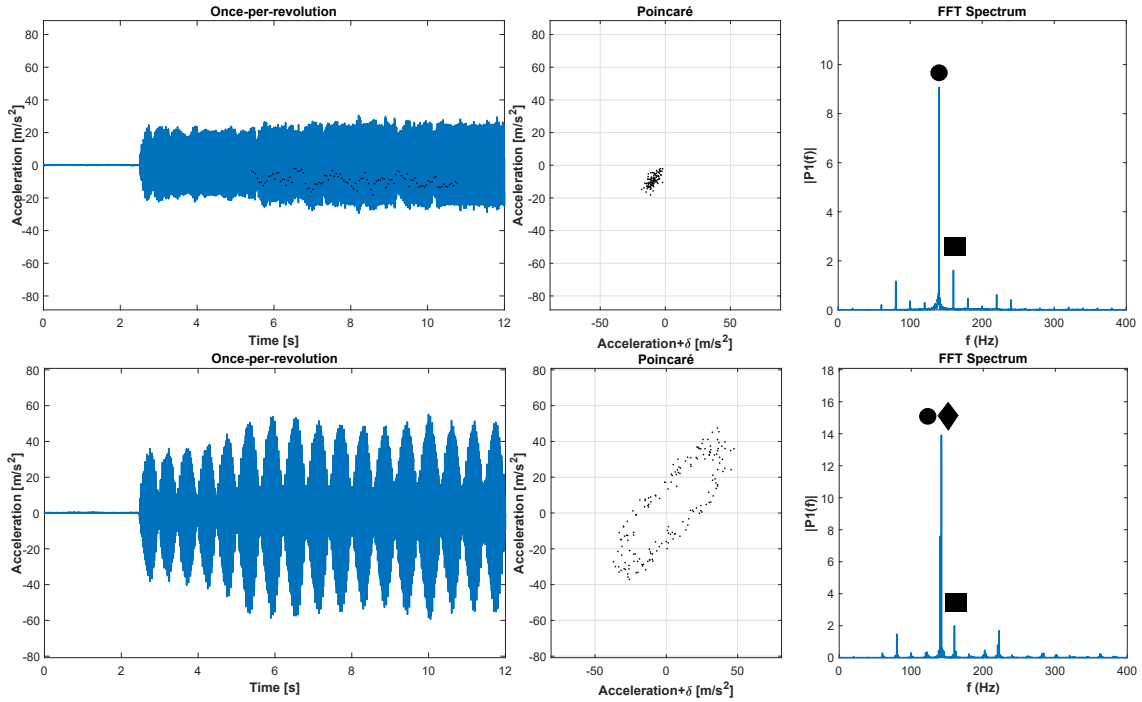


Fig. C.2 Once per revolution samples, Poincaré map and the FFT spectrum for stable cut (1000 rpm, 5 mm), chatter cut (1100 rpm, 5 mm), stable cut (1200 rpm, 3 mm), chatter cut (1200 rpm, 4 mm), respectively. Spindle frequency (runout) (●), tooth passing frequency (■), chatter frequency (⧫)

# C.3 LQR

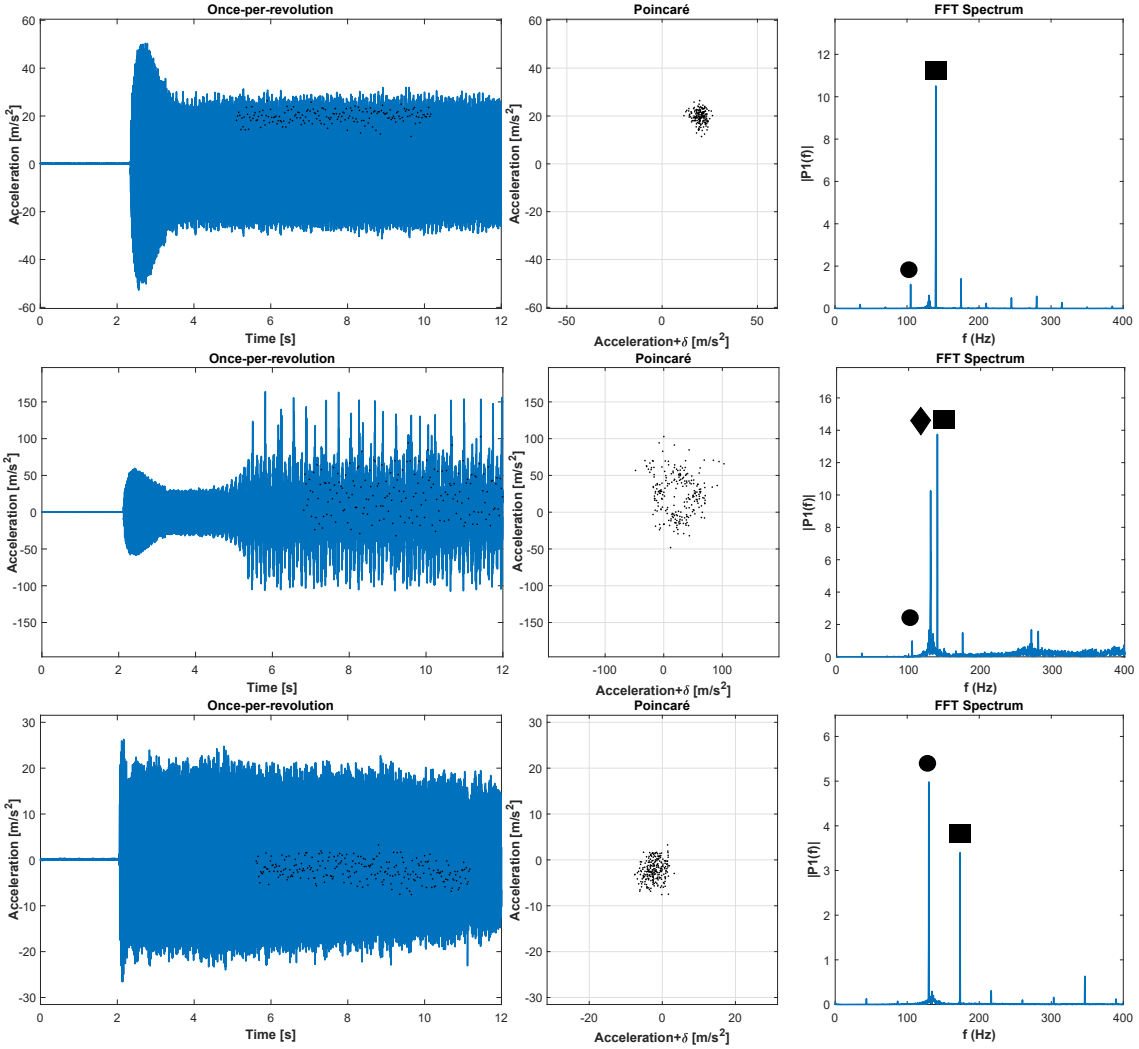
Once-per-revolution
Acceleration [m/s$^2$]
Time [s]
Poincaré
Acceleration+$\delta$ [m/s$^2$]
FFT Spectrum
|P1(f)|
f (Hz)
Once-per-revolution
Acceleration [m/s$^2$]
Time [s]
Poincaré
Acceleration+$\delta$ [m/s$^2$]
FFT Spectrum
|P1(f)|
f (Hz)
Once-per-revolution
Acceleration [m/s$^2$]
Time [s]
Poincaré
Acceleration+$\delta$ [m/s$^2$]
FFT Spectrum
|P1(f)|
f (Hz)

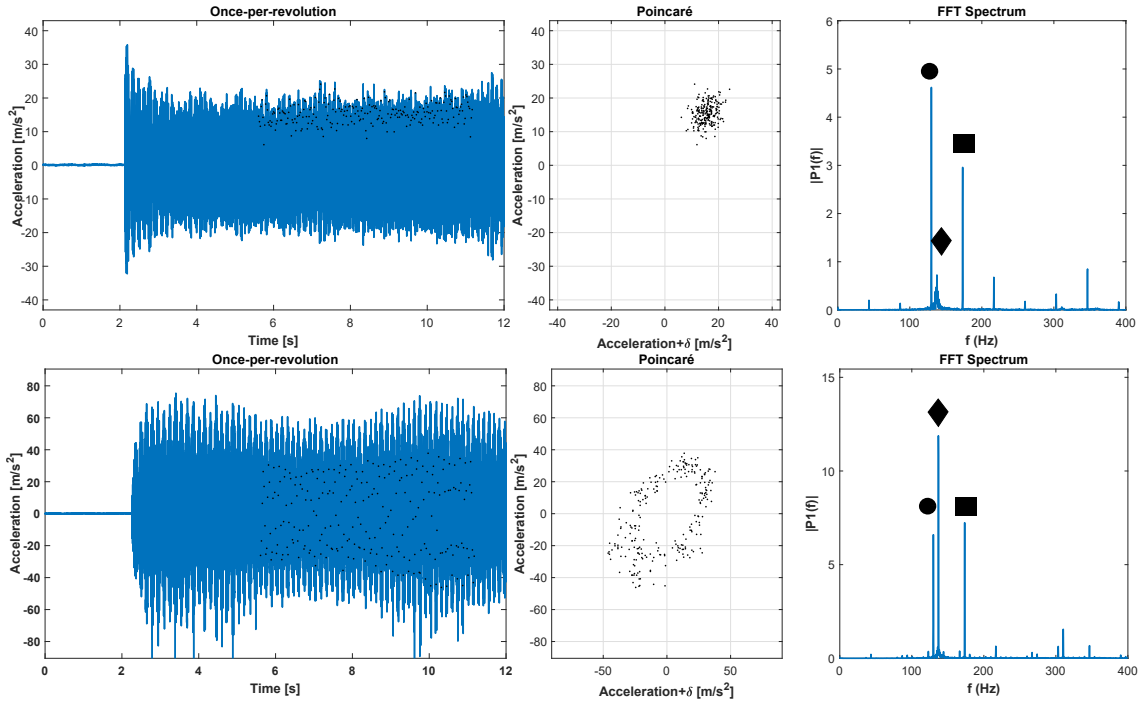


Fig. C.3 Once per revolution samples, Poincaré map and the FFT spectrum for stable cut (2100 rpm, 4 mm), chatter cut (2100 rpm, 5 mm), stable cut (2600 rpm, 2 mm), marginal cut (2600 rpm, 3 mm, chatter cut (2600 rpm, 4 mm), respectively. Spindle frequency (runout) (●), tooth passing frequency (■), chatter frequency (⧫)

# C.4 $H_\infty$

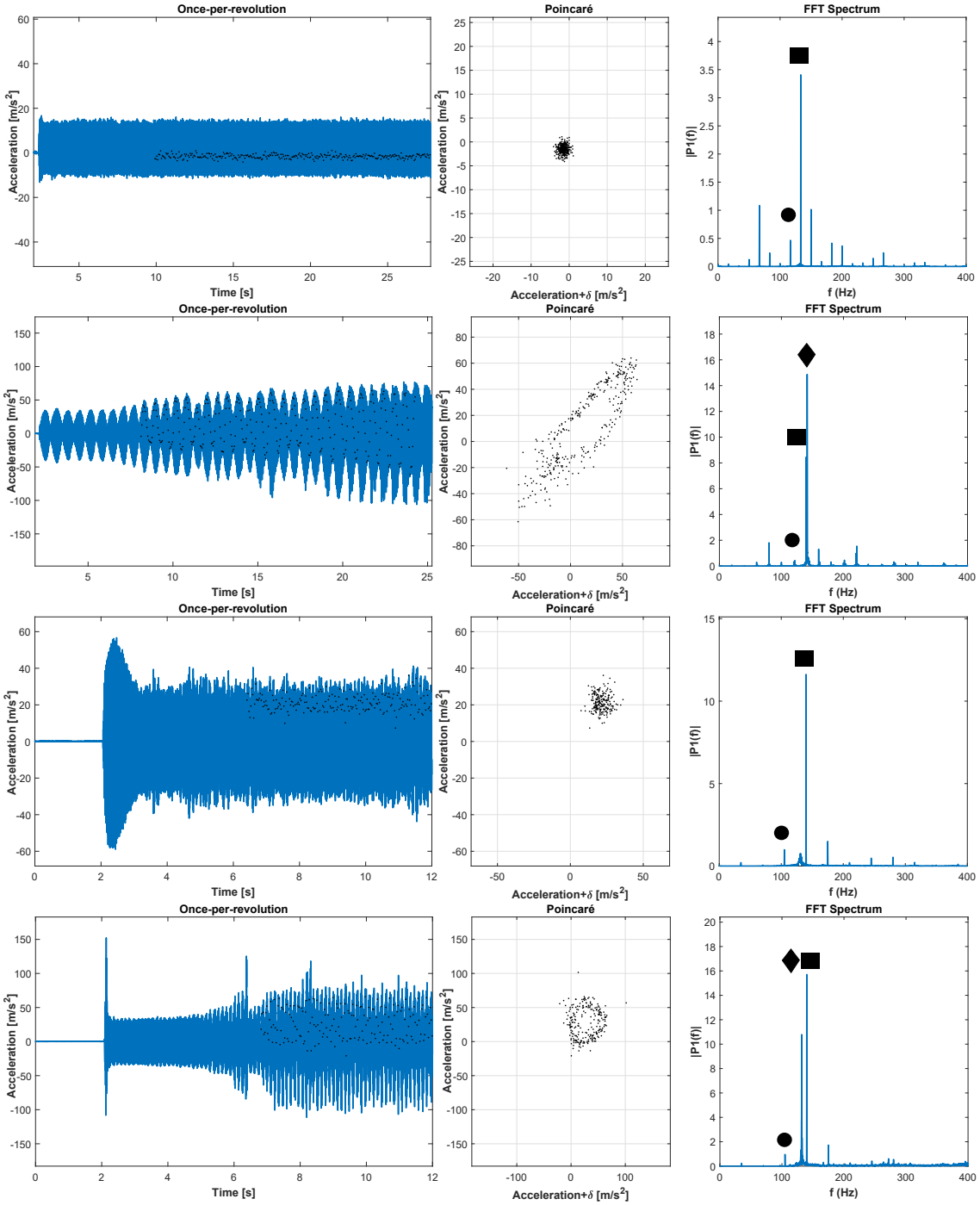
Once-per-revolution
Acceleration [m/s$^2$]
Time [s]
Poincaré
Acceleration [m/s$^2$]
Acceleration+$\delta$ [m/s$^2$]
FFT Spectrum
|P1(f)|
f (Hz)
Once-per-revolution
Acceleration [m/s$^2$]
Time [s]
Poincaré
Acceleration [m/s$^2$]
Acceleration+$\delta$ [m/s$^2$]
FFT Spectrum
|P1(f)|
f (Hz)
Once-per-revolution
Acceleration [m/s$^2$]
Time [s]
Poincaré
Acceleration [m/s$^2$]
Acceleration+$\delta$ [m/s$^2$]
FFT Spectrum
|P1(f)|
f (Hz)
Once-per-revolution
Acceleration [m/s$^2$]
Time [s]
Poincaré
Acceleration [m/s$^2$]
Acceleration+$\delta$ [m/s$^2$]
FFT Spectrum
|P1(f)|
f (Hz)

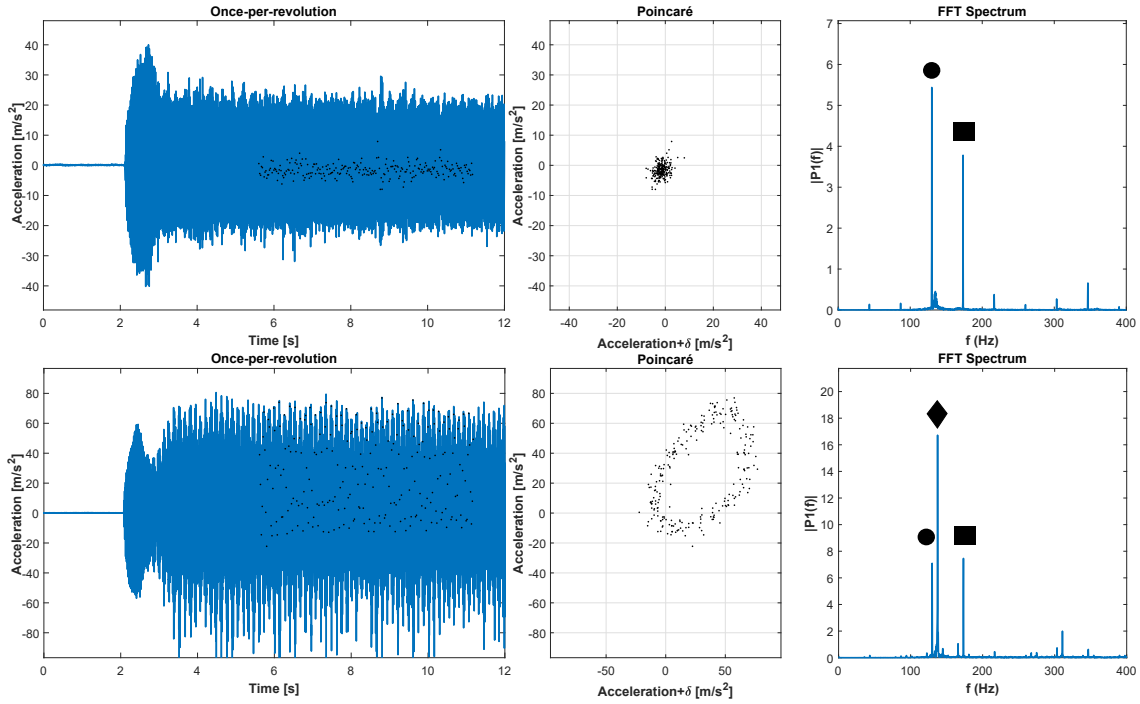


Fig. C.4 Once per revolution samples, Poincaré map and the FFT spectrum for stable cut (1000 rpm, 5 mm), chatter cut (1100 rpm, 5 mm), stable cut (2100 rpm, 4 mm), chatter cut (2100 rpm, 5 mm), stable cut (2600 rpm, 2 mm), chatter cut (2600 rpm, 4 mm), respectively. Spindle frequency (runout) (●), tooth passing frequency (■), chatter frequency (⧫)

# C.5 $\mu$ *synthesis*

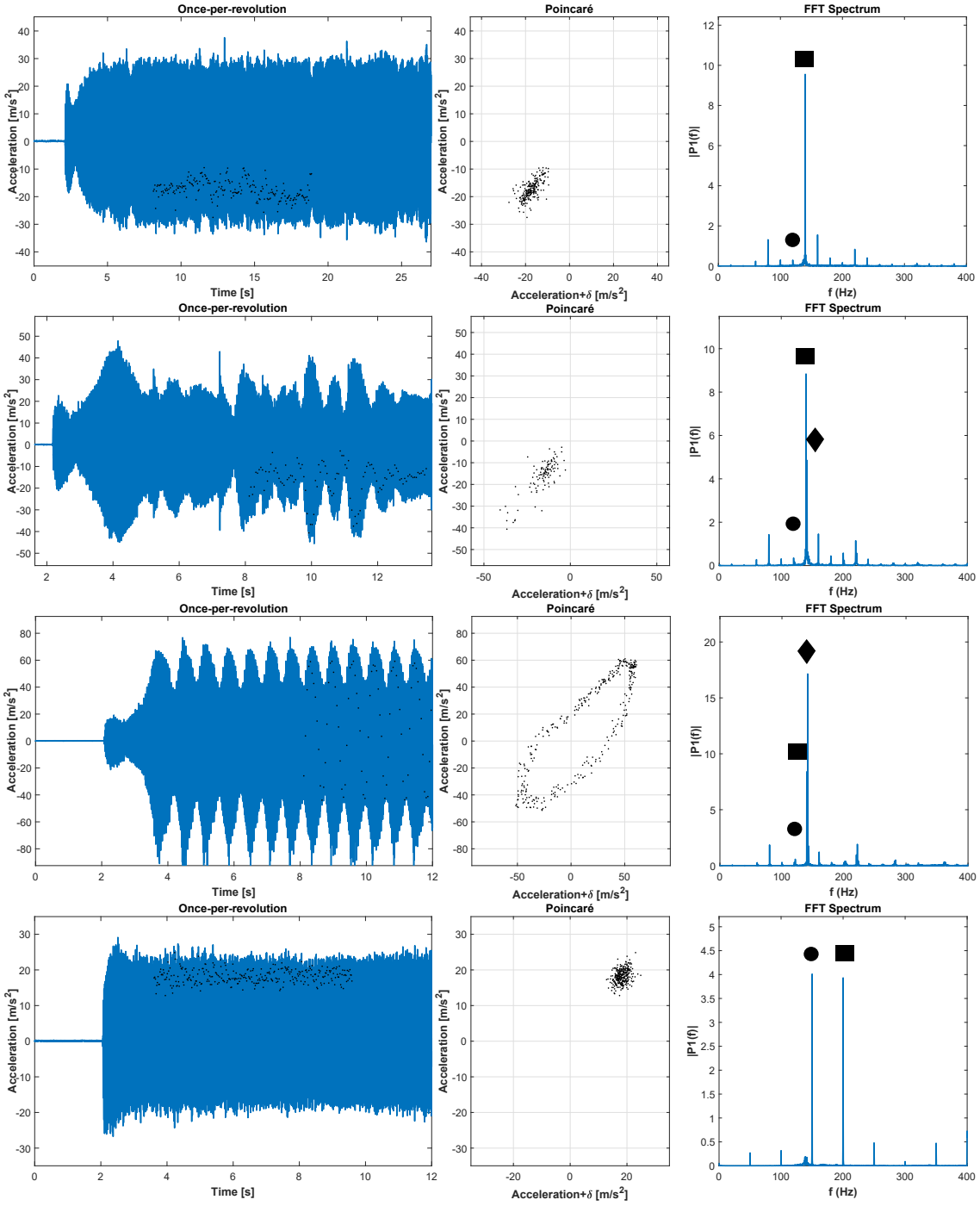

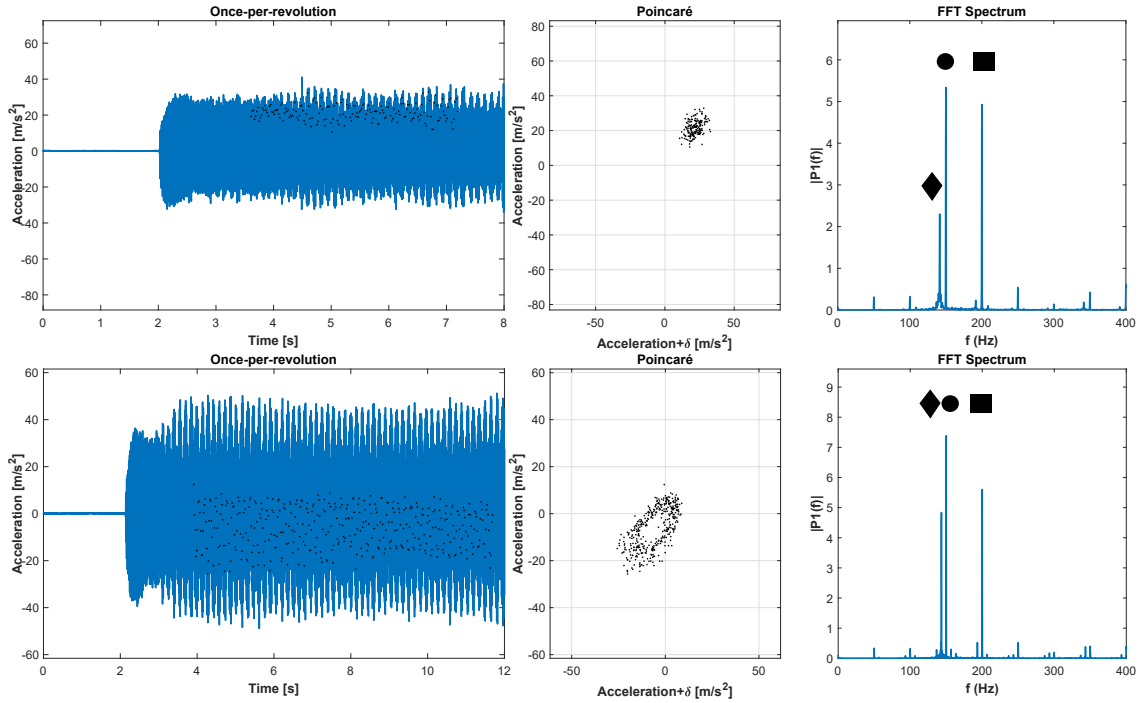


Fig. C.5 Once per revolution samples, Poincaré map and the FFT spectrum for stable cut (1200 rpm, 3 mm), marginal cut (1200 rpm, 4 mm), chatter cut (1200 rpm, 5 mm), stable cut (3000 rpm, 3 mm), marginal cut (3000 rpm, 4 mm), chatter cut (3000 rpm, 5 mm), respectively. Spindle frequency (runout) (●), tooth passing frequency (■), chatter frequency (♦)

# Appendix D

# Research papers

## D.1 Papers from thesis

1. M. Ozsoy, N. Sims, and E. Ozturk, "Investigation of an actively controlled robot arm for vibration suppression in milling," in EURODYN 2020: Proceedings of the XI International Conference on Structural Dynamics. European Association for Structural Dynamics (EASD), 2020, pp. 4577–4589.

2. M. Ozsoy, N. D. Sims, and E. Ozturk, "Robotically assisted active vibration control in milling: A feasibility study," Mechanical Systems and Signal Processing, vol. 177, p. 109152, 2022.

3. M. Ozsoy, N. Sims, and E. Ozturk, "Improving chatter stability of flexible structure milling in robotic assisted machining," in ISMA 2022: Proceedings of the International Conference on Noise and Vibration Engineering, 2022. (Submitted)

4. M. Ozsoy, N. D. Sims, and E. Ozturk, "Robotically assisted active vibration control in milling: experimental study," 2022. (In preparation)

5. M. Ozsoy, N. D. Sims, and E. Ozturk, “ Actuator saturation model in frequency domain, 2022. (In preparation)

6. M. Ozsoy, N. Sims, and E. Ozturk, “The effect of optimisation strategies of active chatter control on actuator saturation in milling,” in CMMO 2023: 19th CIRP Conference on Modeling of Machining Operations, 2023. (Submitted)

## D.2 Collaborations

1. M. Ozsoy, H. Dogan, E. Ozturk, D. J. Wagg, and N. D. Sims, “ Active chatter suppression through virtual inerter-based passive absorber control, in MIC 2022: MIC Procedia. (Published)

2. M. Ozsoy, H. Dogan, E. Ozturk, D. J. Wagg, and N. D. Sims, “ Active chatter suppression through virtual inerter-based passive absorber control, 2022. (In preparation for a journal)

# References


[1] M. Zupan, M. F. Ashby, and N. A. Fleck, "Actuator classification and selection-the development of a database," *Advanced Engineering Materials*, vol. 4, no. 12, pp. 933–940, 2002.

[2] Operational and M. Manual, *Micromega Dynamics*. Belgium, 2019.

[3] N. D. Sims, "The self-excitation damping ratio: a chatter criterion for time-domain milling simulations," 2005.

[4] S. Tobias and W. Fishwick, "Theory of regenerative machine tool chatter," *The engineer*, vol. 205, no. 7, pp. 199–203, 1958.

[5] C. Andrew and S. Tobias, "A critical comparison of two current theories of machine tool chatter," *International Journal of Machine Tool Design and Research*, vol. 1, no. 4, pp. 325–335, 1961.

[6] S. Tobias, *Machine Tool Vibration*. Blackie, London, 1965.

[7] J. Tlusty, F. Ismail, and W. Zaton, "Use of special milling cutters against chatter," in *NAMRC*, vol. 11, no. 599, 1983, pp. 408–415.

[8] J. Tlusty, *Manufacturing processes and equipment*, 2000.

[9] J. Tlusty and M. Polacek, "The stability of machine tools against self-excited vibrations in machining, 1963," *Proceedings of the ASME International*.

[10] J. Tlusty, "A method of analysis of machine tool stability," in *Proc. 6th MTDR*, vol. 5, 1965.

[11] E. Ozturk, A. Barrios, C. Sun, S. Rajabi, and J. Munoa, "Robotic assisted milling for increased productivity," *CIRP Annals*, 2018.

[12] N. Esfandi and T.-C. Tsao, "Robot assisted machining of thin-walled structures," *IFAC-PapersOnLine*, vol. 50, no. 1, pp. 14 594–14 599, 2017.

[13] M. Ozsoy, N. Sims, and E. Ozturk, "Investigation of an actively controlled robot arm for vibration suppression in milling," in *EURODYN 2020: Proceedings of the XI International Conference on Structural Dynamics*. European Association for Structural Dynamics (EASD), 2020, pp. 4577–4589.

[14] M. Ozsoy, N. D. Sims, and E. Ozturk, "Robotically assisted active vibration control in milling: A feasibility study," *Mechanical Systems and Signal Processing*, vol. 177, p. 109152, 2022.

[15] M. E. Merchant, "Twentieth century evolution of machining in the united states—an interpretative review," *Sadhana*, vol. 28, no. 5, pp. 867–874, 2003.

[16] F. W. Taylor, *On the Art of Cutting Metals...* American society of mechanical engineers, 1906.

[17] M. E. Merchant, "Mechanics of the metal cutting process. i. orthogonal cutting and a type 2 chip," *Journal of applied physics*, vol. 16, no. 5, pp. 267–275, 1945.

[18] M. E. Merchantt, "Mechanics of the metal cutting process. ii. plasticity conditions in orthogonal cutting," *Journal of applied physics*, vol. 16, no. 6, pp. 318–324, 1945.

[19] M. E. Merchant, *Basic mechanics of the metal-cutting process*, 1944.

[20] H. Ernst, *Physics of metal cutting*. Cincinnati Milling Machine Company, 1938.

[21] R. Arnold, "Cutting tools research: report of subcommittee on carbide tools: the mechanism of tool vibration in the cutting of steel," *Proceedings of the institution of mechanical engineers*, vol. 154, no. 1, pp. 261–284, 1946.

[22] R. Arnold and G. Hankins, "The mechanics of the cutting operation," *Proceedings of the Institution of Mechanical Engineers*, vol. 155, no. 1, pp. 238–240, 1946.

[23] Y. Altintaş and E. Budak, "Analytical prediction of stability lobes in milling," *CIRP Annals-Manufacturing Technology*, vol. 44, no. 1, pp. 357–362, 1995.

[24] E. Budak and Y. Altintas, "Analytical prediction of chatter stability in milling—part i: general formulation," 1998.

[25] Y. Altintas, "Analytical prediction of three dimensional chatter stability in milling," *JSME International Journal Series C Mechanical Systems, Machine Elements and Manufacturing*, vol. 44, no. 3, pp. 717–723, 2001.

[26] E. Budak and Y. Altintas, "Analytical prediction of chatter stability in milling—part ii: application of the general formulation to common milling systems," 1998.

[27] T. Insperger and G. Stépán, "Semi-discretization method for delayed systems," *International Journal for numerical methods in engineering*, vol. 55, no. 5, pp. 503–518, 2002.

[28] T. Insperger and G. Stépan, "Stability of the milling process," *Periodica polytechnica mechanical engineering*, vol. 44, no. 1, pp. 47–57, 2000.

[29] T. Insperger and G. Stépán, "Updated semi-discretization method for periodic delay-differential equations with discrete delay," *International Journal for Numerical Methods in Engineering*, vol. 61, no. 1, pp. 117–141, 2004.

[30] Y. Ding, L. Zhu, X. Zhang, and H. Ding, "A full-discretization method for prediction of milling stability," *International Journal of Machine Tools and Manufacture*, vol. 50, no. 5, pp. 502–509, 2010.

[31] G. Quintana and J. Ciurana, "Chatter in machining processes: A review," *International Journal of Machine Tools and Manufacture*, vol. 51, no. 5, pp. 363 – 376, 2011.

[32] Y. Altintas, G. Stepan, E. Budak, T. Schmitz, and Z. M. Kilic, "Chatter stability of machining operations," *Journal of Manufacturing Science and Engineering*, vol. 142, no. 11, 2020.

[33] E. Budak, L. T. Tunç, S. Alan, and H. N. Özgüven, "Prediction of workpiece dynamics and its effects on chatter stability in milling," *CIRP Annals-Manufacturing Technology*, vol. 61, no. 1, pp. 339–342, 2012.

[34] Y. Altintas and Z. Kilic, "Generalized dynamic model of metal cutting operations," *CIRP Annals-Manufacturing Technology*, vol. 62, no. 1, pp. 47–50, 2013.

[35] J. Munoa, X. Beudaert, Z. Dombovari, Y. Altintas, E. Budak, C. Brecher, and G. Stepan, "Chatter suppression techniques in metal cutting," *CIRP Annals*, vol. 65, no. 2, pp. 785–808, 2016.

[36] T. Insperger, "Full-discretization and semi-discretization for milling stability prediction: some comments," *International Journal of Machine Tools and Manufacture*, vol. 50, no. 7, pp. 658–662, 2010.

[37] G. Quintana, J. Ciurana, and D. Teixidor, "A new experimental methodology for identification of stability lobes diagram in milling operations," *International Journal of Machine Tools and Manufacture*, vol. 48, no. 15, pp. 1637–1645, 2008.

[38] D. Ewins, "Modal testing: theory, practice and application (mechanical engineering research studies: engineering dynamics series)," *Research studies Pre, 2nd ed., ISBN-13*, pp. 978–0 863 802 188, 2000.

[39] H. Caliskan, Z. M. Kilic, and Y. Altintas, "On-line energy-based milling chatter detection," *Journal of Manufacturing Science and Engineering*, vol. 140, no. 11, p. 111012, 2018.

[40] Y. Liao and Y. Young, "A new on-line spindle speed regulation strategy for chatter control," *International Journal of Machine Tools and Manufacture*, vol. 36, no. 5, pp. 651–660, 1996.

[41] I. Bediaga, M. Zatarain, J. Munoa, and R. Lizarralde, "Application of continuous spindle speed variation for chatter avoidance in roughing milling," *Proceedings of the Institution of Mechanical Engineers, Part B: Journal of Engineering Manufacture*, vol. 225, no. 5, pp. 631–640, 2011.

[42] I. Bediaga, M. Zatarain, J. Munoa, R. Lizarralde, and L. N. L. de Lacalle, "Application of continuous spindle speed variation for chatter avoidance in milling. optimisation of speed variation parameters," in *7th International CIRP Conference on High Speed Machining*, no. 41-46, 2008.

[43] E. Al-Regib, J. Ni, and S.-H. Lee, "Programming spindle speed variation for machine tool chatter suppression," *International Journal of Machine Tools and Manufacture*, vol. 43, no. 12, pp. 1229–1240, 2003.

[44] S. Sastry, S. G. Kapoor, and R. E. DeVor, "Floquet theory based approach for stability analysis of the variable speed face-milling process," *Journal of manufacturing science and engineering*, vol. 124, no. 1, pp. 10–17, 2002.

[45] S. Seguy, T. Insperger, L. Arnaud, G. Dessein, and G. Peigné, "On the stability of high-speed milling with spindle speed variation," *The International Journal of Advanced Manufacturing Technology*, vol. 48, no. 9-12, pp. 883–895, 2010.

[46] A. Yilmaz, A.-R. Emad, and J. Ni, "Machine tool chatter suppression by multi-level random spindle speed variation," *Journal of manufacturing science and engineering*, vol. 124, no. 2, pp. 208–216, 2002.

[47] T. Delio, J. Tlusty, and S. Smith, "Use of audio signals for chatter detection and control," *Journal of engineering for industry*, vol. 114, no. 2, pp. 146–157, 1992.

[48] W. L. Weingaertner, R. B. Schroeter, M. L. Polli, and J. de Oliveira Gomes, "Evaluation of high-speed end-milling dynamic stability through audio signal measurements," *Journal of Materials Processing Technology*, vol. 179, no. 1-3, pp. 133–138, 2006.

[49] T. L. Schmitz, M. A. Davies, K. Medicus, and J. Snyder, "Improving high-speed machining material removal rates by rapid dynamic analysis," *CIRP Annals-Manufacturing Technology*, vol. 50, no. 1, pp. 263–268, 2001.

[50] T. L. Schmitz, K. Medicus, and B. Dutterer, "Exploring once-per-revolution audio signal variance as a chatter indicator," *Machining Science and Technology*, vol. 6, no. 2, pp. 215–233, 2002.

[51] T. L. Schmitz, "Chatter recognition by a statistical evaluation of the synchronously sampled audio signal," *Journal of Sound and Vibration*, vol. 262, no. 3, pp. 721–730, 2003.

[52] O. Tuysuz and Y. Altintas, "Frequency domain updating of thin-walled workpiece dynamics using reduced order substructuring method in machining," *Journal of Manufacturing Science and Engineering*, vol. 139, no. 7, p. 071013, 2017.

[53] C. Sun and Y. Altintas, "Chatter free tool orientations in 5-axis ball-end milling," *International Journal of Machine Tools and Manufacture*, vol. 106, pp. 89–97, 2016.

[54] O. Tuysuz and Y. Altintas, "Time-domain modeling of varying dynamic characteristics in thin-wall machining using perturbation and reduced-order substructuring methods," *Journal of Manufacturing Science and Engineering*, vol. 140, no. 1, p. 011015, 2018.

[55] J. Den Hartog, "Mechanical vibrations,(1934), 122," *McGraw, Hill*.

[56] N. D. Sims, "Vibration absorbers for chatter suppression: a new analytical tuning methodology," *Journal of Sound and Vibration*, vol. 301, no. 3-5, pp. 592–607, 2007.

[57] R. Hahn, "Design of lanchester damper for elimination of metal cutting chatter," *Trans. ASME*, vol. 73, p. 331, 1951.

[58] K. Kolluru, D. Axinte, and A. Becker, "A solution for minimising vibrations in milling of thin walled casings by applying dampers to workpiece surface," *CIRP Annals-Manufacturing Technology*, vol. 62, no. 1, pp. 415–418, 2013.

[59] M. Zatarain, J. Munoa, G. Peigné, and T. Insperger, "Analysis of the influence of mill helix angle on chatter stability," *CIRP Annals-Manufacturing Technology*, vol. 55, no. 1, pp. 365–368, 2006.

[60] T. Insperger, J. Munoa, M. a. Zatarain, and G. Peigné, "Unstable islands in the stability chart of milling processes due to the helix angle," in *CIRP 2nd International Conference on High Performance Cutting*, 2006, pp. 12–13.

[61] B. Patel, B. Mann, and K. Young, "Uncharted islands of chatter instability in milling," *International Journal of Machine Tools and Manufacture*, vol. 48, no. 1, pp. 124–134, 2008.

[62] N. Sims, B. Mann, and S. Huyanan, "Analytical prediction of chatter stability for variable pitch and variable helix milling tools," *Journal of Sound and Vibration*, vol. 317, no. 3-5, pp. 664–686, 2008.

[63] G. Aguirre, M. Gorostiaga, T. Porchez, and J. Muñoa, "Self-tuning semi-active tuned-mass damper for machine tool chatter suppression," *ISMA2012-USD2012*, pp. 109–124, 2012.

[64] J. Munoa, A. Iglesias, A. Olarra, Z. Dombovari, M. Zatarain, and G. Stepan, "Design of self-tuneable mass damper for modular fixturing systems," *CIRP Annals*, vol. 65, no. 1, pp. 389–392, 2016.

[65] J. Burtscher and J. Fleischer, "Adaptive tuned mass damper with variable mass for chatter avoidance," *CIRP Annals*, vol. 66, no. 1, pp. 397–400, 2017.

[66] H. Moradi, G. Vossoughi, M. Behzad, and M. R. Movahhedy, "Vibration absorber design to suppress regenerative chatter in nonlinear milling process: application for machining of cantilever plates," *Applied Mathematical Modelling*, vol. 39, no. 2, pp. 600–620, 2015.

[67] L. Yuan, S. Sun, Z. Pan, D. Ding, O. Gienke, and W. Li, "Mode coupling chatter suppression for robotic machining using semi-active magnetorheological elastomers absorber," *Mechanical Systems and Signal Processing*, vol. 117, pp. 221–237, 2019.

[68] H. Merritt, "Theory of self-excited machine-tool chatter: contribution to machine-tool chatter research—," *Journal of engineering for industry*, vol. 87, no. 4, pp. 447–454, 1965.

[69] R. Kegg, "Cutting dynamics in machine tool chatter: Contribution to machine-tool chatter research—3," 1965.

[70] R. Sridhar, R. Hohn, and G. Long, "A general formulation of the milling process equation: contribution to machine tool chatter research—5," 1968.

[71] R. Sridhar, R. Hohnn, and G. Long, "A stability algorithm for the general milling process: contribution to machine tool chatter research—7," 1968.

[72] F. Koenigsberger and J. Tlusty, *Machine tool structures*. Elsevier, 2016.

[73] H. Opitz, "Chatter behavior of heavy machine tools," TECHNISCHE HOCHSCHULE AACHEN (GERMANY FR) LABORATORIUM FUER ..., Tech. Rep., 1968.

[74] H. Opitzz, "Investigation and calculation of the chatter behavior of: Lathes and milling machines," *Annals of the CIRP*, vol. 18, pp. 335–342, 1979.

[75] J. Tlusty and F. Ismail, "Basic non-linearity in machining chatter," *CIRP Annals*, vol. 30, no. 1, pp. 299–304, 1981.

[76] J. Tlusty, W. Zaton, and F. Ismail, "Stability lobes in milling," *CIRP Annals*, vol. 32, no. 1, pp. 309–313, 1983.

[77] J. Tlusty and F. Ismail, "Special aspects of chatter in milling," 1983.

[78] J. Tlusty, "Dynamics of high-speed milling," 1986.

[79] Y. Altintas, D. Montgomery, and E. Budak, "Dynamic peripheral milling of flexible structures," 1992.

[80] S. Smith and J. Tlusty, "Efficient simulation programs for chatter in milling," *CIRP annals*, vol. 42, no. 1, pp. 463–466, 1993.

[81] I. Minis and R. Yanushevsky, "A new theoretical approach for the prediction of machine tool chatter in milling," *Journal of Engineering for Industry*, vol. 115, pp. 1–8, 1993.

[82] M. A. Davies, J. R. Pratt, B. S. Dutterer, and T. J. Burns, "The stability of low radial immersion milling," *CIRP Annals*, vol. 49, no. 1, pp. 37–40, 2000.

[83] M. A. Davies, J. R. Pratt, B. Dutterer, and T. J. Burns, "Stability prediction for low radial immersion milling," *J. Manuf. Sci. Eng.*, vol. 124, no. 2, pp. 217–225, 2002.

[84] P. V. Bayly, B. P. Mann, T. L. Schmitz, D. A. Peters, G. Stepan, and T. Insperger, "Effects of radial immersion and cutting direction on chatter instability in end-milling," in *ASME International Mechanical Engineering Congress and Exposition*, vol. 3641, 2002, pp. 351–363.

[85] P. Bayly, J. Halley, B. P. Mann, and M. Davies, "Stability of interrupted cutting by temporal finite element analysis," *J. Manuf. Sci. Eng.*, vol. 125, no. 2, pp. 220–225, 2003.

[86] T. Insperger, G. Stépán, and J. Turi, "On the higher-order semi-discretizations for periodic delayed systems," *Journal of Sound and Vibration*, vol. 313, no. 1-2, pp. 334–341, 2008.

[87] G. Stepan, D. Hajdu, A. Iglesias, D. Takacs, and Z. Dombovari, "Ultimate capability of variable pitch milling cutters," *CIRP Annals*, vol. 67, no. 1, pp. 373–376, 2018.

[88] S. Merdol and Y. Altintas, "Multi frequency solution of chatter stability for low immersion milling," *J. Manuf. Sci. Eng.*, vol. 126, no. 3, pp. 459–466, 2004.

[89] D. Bachrathy and G. Stepan, "Improved prediction of stability lobes with extended multi frequency solution," *CIRP Annals*, vol. 62, no. 1, pp. 411–414, 2013.

[90] S. Smith and J. Tlusty, "Update on high-speed milling dynamics," 1990.

[91] S. Smith and T. Delio, "Sensor-based chatter detection and avoidance by spindle speed selection," 1992.

[92] S. Smith and J. Tlusty, "Stabilizing chatter by automatic spindle speed regulation," *CIRP annals*, vol. 41, no. 1, pp. 433–436, 1992.

[93] Y. Tarng and T. Li, "The change of spindle speed for the avoidance of chatter in end milling," *Journal of materials processing technology*, vol. 41, no. 2, pp. 227–236, 1994.

[94] Y. Tarng, Y. Hseih, and T. Li, "Automatic selection of spindle speed for suppression of regenerative chatter in turning," *The International Journal of Advanced Manufacturing Technology*, vol. 11, no. 1, pp. 12–17, 1996.

[95] J. Sexton, B. Stone *et al.*, "The stability of machining with continuously varying spindle speed," *Annals of the CIRP*, vol. 27, no. 1, pp. 321–326, 1978.

[96] T. s. Insperger, T. L. Schmitz, T. J. Burns, and G. b. Ste´ pa´ n, "Comparison of analytical and numerical simulations for variable spindle speed turning," in *ASME International Mechanical Engineering Congress and Exposition*, vol. 37203, 2003, pp. 41–47.

[97] A. Otto, G. Kehl, M. Mayer, and G. Radons, "Stability analysis of machining with spindle speed variation," in *Advanced Materials Research*, vol. 223. Trans Tech Publ, 2011, pp. 600–609.

[98] S. Jayaram, S. Kapoor, and R. DeVor, "Analytical stability analysis of variable spindle speed machining," *J. Manuf. Sci. Eng.*, vol. 122, no. 3, pp. 391–397, 2000.

[99] S. Lin, R. DeVor, and S. G. Kapoor, "The effects of variable speed cutting on vibration control in face milling," 1990.

[100] Y. Altintas and P. K. Chan, "In-process detection and suppression of chatter in milling," *International Journal of Machine Tools and Manufacture*, vol. 32, no. 3, pp. 329–347, 1992.

[101] M. Zatarain, I. Bediaga, J. Munoa, and R. Lizarralde, "Stability of milling processes with continuous spindle speed variation: analysis in the frequency and time domains, and experimental correlation," *CIRP annals*, vol. 57, no. 1, pp. 379–384, 2008.

[102] S. Kato, E. Marui, and H. Kurita, "Some considerations on prevention of chatter vibration in boring operations," 1969.

[103] S. Ema and E. Marui, "Damping characteristics of an impact damper and its application," *International Journal of machine tools and manufacture*, vol. 36, no. 3, pp. 293–306, 1996.

[104] E. Marui, S. Ema, M. Hashimoto, and Y. Wakasawa, "Plate insertion as a means to improve the damping capacity of a cutting tool system," *International Journal of Machine Tools and Manufacture*, vol. 38, no. 10-11, pp. 1209–1220, 1998.

[105] S. Ema and E. Marui, "Suppression of chatter vibration of boring tools using impact dampers," *International Journal of Machine Tools and Manufacture*, vol. 40, no. 8, pp. 1141–1156, 2000.

[106] J. C. Ziegert, C. Stanislaus, T. L. Schmitz, and R. Sterling, "Enhanced damping in long slender end mills," *Journal of Manufacturing Processes*, vol. 8, no. 1, pp. 39–46, 2006.

[107] E. Edhi and T. Hoshi, "Stabilization of high frequency chatter vibration in fine boring by friction damper," *Precision engineering*, vol. 25, no. 3, pp. 224–234, 2001.

[108] K. SETO and N. TOMINARI, "Effect of a variable stiffness-type dynamic damper on machine tools with long overhung ram," *Bulletin of JSME*, vol. 19, no. 137, pp. 1270–1277, 1976.

[109] K. Liu and K. Rouch, "Optimal passive vibration control of cutting process stability in milling," *Journal of materials processing technology*, vol. 28, no. 1-2, pp. 285–294, 1991.

[110] Y. Yang, J. Munoa, and Y. Altintas, "Optimization of multiple tuned mass dampers to suppress machine tool chatter," *International Journal of Machine Tools and Manufacture*, vol. 50, no. 9, pp. 834–842, 2010.

[111] Y. Nakano, H. Takahara, and E. Kondo, "Countermeasure against chatter in end milling operations using multiple dynamic absorbers," *Journal of Sound and Vibration*, vol. 332, no. 6, pp. 1626–1638, 2013.

[112] M. Wang, T. Zan, Y. Yang, and R. Fei, "Design and implementation of nonlinear tmd for chatter suppression: An application in turning processes," *International Journal of Machine Tools and Manufacture*, vol. 50, no. 5, pp. 474–479, 2010.

[113] M. Wang, "Feasibility study of nonlinear tuned mass damper for machining chatter suppression," *Journal of Sound and Vibration*, vol. 330, no. 9, pp. 1917–1930, 2011.

[114] G. Habib, G. Kerschen, and G. Stepan, "Chatter mitigation using the nonlinear tuned vibration absorber," *International Journal of Non-Linear Mechanics*, vol. 91, pp. 103–112, 2017.

[115] K. Kim and J. Ha, "Suppression of machine tool chatter using a viscoelastic dynamic damper," 1987.

[116] A. Rashid and C. M. Nicolescu, "Design and implementation of tuned viscoelastic dampers for vibration control in milling," *International Journal of Machine Tools and Manufacture*, vol. 48, no. 9, pp. 1036–1053, 2008.

[117] J. Saffury and E. Altus, "Optimized chatter resistance of viscoelastic turning bars," *Journal of Sound and Vibration*, vol. 324, no. 1-2, pp. 26–39, 2009.

[118] Y. Yang, D. Xu, and Q. Liu, "Milling vibration attenuation by eddy current damping," *The International Journal of Advanced Manufacturing Technology*, vol. 81, no. 1-4, pp. 445–454, 2015.

[119] Y. Yang, R. Xie, and Q. Liu, "Design of a passive damper with tunable stiffness and its application in thin-walled part milling," *The International Journal of Advanced Manufacturing Technology*, vol. 89, no. 9-12, pp. 2713–2720, 2017.

[120] M. A. Butt, Y. Yang, X. Pei, and Q. Liu, "Five-axis milling vibration attenuation of freeform thin-walled part by eddy current damping," *Precision Engineering*, vol. 51, pp. 682–690, 2018.

[121] Z. Zhang, H. Li, G. Meng, and S. Ren, "Milling chatter suppression in viscous fluid: a feasibility study," *International Journal of Machine Tools and Manufacture*, vol. 120, pp. 20–26, 2017.

[122] Z. Zhang, H. Li, X. Liu, W. Zhang, and G. Meng, "Chatter mitigation for the milling of thin-walled workpiece," *International Journal of Mechanical Sciences*, vol. 138, pp. 262–271, 2018.

[123] J. Fei, B. Lin, S. Yan, M. Ding, J. Xiao, J. Zhang, X. Zhang, C. Ji, and T. Sui, "Chatter mitigation using moving damper," *Journal of Sound and Vibration*, vol. 410, pp. 49–63, 2017.

[124] J. Fei, B. Lin, J. Xiao, M. Ding, S. Yan, X. Zhang, and J. Zhang, "Investigation of moving fixture on deformation suppression during milling process of thin-walled structures," *Journal of Manufacturing Processes*, vol. 32, pp. 403–411, 2018.

[125] J. Munoa, M. Sanz-Calle, Z. Dombovari, A. Iglesias, J. Pena-Barrio, and G. Stepan, "Tuneable clamping table for chatter avoidance in thin-walled part milling," *CIRP Annals*, vol. 69, no. 1, pp. 313–316, 2020.

[126] M. Wan, T.-Q. Gao, J. Feng, and W.-H. Zhang, "On improving chatter stability of thin-wall milling by prestressing," *Journal of Materials Processing Technology*, vol. 264, pp. 32–44, 2019.

[127] R. Hahn, "Metal-cutting chatter and its elimination," *Transactions of the American Society of Mechanical Engineers*, vol. 75, no. 6, pp. 1073–1078, 1953.

[128] A. Iglesias, Z. Dombovari, G. Gonzalez, J. Munoa, and G. Stepan, "Optimum selection of variable pitch for chatter suppression in face milling operations," *Materials*, vol. 12, no. 1, p. 112, 2018.

[129] J. Slavicek, "The effect of irregular tooth pitch on stability of milling," in *Proceedings of the 6th MTDR Conference*, vol. 1. Pergamon Press London, 1965, pp. 15–22.

[130] Y. Altıntas, S. Engin, and E. Budak, "Analytical stability prediction and design of variable pitch cutters," 1999.

[131] E. Budak, "An analytical design method for milling cutters with nonconstant pitch to increase stability, part i: theory," *J. Manuf. Sci. Eng.*, vol. 125, no. 1, pp. 29–34, 2003.

[132] E. Budakk, "An analytical design method for milling cutters with nonconstant pitch to increase stability, part 2: application," *J. Manuf. Sci. Eng.*, vol. 125, no. 1, pp. 35–38, 2003.

[133] S. Turner, D. Merdol, Y. Altintas, and K. Ridgway, "Modelling of the stability of variable helix end mills," *International Journal of Machine Tools and Manufacture*, vol. 47, no. 9, pp. 1410–1416, 2007.

[134] N. D. Sims, "Multi-frequency chatter analysis using the shift theorem," *Procedia IUTAM*, vol. 22, pp. 3–9, 2017.

[135] A. R. Yusoff and N. D. Sims, "Optimisation of variable helix tool geometry for regenerative chatter mitigation," *International Journal of Machine Tools and Manufacture*, vol. 51, no. 2, pp. 133–141, 2011.

[136] Y.-z. Lei, "Use of the electrorheological technique (ert) for chatter control," in *International Conference on Intelligent Manufacturing*, vol. 2620. International Society for Optics and Photonics, 1995, pp. 762–766.

[137] T. Aoyama and I. Inasaki, "Application of electrorheological fluid dampers to machine tool elements," *CIRP Annals*, vol. 46, no. 1, pp. 309–312, 1997.

[138] M. Wang and R. Fei, "Chatter suppression based on nonlinear vibration characteristic of electrorheological fluids," *International Journal of Machine Tools and Manufacture*, vol. 39, no. 12, pp. 1925–1934, 1999.

[139] Y. Zhou and Y. Zhang, "Optimal design of a shear magnetorheological damper for turning vibration suppression," *Smart materials and structures*, vol. 22, no. 9, p. 095012, 2013.

[140] Y. Zhang, N. M. Wereley, W. Hu, M. Hong, and W. Zhang, "Magnetic circuit analyses and turning chatter suppression based on a squeeze-mode magnetorheological damping turning tool," *Shock and Vibration*, vol. 2015, 2015.

[141] A. Som, D.-H. Kim, and H. Son, "Semiactive magnetorheological damper for high aspect ratio boring process," *IEEE/ASME Transactions on Mechatronics*, vol. 20, no. 5, pp. 2575–2582, 2015.

[142] N. D. Sims, N. Holmes, and R. Stanway, "A unified modelling and model updating procedure for electrorheological and magnetorheological vibration dampers," *Smart materials and structures*, vol. 13, no. 1, p. 100, 2003.

[143] D. Batterbee and N. D. Sims, "Temperature sensitive controller performance of mr dampers," *Journal of Intelligent Material Systems and Structures*, vol. 20, no. 3, pp. 297–309, 2009.

[144] D. J. Segalman and J. M. Redmond, "Chatter supression through variable impedance and smart fluids," in *Smart Structures and Materials 1996: Industrial and Commercial Applications of Smart Structures Technologies*, vol. 2721. International Society for Optics and Photonics, 1996, pp. 353–363.

[145] D. Mei, Z. Yao, T. Kong, and Z. Chen, "Parameter optimization of time-varying stiffness method for chatter suppression based on magnetorheological fluid-controlled boring bar," *The International Journal of Advanced Manufacturing Technology*, vol. 46, no. 9-12, pp. 1071–1083, 2010.

[146] D. Mei, T. Kong, A. J. Shih, and Z. Chen, "Magnetorheological fluid-controlled boring bar for chatter suppression," *journal of materials processing technology*, vol. 209, no. 4, pp. 1861–1870, 2009.

[147] R. Klein and C. Nachtigal, "The application of active control to improve boring bar performance," 1975.

[148] R. Klein and C. Nachtigall, "A theoretical basis for the active control of a boring bar operation," 1975.

[149] D. Glaser and C. Nachtigal, "Development of a hydraulic chambered, actively controlled boring bar," 1979.

[150] S. G. Tewani, K. E. Rouch, and B. L. Walcott, "A study of cutting process stability of a boring bar with active dynamic absorber," *International Journal of Machine Tools and Manufacture*, vol. 35, no. 1, pp. 91–108, 1995.

[151] H. Tanaka, F. Obata, T. Matsubara, and H. Mizumoto, "Active chatter suppression of slender boring bar using piezoelectric actuators," *JSME international journal. Ser. C, Dynamics, control, robotics, design and manufacturing*, vol. 37, no. 3, pp. 601–606, 1994.

[152] J. R. Pratt and A. H. Nayfeh, "Chatter control and stability analysis of a cantilever boring bar under regenerative cutting conditions," *Philosophical Transactions of the Royal Society of London A: Mathematical, Physical and Engineering Sciences*, vol. 359, no. 1781, pp. 759–792, 2001.

[153] M. Fallah and B. Moetakef-Imani, "Design, analysis, and implementation of a new adaptive chatter control system in internal turning," *The International Journal of Advanced Manufacturing Technology*, vol. 104, no. 5-8, pp. 1637–1659, 2019.

[154] X. Lu, F. Chen, and Y. Altintas, "Magnetic actuator for active damping of boring bars," *CIRP Annals*, vol. 63, no. 1, pp. 369–372, 2014.

[155] F. Chen, X. Lu, and Y. Altintas, "A novel magnetic actuator design for active damping of machining tools," *International Journal of Machine Tools and Manufacture*, vol. 85, pp. 58–69, 2014.

[156] F. Chen, "Active damping of machine tools with magnetic actuators," Ph.D. dissertation, University of British Columbia, 2014.

[157] B. Chung, S. Smith, and J. Tlusty, "Active damping of structural modes in high-speed machine tools," *Journal of vibration and control*, vol. 3, no. 3, pp. 279–295, 1997.

[158] J. Munoa, I. Mancisidor, N. Loix, L. Uriarte, R. Barcena, and M. Zatarain, "Chatter suppression in ram type travelling column milling machines using a biaxial inertial actuator," *CIRP Annals-Manufacturing Technology*, vol. 62, no. 1, pp. 407–410, 2013.

[159] J. Monnin, F. Kuster, and K. Wegener, "Optimal control for chatter mitigation in milling—part 1: Modeling and control design," *Control Engineering Practice*, vol. 24, pp. 156–166, 2014.

[160] J. Monnin, F. Kuster, and K. Wegenerr, "Optimal control for chatter mitigation in milling—part 2: Experimental validation," *Control Engineering Practice*, vol. 24, pp. 167–175, 2014.

[161] C. Wang, X. Zhang, H. Cao, X. Chen, and J. Xiang, "Milling stability prediction and adaptive chatter suppression considering helix angle and bending," *The International Journal of Advanced Manufacturing Technology*, vol. 95, no. 9, pp. 3665–3677, 2018.

[162] Z. Chen, H.-T. Zhang, X. Zhang, and H. Ding, "Adaptive active chatter control in milling processes," *Journal of Dynamic Systems, Measurement, and Control*, vol. 136, no. 2, p. 021007, 2014.

[163] D. Li, H. Cao, X. Zhang, X. Chen, and R. Yan, "Model predictive control based active chatter control in milling process," *Mechanical Systems and Signal Processing*, vol. 128, pp. 266–281, 2019.

[164] F. Shi, H. Cao, X. Zhang, and X. Chen, "A chatter mitigation technique in milling based on h∞-addpms and piezoelectric stack actuators," *The International Journal of Advanced Manufacturing Technology*, vol. 101, no. 9-12, pp. 2233–2248, 2019.

[165] P. Ruttanatri, M. O. Cole, R. Pongvuthithum, and S. Huyanan, "H-infinity controller design for chatter suppression in machining based on integrated cutting and flexible structure model," *Automatica*, p. 109643, 2021.

[166] X. Zhang, C. Wang, J. Liu, R. Yan, H. Cao, and X. Chen, "Robust active control based milling chatter suppression with perturbation model via piezoelectric stack actuators," *Mechanical Systems and Signal Processing*, vol. 120, pp. 808–835, 2019.

[167] Y. He, X. Chen, Z. Liu, and Y. Chen, "Active vibration control of motorized spindle based on mixed h∞/kalman filter robust state feedback control," *Journal of Vibration and control*, vol. 25, no. 6, pp. 1279–1293, 2019.

[168] Y. Zhang and N. D. Sims, "Milling workpiece chatter avoidance using piezoelectric active damping: a feasibility study," *Smart materials and structures*, vol. 14, no. 6, p. N65, 2005.

[169] J.-H. Kyung and C.-W. Lee, "Controller design for a magnetically suspended milling spindle based on chatter stability analysis," *JSME International Journal Series C Mechanical Systems, Machine Elements and Manufacturing*, vol. 46, no. 2, pp. 416–422, 2003.

[170] N. Van de Wouw, N. van Dijk, A. Schiffler, H. Nijmeijer, and E. Abele, "Experimental validation of robust chatter control for high-speed milling processes," in *Time Delay Systems*. Springer, 2017, pp. 315–331.

[171] Y. Wu, H.-T. Zhang, T. Huang, G. Ren, and H. Ding, "Robust chatter mitigation control for low radial immersion machining processes," *IEEE Transactions on Automation Science and Engineering*, vol. 15, no. 4, pp. 1972–1979, 2018.

[172] T. Huang, Z. Chen, H.-T. Zhang, and H. Ding, "Active control of an active magnetic bearings supported spindle for chatter suppression in milling process," *Journal of Dynamic Systems, Measurement, and Control*, vol. 137, no. 11, p. 111003, 2015.

[173] S. Wan, X. Li, W. Su, J. Yuan, J. Hong, and X. Jin, "Active damping of milling chatter vibration via a novel spindle system with an integrated electromagnetic actuator," *Precision Engineering*, vol. 57, pp. 203–210, 2019.

[174] C. R. Knospe, "Active magnetic bearings for machining applications," *Control Engineering Practice*, vol. 15, no. 3, pp. 307–313, 2007.

[175] S. Huyanan and N. D. Sims, "Vibration control strategies for proof-mass actuators," *Journal of Vibration and Control*, vol. 13, no. 12, pp. 1785–1806, 2007.

[176] S. Huyanan, "An active vibration absorber for chatter reduction in machining," Ph.D. dissertation, University of Sheffield, 2007.

[177] X. Beudaert, K. Erkorkmaz, and J. Munoa, "Portable damping system for chatter suppression on flexible workpieces," *CIRP Annals*, vol. 68, no. 1, pp. 423–426, 2019.

[178] M. Zaeh, R. Kleinwort, P. Fagerer, and Y. Altintas, "Automatic tuning of active vibration control systems using inertial actuators," *CIRP Annals*, vol. 66, no. 1, pp. 365–368, 2017.

[179] R. Kleinwort, J. Herb, P. Kapfinger, M. Sellemond, C. Weiss, M. Buschka, and M. Zaeh, "Experimental comparison of different automatically tuned control strategies for active vibration control," *CIRP Journal of Manufacturing Science and Technology*, vol. 35, pp. 281–297, 2021.

[180] R. Kleinwort, J. Platz, and M. F. Zaeh, "Adaptive active vibration control for machine tools with highly position-dependent dynamics," *International Journal of Automation Technology*, vol. 12, no. 5, pp. 631–641, 2018.

[181] Y. Altintas, A. Verl, C. Brecher, L. Uriarte, and G. Pritschow, "Machine tool feed drives," *CIRP annals*, vol. 60, no. 2, pp. 779–796, 2011.

[182] M. Zatarain, I. R. De Argandoña, A. Illarramendi, J. Azpeitia, and R. Bueno, "New control techniques based on state space observers for improving the precision and dynamic behaviour of machine tools," *CIRP Annals-Manufacturing Technology*, vol. 1, no. 54, pp. 393–396, 2005.

[183] D. Dumur, P. Boucher, and G. Ramond, "Direct adaptive generalized predictive control. application to motor drives with flexible modes," *CIRP Annals*, vol. 49, no. 1, pp. 271–274, 2000.

[184] K. Erkorkmaz and A. Kamalzadeh, "High bandwidth control of ball screw drives," *CIRP annals*, vol. 55, no. 1, pp. 393–398, 2006.

[185] A. Kamalzadeh and K. Erkorkmaz, "Compensation of axial vibrations in ball screw drives," *CIRP annals*, vol. 56, no. 1, pp. 373–378, 2007.

[186] D. Alter and T.-C. Tsao, "Stability of turning processes with actively controlled linear motor feed drives," *Journal of engineering for industry*, vol. 116, no. 3, pp. 298–307, 1994.

[187] D. M. Alter and T.-C. Tsao, "Control of linear motors for machine tool feed drives: design and implementation of h∞ optimal feedback control," 1996.

[188] J. Munoa, X. Beudaert, K. Erkorkmaz, A. Iglesias, A. Barrios, and M. Zatarain, "Active suppression of structural chatter vibrations using machine drives and accelerometers," *CIRP Annals*, vol. 64, no. 1, pp. 385–388, 2015.

[189] G. Campatelli, L. Sallese, and A. Scippa, "Design of an active workpiece holder," *Procedia CIRP*, vol. 34, pp. 217–222, 2015.

[190] E. Abele, H. Hanselka, F. Haase, D. Schlote, and A. Schiffler, "Development and design of an active work piece holder driven by piezo actuators," *Production Engineering*, vol. 2, no. 4, pp. 437–442, 2008.

[191] C. Brecher, D. Manoharan, U. Ladra, and H.-G. Köpken, "Chatter suppression with an active workpiece holder," *production engineering*, vol. 4, no. 2-3, pp. 239–245, 2010.

[192] L. Sallese, N. Grossi, A. Scippa, and G. Campatelli, "Numerical investigation of chatter suppression in milling using active fixtures in open-loop control," *Journal of Vibration and Control*, vol. 24, no. 9, pp. 1757–1773, 2018.

[193] L. Sallese, A. Scippa, N. Grossi, and G. Campatelli, "Investigating actuation strategies in active fixtures for chatter suppression," *Procedia CIRP*, vol. 46, pp. 311–314, 2016.

[194] L. Sallese, N. Grossi, J. Tsahalis, A. Scippa, and G. Campatelli, "Intelligent fixtures for active chatter control in milling," *Procedia CIRP*, vol. 55, pp. 176–181, 2016.

[195] H.-C. Möhring and P. Wiederkehr, "Intelligent fixtures for high performance machining," *Procedia CIRP*, vol. 46, pp. 383–390, 2016.

[196] C. Brecher, A. Schulz, and M. Week, "Electrohydraulic active damping system," *CIRP Annals-Manufacturing Technology*, vol. 54, no. 1, pp. 389–392, 2005.

[197] E. Mizrachi, S. Basovich, and S. Arogeti, "Robust time-delayed h∞ synthesis for active control of chatter in internal turning," *International Journal of Machine Tools and Manufacture*, vol. 158, p. 103612, 2020.

[198] N. van Dijk, N. van de Wouw, E. Doppenberg, H. Oosterling, and H. Nijmeijer, "Chatter control in the high-speed milling process using $\mu$-synthesis," in *Proceedings of the 2010 American Control Conference*. IEEE, 2010, pp. 6121–6126.

[199] N. J. van Dijk, N. van de Wouw, E. J. Doppenberg, H. A. Oosterling, and H. Nijmeijer, "Robust active chatter control in the high-speed milling process," *IEEE Transactions on Control Systems Technology*, vol. 20, no. 4, pp. 901–917, 2011.

[200] M. M. Daniali and G. Vossoughi, "Intelligent active vibration control of constrained manipulaors in robotic deburring," in *2009 International Conference on Industrial Mechatronics and Automation*. IEEE, 2009, pp. 76–80.

[201] V. Nguyen, J. Johnson, and S. Melkote, "Active vibration suppression in robotic milling using optimal control," *International Journal of Machine Tools and Manufacture*, vol. 152, p. 103541, 2020.

[202] Q. Wang, W. Wang, L. Zheng, and C. Yun, "Force control-based vibration suppression in robotic grinding of large thin-wall shells," *Robotics and Computer-Integrated Manufacturing*, vol. 67, p. 102031, 2021.

[203] O. Sörnmo, B. Olofsson, U. Schneider, A. Robertsson, and R. Johansson, "Increasing the milling accuracy for industrial robots using a piezo-actuated high-dynamic micro manipulator," in *2012 IEEE/ASME international conference on advanced intelligent mechatronics (AIM)*. IEEE, 2012, pp. 104–110.

[204] Z. Wang and P. Keogh, "Active vibration control for robotic machining," in *ASME International Mechanical Engineering Congress and Exposition*, vol. 58356. American Society of Mechanical Engineers, 2017, p. V002T02A079.

[205] I. Del Sol, A. Rivero, L. N. López de Lacalle, and A. J. Gamez, "Thin-wall machining of light alloys: A review of models and industrial approaches," *Materials*, vol. 12, no. 12, p. 2012, 2019.

[206] F. Rafieian, F. Girardin, Z. Liu, M. Thomas, and B. Hazel, "Angular analysis of the cyclic impacting oscillations in a robotic grinding process," *Mechanical Systems and Signal Processing*, vol. 44, no. 1-2, pp. 160–176, 2014.

[207] B. Tao, X. Zhao, and H. Ding, "Mobile-robotic machining for large complex components: A review study," *Science China Technological Sciences*, vol. 62, no. 8, pp. 1388–1400, 2019.

[208] D. Zhu, X. Feng, X. Xu, Z. Yang, W. Li, S. Yan, and H. Ding, "Robotic grinding of complex components: a step towards efficient and intelligent machining–

challenges, solutions, and applications," *Robotics and Computer-Integrated Manufacturing*, vol. 65, p. 101908, 2020.

[209] P. Zhou, X. Zhao, B. Tao, and H. Ding, "Time-varying isobaric surface reconstruction and path planning for robotic grinding of weak-stiffness workpieces," *Robotics and Computer-Integrated Manufacturing*, vol. 64, p. 101945, 2020.

[210] H. Susemihl, C. Moeller, S. Kothe, H. C. Schmidt, N. Shah, C. Brillinger, J. Wollnack, and W. Hintze, "High accuracy mobile robotic system for machining of large aircraft components," *SAE International Journal of Aerospace*, vol. 9, no. 2, p. 231, 2016.

[211] D. Hao, W. Wang, Z. Liu, and C. Yun, "Experimental study of stability prediction for high-speed robotic milling of aluminum," *Journal of Vibration and Control*, vol. 26, no. 7-8, pp. 387–398, 2020.

[212] A. Verl, A. Valente, S. Melkote, C. Brecher, E. Ozturk, and L. T. Tunc, "Robots in machining," *CIRP Annals*, vol. 68, no. 2, pp. 799–822, 2019.

[213] M. Wan, X.-B. Dang, W.-H. Zhang, and Y. Yang, "Chatter suppression in the milling process of the weakly-rigid workpiece through a moving fixture," *Journal of Materials Processing Technology*, vol. 299, p. 117293, 2022.

[214] Y. Zhao, Z. Wang, H. Wang, J. Hao, and H. Yu, "Stiffness analysis and optimization of supporting mechanism based on tricept for thin-walled part milling system," in *The 14th IFToMM World Congress, Taipei, Taiwan*, 2015, pp. 25–30.

[215] C. Sun, P. L. Kengne, A. Barrios, S. Mata, and E. Ozturk, "Form error prediction in robotic assisted milling," in *Procedia CIRP*, vol. 82. Elsevier, 2019, pp. 491–496.

[216] Q. Bo, H. Liu, M. Lian, Y. Wang, and K. Liu, "The influence of supporting force on machining stability during mirror milling of thin-walled parts," *The International Journal of Advanced Manufacturing Technology*, pp. 1–13, 2018.

[217] Y. Bao, R. Kang, Z. Dong, X. Zhu, C. Wang, and D. Guo, "Multipoint support technology for mirror milling of aircraft skins," *Materials and Manufacturing Processes*, vol. 33, no. 9, pp. 996–1002, 2018.

[218] Y. Bao, X. Zhu, R. Kang, Z. Dong, B. Zhang, and D. Guo, "Optimization of support location in mirror-milling of aircraft skins," *Proceedings of the Institution of Mechanical Engineers, Part B: Journal of Engineering Manufacture*, vol. 232, no. 9, pp. 1569–1576, 2018.

[219] Y. Bao, R. Kang, Z. Dong, X. Zhu, C. Wang, and D. Guo, "Model for surface topography prediction in mirror-milling of aircraft skin parts," *The International Journal of Advanced Manufacturing Technology*, vol. 95, no. 5-8, pp. 2259–2268, 2018.

[220] Q. Bi, X. Wang, Q. Wu, L. Zhu, and H. Ding, "Fv-svm-based wall-thickness error decomposition for adaptive machining of large skin parts," *IEEE Transactions on Industrial Informatics*, vol. 15, no. 4, pp. 2426–2434, 2018.

[221] X. Wang, Z. Li, Q. Bi, L. Zhu, and H. Ding, "An accelerated convergence approach for real-time deformation compensation in large thin-walled parts machining," *International Journal of Machine Tools and Manufacture*, vol. 142, pp. 98–106, 2019.

[222] X. Wang, Q. Bi, L. Zhu, and H. Ding, "Improved forecasting compensatory control to guarantee the remaining wall thickness for pocket milling of a large thin-walled part," *The International Journal of Advanced Manufacturing Technology*, vol. 94, no. 5-8, pp. 1677–1688, 2018.

[223] J. Fei, B. Lin, T. Huang, and J. Xiao, "Thin floor milling using moving support," 2021.

[224] J.-L. Xiao, S.-L. Zhao, H. Guo, T. Huang, and B. Lin, "Research on the collaborative machining method for dual-robot mirror milling," *The International Journal of Advanced Manufacturing Technology*, vol. 105, no. 10, pp. 4071–4084, 2019.

[225] R. Torres, S. González, I. Elguea, J. Aginaga, X. Iriarte, N. Agirre, and I. Inziarte, "Robotic assisted thin-wall machining with a collaborative robot," in *2020 IEEE 16th International Conference on Automation Science and Engineering (CASE)*. IEEE, 2020, pp. 1505–1508.

[226] X. Yang, H. Liu, J. Xiao, W. Zhu, Q. Liu, G. Gong, and T. Huang, "Continuous friction feedforward sliding mode controller for a trimule hybrid robot," *IEEE/ASME Transactions on Mechatronics*, vol. 23, no. 4, pp. 1673–1683, 2018.

[227] R. Fu, P. Curley, C. Higgins, Z. M. Kilic, D. Sun, A. Murphy, and Y. Jin, "Double-sided milling of thin-walled parts by dual collaborative parallel kinematic machines," *Journal of Materials Processing Technology*, vol. 299, p. 117395, 2022.

[228] J. Xiao, Q. Zhang, H. Liu, T. Huang, and X. Shan, "Research on vibration suppression by a multi-point flexible following support head in thin-walled parts mirror milling," *The International Journal of Advanced Manufacturing Technology*, pp. 1–10, 2020.

[229] J. Lan, B. Lin, T. Huang, J.-L. Xiao, X.-F. Zhang, and J.-X. Fei, "Path planning for support heads in mirror-milling machining system," *The International Journal of Advanced Manufacturing Technology*, vol. 91, no. 1-4, pp. 617–628, 2017.

[230] S. Veeramani, S. Muthuswamy, K. Sagar, and M. Zoppi, "Artificial intelligence planners for multi-head path planning of swarmitfix agents," *Journal of Intelligent Manufacturing*, vol. 31, no. 4, pp. 815–832, 2020.

[231] Y. Wang, Q. Bo, H. Liu, L. Hu, and H. Zhang, "Mirror milling chatter identification using q-factor and svm," *The International Journal of Advanced Manufacturing Technology*, vol. 98, no. 5, pp. 1163–1177, 2018.

[232] Y. Altintas, *Manufacturing automation: metal cutting mechanics, machine tool vibrations, and CNC design*. Cambridge university press, 2012.

[233] J. Gradišek, M. Kalveram, T. Insperger, K. Weinert, G. Stépán, E. Govekar, and I. Grabec, "On stability prediction for milling," *International Journal of Machine Tools and Manufacture*, vol. 45, no. 7-8, pp. 769–781, 2005.

[234] A. Preumont, *Vibration control of active structures*. Springer, 1997, vol. 2.

[235] I. Mancisidor, J. Munoa, R. Barcena, X. Beudaert, and M. Zatarain, "Coupled model for simulating active inertial actuators in milling processes," *The International Journal of Advanced Manufacturing Technology*, vol. 77, no. 1-4, pp. 581–595, 2015.

[236] A. Bilbao-Guillerna, I. Azpeitia, S. Luyckx, N. Loix, and J. Munoa, "Low frequency chatter suppression using an inertial actuator," 2012.

[237] Y. Tarng, J. Kao, and E. Lee, "Chatter suppression in turning operations with a tuned vibration absorber," *Journal of materials processing technology*, vol. 105, no. 1-2, pp. 55–60, 2000.

[238] E. I. Rivin and H. Kang, "Enhancement of dynamic stability of cantilever tooling structures," *International Journal of Machine Tools and Manufacture*, vol. 32, no. 4, pp. 539–561, 1992.

[239] S. Skogestad and I. Postlethwaite, *Multivariable feedback control: analysis and design*. Wiley New York, 2007, vol. 2.

[240] H. O. Bansal, R. Sharma, and P. Shreeraman, "Pid controller tuning techniques: a review," *Journal of control engineering and technology*, vol. 2, no. 4, pp. 168–176, 2012.

[241] S. Paul and R. Morales-Menendez, "Active control of chatter in milling process using intelligent pd/pid control," *IEEE Access*, vol. 6, pp. 72 698–72 713, 2018.

[242] C.-H. Yeung, Y. Altintas, and K. Erkorkmaz, "Virtual cnc system. part i. system architecture," *International Journal of Machine Tools and Manufacture*, vol. 46, no. 10, pp. 1107–1123, 2006.

[243] N. Esfandi, "Stability and control for machining of thin-walled structures-a time-varying delayed distributed parameter system," Ph.D. dissertation, UCLA, 2017.

[244] R. Kleinwort, M. Schweizer, and M. F. Zaeh, "Comparison of different control strategies for active damping of heavy duty milling operations," *Procedia Cirp*, vol. 46, pp. 396–399, 2016.

[245] G. S. Duncan, M. H. Kurdi, T. L. Schmitz, and J. P. Snyder, "Uncertainty propagation for selected analytical milling stability limit analyses."

[246] D. Hajdu, T. Insperger, D. Bachrathy, and G. Stepan, "Prediction of robust stability boundaries for milling operations with extended multi-frequency solution and structured singular values," *Journal of Manufacturing Processes*, vol. 30, pp. 281–289, 2017.

[247] D. Hajdu, T. Insperger, and G. Stepan, "Robust stability analysis of machining operations," *The International Journal of Advanced Manufacturing Technology*, vol. 88, no. 1-4, pp. 45–54, 2017.

[248] J. C. Doyle, "Synthesis of robust controllers and filters," in *The 22nd IEEE Conference on Decision and Control*. IEEE, 1983, pp. 109–114.

[249] A. Packard and J. Doyle, "The complex structured singular value," *Automatica*, vol. 29, no. 1, pp. 71–109, 1993.

[250] P. M. Young, "Controller design with mixed uncertainties," in *Proceedings of 1994 American Control Conference-ACC'94*, vol. 2. IEEE, 1994, pp. 2333–2337.

[251] P. M. Wortelboer and O. H. Bosgra, "Generalized frequency weighted balanced reduction," in *[1992] Proceedings of the 31st IEEE Conference on Decision and Control*. IEEE, 1992, pp. 2848–2849.

[252] MATLAB, *9.7.0.1190202 (R2019b)*. Natick, Massachusetts: The MathWorks Inc., 2018.

[253] M. L. Campomanes and Y. Altintas, "An improved time domain simulation for dynamic milling at small radial immersions," *J. Manuf. Sci. Eng.*, vol. 125, no. 3, pp. 416–422, 2003.

[254] R. Storn and K. Price, "Differential evolution–a simple and efficient heuristic for global optimization over continuous spaces," *Journal of global optimization*, vol. 11, no. 4, pp. 341–359, 1997.

[255] A. K. Qin and P. N. Suganthan, "Self-adaptive differential evolution algorithm for numerical optimization," in *2005 IEEE congress on evolutionary computation*, vol. 2. IEEE, 2005, pp. 1785–1791.

[256] K. Worden and G. Manson, "On the identification of hysteretic systems. part i: Fitness landscapes and evolutionary identification," *Mechanical Systems and Signal Processing*, vol. 29, pp. 201–212, 2012.

[257] Y. Altintas and M. Weck, "Chatter stability of metal cutting and grinding," *CIRP annals*, vol. 53, no. 2, pp. 619–642, 2004.

[258] T. L. Schmitz and K. S. Smith, *Machining dynamics*. Springer, 2014.

[259] T. L. Schmitz and B. P. Mann, "Closed-form solutions for surface location error in milling," *International Journal of Machine Tools and Manufacture*, vol. 46, no. 12-13, pp. 1369–1377, 2006.

[260] T. Insperger, B. P. Mann, T. Surmann, and G. Stépán, "On the chatter frequencies of milling processes with runout," *International Journal of Machine Tools and Manufacture*, vol. 48, no. 10, pp. 1081–1089, 2008.

[261] T. Insperger, G. Stépán, P. Bayly, and B. Mann, "Multiple chatter frequencies in milling processes," *Journal of sound and vibration*, vol. 262, no. 2, pp. 333–345, 2003.

[262] M. A. Davies, B. Dutterer, J. R. Pratt, A. Schaut, and J. Bryan, "On the dynamics of high-speed milling with long, slender endmills," *CIRP Annals*, vol. 47, no. 1, pp. 55–60, 1998.